博士論文

Mammalian methionine adenosyltransferase 2A promotes rRNA processing and methylation of translation factors to induce translation in an mTORC1-independent manner

（哺乳類メチオニンアデノシルトランスフェラーゼ 2A はリボゾーム RNA プロセシングおよび翻訳因子のメチル化を促進し mTORC1 非依存的に翻訳を誘導する）

東北大学大学院医学系研究科医科学専攻

細胞生物学講座　生物化学分野

MAHABUB ALAM

Table of Contents

Abbreviations

18S rRNA	18S subunit ribosomal RNA
28S rRNA	28S subunit ribosomal RNA
4E-BP	Eukaryotic translation initiation factor 4E-binding protein
ATP	Adenosine triphosphate
BSA	Bovine serum albumin
CBB	Coomassie brilliant blue
CHX	Cycloheximide
DMEM	Dulbecco's Modified Eagle Medium
EDTA	Ethylenediaminetetraacetic acid
eIF4A	Eukaryotic translation initiation factor 4A
eIF4B	Eukaryotic translation initiation factor 4B
eIF4E	Eukaryotic translation initiation factor 4E
eIF4F	Eukaryotic translation initiation factor 4F
FBS	Fetal bovine serum
GO	Gene ontology
LC-MS/MS	Liquid chromatography with tandem mass spectrometry
MAPK	Mitogen-activated protein kinase
MAT	Methionine adenosyltransferase
mM	Millimole
mTOR	Mechanistic target of rapamycin
mTORC1	Mechanistic target of rapamycin complex 1
mM	Nanomolar concentration
PBS	Phosphate-buffered saline
PI3K	Phosphoinositide 3-kinase

Abbreviations (Continue)

PVDF	Polyvinylidene Fluoride
qPCR	Quantitative polymerase chain reaction
rRNA	Ribosomal RNA
RT-qPCR	Quantitative reverse transcription polymerase chain reaction
S6K	P70-S6 Kinase 1
SAM	S-adenosylmethionine
SDS-PAGE	Sodium dodecyl sulphate-polyacrylamide gel electrophoresis
snoRNP	Small nucleolar ribonucleoproteins
SUnSET	Surface sensing of translation
TE	Translation efficiency
µl	Microliter
µM	Micromole
M	Mole
g	Gravitational constant
ACN	Acetonitrile

Abstract

Background: Translation, one of the essential steps of gene expression, consumes a huge amount of energy of the cells. Therefore, translation is a tightly controlled process to maintain cell energy homeostasis. Due to the high demand for growth, protein synthesis is induced in rapidly proliferative cells such as in cancers. In cancer, the activity of mammalian mechanistic target of rapamycin complex (mTOR) particularly mTORC1 induces translation. Therefore, mTORC1 inhibitor have been used as anti-cancer therapy. One of the major problems of mTORC1 inhibitor treatment is that many cancers develop resistant to such inhibition. Therefore, it is essential to discover mTORC1 independent translational regulation to invent new drug targets. Interestingly, cancer cells are highly dependent on methionine and other methionine cycle metabolites for proliferation which links the methionine metabolic cycle with cancer. The enzyme Methionine adenosyltransferase (MAT) catalyzes the synthesis of S-adenosylmethonine (SAM) in the first reaction of the methionine cycle. SAM is the essential methyl-donor required for the methylation of various biomolecules including DNA, RNA, histone and non-histone proteins. The level of intracellular SAM affects gene expression by changing methylation of these molecules. Gene expression control by histone proteins or mRNA methylation have been extensively studied. However, little is known about influence of gene expression by the methylation of structural and functional components of translation machinery. Various studies identified multiple methylation sites on rRNA, ribosomal proteins and translation factors. Although the biological significance of ribosomal protein methylation is still unknown, some specific methylation of rRNA and translation factors appears important for translation. In mammals, three MATs isozymes are liver specific MAT1 and 3, and the ubiquitous MAT2. Expression of MAT2A, the catalytic subunit of the MAT2 isozyme, is positively correlated with proliferation of various cancer cells. However, the specific functions of MAT2A in cancer cells is unclear. Considering this upregulation in cancer and methionine

dependency of cancer cells, it is assumable that MAT2A might be required for methylation of translation machinery by the production of SAM to facilitate translation in proliferating cancer cells. **Hypothesis:** Given that the protein synthesis is induced in proliferating cells and that RNA and protein components of translation machinery are methylated, we hypothesized that MAT2 and its catalytic product SAM are necessary for protein synthesis. **Methods:** In various experiments, MAT2A was depleted by RNAi or was chemically inhibited by cycloleucine (cLEU). The gene expression was quantified either by RT-qPCR or high throughput sequencing. The polysome analysis was performed by sucrose gradient ultra-centrifugation. We used quantitative mass spectrometry for proteomic studies and methylated peptides quantification. **Results:** In this study we discovered that MAT2A and SAM stimulate protein synthesis by facilitating the biogenesis of 18S rRNA and by dynamic methylation of translation factors in an mTORC1-independent manner. We revealed that both depletion and inhibition of MAT2A reduced protein synthesis in mammalian cells. Overexpression of MAT2A enhanced protein synthesis, indicating that SAM is limiting under the normal culture conditions. These effects of MAT2 manipulations did not accompany a reduction in the mTORC1 activity. Moreover, MAT2A inhibition reduced polysome formation. Sequencing of the polysome-bound RNA revealed that MAT2 inhibition decreased the translation efficiency (TE) of a fraction of mRNAs. We found that MAT2A interacts with proteins involved in rRNA processing and ribosome biogenesis. Depletion and inhibition of MAT2 reduced the 18S rRNA abundance. In addition, we observed that some translation factors were dynamically methylated in response to the activity of MAT2A or the availability of SAM. **Conclusion:** These observations suggest that cells possess an mTOR-independent regulatory mechanism that tunes translation in response to the amount of SAM. Such a system may acclimate cells for survival when SAM synthesis is reduced whereas it may support proliferation when SAM

is sufficient. Therefore, MAT2A could be a targetable molecule for cancer therapy to suppress translation in cancer cells in an mTORC1-independent manner.

Background

1. Translation is a key control point of gene expression

Cellular transcriptomes are partly correlated with protein levels. In general, the correlation between mRNA and protein levels in eukaryotes is around 40%[1–3], which represents the transcriptional regulation and the remaining 60% regulated in other ways. The partial correlation between transcriptomes and proteomes suggests the existence and importance of post-transcriptional regulation in gene expression. When a gene is expressed, it needs to be transcribed into mRNA, and then mRNA needs to be processed and to be translated into protein[4]. Translation itself is a multitier process regulated at the levels of initiation, elongation, ribosome turnover and mRNA composition[5–8]. In general, translation is regulated by translation machineries or by the limiting of proteins involved in translation (translation factors). But the translational regulation can be derived from the mRNA itself which is often resulting from the structural attributes. Translation initiation is the most important rate-limiting steps of protein synthesis[9].

2. Translation regulation by mTORC1

Since aberrant translation leads to dissipation of energy resources and various pathological consequences, translation is tightly regulated by various pathways in the cells[10]. In mammals, mRNAs are translated in two principal pathways: the cap-dependent and independent. In the cap-dependent translation the 5′ cap of mRNA allows binding of initiation complex and 40S ribosomal subunit to initiate translation[11,12]. The cap-independent translation is mediated by specialized mRNA structure called internal ribosome entry site (IRES) which recruits ribosome independent of cap structure and initiation complex[13]. The cap-dependent translation, which is the major pathway of mammalian translation, is mainly regulated by mTORC1 signaling[14]. So far as explored, the phosphoinositide 3-kinase (PI3K)–AKT and the

mitogen-activated protein kinase (MAPK) pathways are well known upstream of mTORC1. PI3K–AKT and MAPK/ERK signaling converge on mTORC1 to control translation[15] which are activated by the binding of growth factors such as insulin, fibroblast growth factor, epidermal growth factors, cytokines and hormones to receptor tyrosine kinases (RTKs) on the cell surface[16,17]. Upon activation, PI3K (p85-p110 heterodimer) is recruited to the plasma membrane where it phosphorylates phosphatidylinositol-4,5-bisphosphate (PIP2) and converts it to second messenger phosphatidylinositol-3,4,5-trisphosphate (PIP3). PIP3-bound AKT is then activated by phosphorylation[18]. Activated AKT phosphorylates and inactivates TSC1/2[19]. The inactivation of TSC1/2 facilitates the accumulation of the GTP-bound Ras-homolog protein RHEB to activate mTORC1[20,21].

The MAPK proteins are activated and recruit the GRB2 and SOS complex to convert inactive GDP-bound Ras to the active GTP-binding form. Activated Ras then phosphorylates and activates RAF. The phosphorylated form of RAF then activates MEK to activate ERK1/2 [22] which inhibit TSC1/2 thus activates the mTORC1 signaling cascade.

In the downstream for translation regulation, mTORC1 activates S6K by phosphorylation[23]. S6K then activates multiple targets including RPS6, PDCD4 and eEF2K. Phosphorylation of RPS6 promotes the recruitment of RPS6 to 7-methylguanosine cap complex which expedites the formation of the translation pre-initiation complex[24]. PDCD4 sequesters eIF4A from eIF4A-eIF4G complex thereby inhibit eIF4A helicase activity and structured mRNA translation[25]. Upon phosphorylation by S6K, PDCD4 is degraded by ubiquitination[26] and induce translation. eEF2K phosphorylation by S6K inhibits its kinase activity on eEF2, phosphorylation of which reduces translation[27]. mTORC1 also phosphorylates 4E-BPs which eliminate binding inhibition to eIF4E to facilitates translation initiation[28].

The activated MAPK also phosphorylates eIF4E in an mTORC1-independent manner through MAPK-interacting kinases 1 and 2 (MNK1/2) to facilitate translation of a specific subset mRNA required for oncogenesis[29].

3. Protein synthesis induction is an anabolic demand for cell proliferation

Cell proliferation is initiated by cell growth where cell anabolic processes including translation are activated to induce protein synthesis. Since translation is an energy-expensive process, the proliferating cells need to balance energy content and translation to maintain homeostasis[30]. A dysregulated translation can generate various pathological consequences including cancer[31]. Cancer cells acquire the ability to induce protein synthesis, growth and proliferation by complex molecular alterations in the cells that facilitate the expression of proteins required for cell survival and growth[32–34]. To induce growth and proliferation, mammalian cells require a signal-mediated stimulation of translation, initiated by the availability of extracellular factors such as various types of growth factors, insulin, nutrition, endocrine secretions, and metabolites. The proliferating cells integrate the presence of these extracellular molecules to induce anabolic processes including translation[35,36]. It has been reported that proliferation of cancer cells was sustained by the increased protein synthesis[37].

Cancer cells induce protein synthesis by activation of the translation signaling pathways which facilitate the expression of the proteins required for cell survival and growth[32–34]. In addition, translation can be induced by post translational modifications of diverse proteins involved in translation. For example, consecutive expression and phosphorylation of eukaryotic initiation factor 4F (eIF4F) accelerate translation initiation[32,38–40], reduced expression or increased phosphorylation of 4E-BP promotes translation in pancreatic cancer[41], and overexpression of eukaryotic initiation factor 3 (eIF3) induced global protein synthesis and increased translation of oncogenic transcripts in fibroblast cancer cells[42]. Considering the

contribution of mTOR to translation, cellular growth and proliferation, various drugs targeting the mTOR signaling proteins are being developed for cancer therapy[43–45]. However, one of the major problems in mTOR inhibition for cancer therapy is that upon inhibition of a protein in the mTOR signaling, cancer cells develop a resistance to the chemotherapy by activating compensatory proteins by various feedback mechanisms[46]. For example, upon inhibition of mTORC1, the AKT and MAPK pathways are activated by feedback mechanisms to promote cell survival[47–51]. Therefore, it is of utmost importance to explore new mTOR-independent translation regulatory mechanisms in the cells to propose novel targets for cancer therapy.

4. Dynamics of methionine metabolism in cancer

In addition to components of proteins, methionine is necessary to synthesize various essential metabolites in the one-carbon metabolic cycle. The first reaction of the cycle is the conversion of methionine to S-adenosylmethionine (SAM). SAM is produced from methionine and ATP by methionine adenosyltransferase (MAT)[52]. In mammals, three isozymes of MAT are known[53,54]. MAT1 and MAT3 are found in the liver whereas MAT2 is expressed in all tissues except for adult liver[55–57]. MAT2 consists of two subunits named MAT2A and MAT2B which form a complex with a molecular ratio of 2:1. MAT2A is the catalytic subunit whereas MAT2B regulates the catalytic activity of MAT2A[58]. A massive metabolic reprogramming happens during cancer development. In addition to metabolism shift from oxidative phosphorylation to glycolysis, the cancer cells become highly dependent on methionine for proliferation. The normal cells and methionine-dependent cancer cells have the similar potential of converting homocysteine to methionine. Interestingly, it has been reported that normal cells can easily maintain proliferation by replacing methionine with its precursor homocysteine but methionine-dependent cancer cells rapidly stopped proliferation in such replacement[59]. Accumulative evidence suggested that this methionine dependency is derived

from decreasing SAM concentration inside the cells[60,61]. In these circumstances, how SAM reduction inhibits cell proliferation is incompletely understood.

5. MAT2A in cellular growth and proliferation

MAT2A expression is high in proliferating fetal hepatocytes and is replaced by MAT1 in adult quiescent hepatocytes[62]. Upon partial hepatectomy, MAT2A is upregulated during regeneration[63]. MAT2A is found to be upregulated in various cancers including liver[64,65], uterine cervix[66], colon[67] and breast cancers[68]. These observations suggest that MAT2A is required for cell growth and proliferation. However, how MAT2A induces cancer cell growth and proliferation is largely unknown. Cellular growth and proliferation are facilitated by activating anabolic pathways, suggesting that MAT2 may be a contributor to the cellular anabolic pathways. Recently, MYC has been shown to induce MAT2A expression[69], which explains how MAT2A is upregulated in proliferative tissue, particularly in cancer. In addition, mTOR was shown to be responsive to one of the one-carbon cycle metabolites, SAM, by a protein named SAMTOR[70]. While SAM may stimulate mTOR via SAMTOR, it remains possible that SAM affects other machinery for cellular growth and proliferation.

6. SAM is required for methylation

SAM is the essential methyl group donor in biological methylation of various biomolecules including DNA, RNA and proteins. MAT2A has been shown to indirectly interact with FTSJ3, a 2-O-methyltransferase for various types of RNA including ribosomal RNA[71]. Previous research showed that FTSJ3 is required for the maturation of the 18S rRNA[72], raising the possibility that MAT2A is also involved in this process along with FTSJ3. Moreover, SAM depletion in *E. coli* showed inefficient assembly of ribosomal subunits due to hypomethylation of U2525 of the 23S rRNA during translation[73]. Besides histones, non-histone

proteins such as ribosomal proteins and translation factors were found to be methylated[74]. Although the biological significance of ribosomal protein methylation is yet to be interrogated, methylation of several translation factors is known to regulate translation. For example, it has been revealed that depletion of the methyltransferase for eEF1A165K induces translation of proteins related to ribosome biogenesis and chromatin whereas it reduced translation of proteins important for unfolded protein response[75]. Methylation of eEF1A55K promoted global translation in a human lung cancer cell line[76].

Aim and objectives of the study

1. Aim

As some of the RNA and protein components of translation machinery are methylated, we hypothesized that MAT2 and SAM are required for protein synthesis in mammalian cells by affecting their methylation.

2. Objectives

1. To examine the importance of MAT2A in global protein synthesis
2. To find out the influence of signaling pathways for translation control in MAT2A-regulated protein synthesis
3. To investigate the characteristics of MAT2A- and SAM-regulated translation by polysome profiling and polysome-bound mRNA sequencing
4. To examine how the interaction of MAT2A with proteins is involved in translation
5. As a part of the mechanistic aspect, to assess how MAT2A and SAM affect rRNA biogenesis and methylation of proteins involved in translation.

Materials and methods

1. Cell culture

Hepa1 and HeLa cells were cultured in Dulbecco's Modified Eagle's Medium (DMEM) containing 4.5 g/l of glucose (D5796, DMEM-high glucose, Sigma-Aldrich, St. Louis, MO) supplemented with 10% fetal bovine serum (FBS) (172012, Sigma Aldrich) and combination of 100 U/ml penicillin and 100 μg/ml streptomycin (15140-122, Penicillin-Streptomycin, Thermo Fisher Scientific, Waltham, MA). In the polysome analysis experiment, HeLa cells were cultured in DMEM containing 4.5 g/l of glucose (08458-16, Nacalai Tesque, Kyoto, Japan) supplemented with 10% FBS (26140079, Thermo Fisher Scientific). HEK293T cells were cultured in DMEM containing 1.0 g/l of glucose (D6046, Sigma Aldrich) supplemented with 10% FBS (172012, Sigma Aldrich). Cells were regularly maintained by passaging every 2-3 days and every 2.5 to 3 months, the cells were replaced with a new stock. In each passage, the cells were stripped using 0.05% trypsin-EDTA (25300-062, Thermo Fisher Scientific). The cells were grown in a cell culture incubator at 37°C supplied with 5% CO_2 in the air with sufficient humidity. Unless specified, cells were harvested by in-situ lysis in cell culture plates or dishes using various types of lysis buffer depending on the experiments.

2. Plasmids

The pEF1α-FLAG-Biotag empty vector (FB-EV) was a gift from Dr. Cantor A. B. (Children's Hospital and Dana Farber Cancer Institute; Harvard Medical School) and pEF1α-FLAG-Biotag-MAT2A (FB-MAT2A) was constructed in a previous research[77] by introducing the mouse *Mat2a* cDNA (Genebank ID: BC003451) into FB-EV. The pEF1α-FLAG-Biotag-BirA (FB-BirA) vector was used for the expression of the bacterial biotin ligase[77,78]. The pcDNA3.1(+)-MAT2A (MAT2A) was constructed and used in previous research[77]. The

pcDNA3.1(+)-RPS2-TEV-3X-FLAG (FL-RPS2) and pcDNA3.1(+)-RPL23A-TEV-3X-FLAG (FL-RPL23A) vectors were constructed in this study. The human RPS2 (NM_002952.3) and RPL23A (NM_000984.5) cDNA were amplified from HEK293T cells using a forward primer including a BamH1 restriction site and a reverse primer including a TEV protease site followed by the 3XFLAG sequence and an Xho1 restriction site. The amplified cDNAs were then introduced into the pcDNA 3.1 (+) vector at the BamH1 and Xho1 sites. Therefore, the resulting contracts encodes C-terminal 3XFLAG-tagged RPS2 and 3XFLAG-tagged RPL23A, respectively. The MSCV-FB-eEF1A1 (FB-eEF1A1) and MSCV-FB-eEF1A1K55R mutant (FB-FB-eEF1A1K55R) plasmids were constructed in this study. Human eEF1A1 cDNA (NM_001402.5) was PCR amplified from ASPC1 cells lines and introduced into BamH1 restriction enzymes site of MSCV vector. MSCV-FB-eEF1A1K55R mutant vector was then constructed by introducing point mutation to MSCV-FB-eEF1A1 plasmid.

3. Histone protein extraction

The histone proteins were extracted from cells by a previously described acid extraction method[79]. About 4×10^6 HeLa cells were grown in a 10-cm culture dish. Cells were washed 2 times with ice-cold PBS and harvested in 15 ml centrifuge tube by scrapping in presence of ice-cold PBS. Cells pellet was made by centrifuges the tubes at 4°C at a speed of 300 × g for 5 minutes. The cells were then re-suspended in ice-cold 900 µL of hypotonic lysis buffer (10 mM Tris–HCl pH 8.0, 1 mM KCl, 1.5 mM $MgCl_2$ and 1 mM DTT) containing protease inhibitor (0469315900, cOmplete® Mini EDTA-free Protease Inhibitor Cocktail Tablets, Roche, Mannheim, Germany). The content was then transferred to 1.5 ml tube and rotate for 30 minutes at 4°C. The nuclei were pelleted by spinning at 10,000 × g for 10 minutes. The supernatant was discarded, and the nuclei were re-suspended in 400 µL of 0.4 N H_2SO_4 and incubates at 4°C with rotation for 30 minutes. The content was then centrifuge at a speed of

16,000 × g for 10 minutes to pelleted down the nuclear debris. The supernatant was collected in a 1.5 ml centrifuge tube for trichloroacetic acid (TCA) precipitation of histones. Briefly, 132 µL of TCA (33% of supernatant) was added to the tube drop by drop and mixed gently. The tube was then incubated on ice for 30 minutes. The content was then centrifuged 16,000 × g for 10 minutes to pellets the histone followed by washing with ice-cold acetone for 2 times. The histone pellets where then air dried for 20 minutes. The pellets were re-suspended in 100 µL of distilled water. The SDS-PAGE and CBB staining were performed to confirm histone extraction. This histone solution was used for western blot analysis to detect the methylated histones.

4. Western blot analysis

Western blot analysis was performed as described in previous studies with modifications[77,80]. Cells were washed with ice-cold Dulbecco's phosphate-buffered saline (PBS) three times followed by *in-situ* lysis in 100-300 µl of 1× SDS sample buffer (62.5 mM Tris-HCl pH 6.8, 1% SDS, 10% glycerol, 1% 2-mercaptoethanol and 0.02% bromophenol blue) containing a protease inhibitor (0469315900, cOmplete® Mini EDTA-free Protease Inhibitor Cocktail Tablets). The lysate was then collated in 1.5-ml tubes and was denatured by heating at 95°C for 5 minutes. Alternatively, cells were lysed by radioimmunoprecipitation assay (RIPA) buffer (50 mM Tris-HCl pH 7.4, 150 mM NaCl, 1 mM EDTA, 1% NP-40, 0.5% Na-deoxycholate and 0.1% SDS) containing the protease inhibitor and a phosphatase inhibitor (04906837001, PhosSTOP®, Roche) for 30 minutes on ice. The lysate was then centrifuged at a speed of 20,000 × *g* for 20 minutes at 4°C. The clarified lysate was transferred to new tubes. To facilitate equal-amount loading in the SDS-PAGE, the total protein amount was quantified by either a protein assay kit (22660, Pierce™ 660nm protein assay reagent, Thermo Fisher Scientific) or SDS-PAGE followed by Coomassie brilliant blue (CBB, 50% methanol, 10%

acetic acid, and 0.1% R-250 or G-250) staining and quantification of stain density using the ImageJ software (Version 1.53i 24 March 2021, National Institutes of Health and the Laboratory for Optical and Computational Instrumentation, University of Wisconsin). Before loading into a gel for SDS-PAGE, the lysate was denatured by heating at 95°C for 5 minutes in the presence of SDS sample buffer. The protein was then separated by SDS-PAGE in an 11% polyacrylamide gel (15% for SUnSET and ribosomal proteins) at 100 V (or 80 V. for SUnSET and LC-MS/MS) in the presence of 1× SDS-PAGE running buffer (25 mM Tris, 192 mM glycine and 0.1% SDS, pH not adjusted). The separated proteins were then transferred onto 0.45-µm PVDF membrane (IPVH00010, Immobilon®-P Transfer Membrane, Merck Millipore Ltd., Ireland) by a wet electro-transfer method at a constant 300-mA current flow for 2.5 hr in the presence of a transfer buffer (25 mM Tris, 192 mM glycine and 10% methanol). After transfer, the PVDF membranes were blocked in 3 to 5% skim milk for 45 to 60 minutes. The membranes were then incubated overnight in hybridization bags at 4°C with primary antibodies diluted in 3 to 5% skim milk with a gentle rocking movement. For detection of phosphorylated proteins, after blocking in skim milk, the membranes were washed in TBS-T (50 mM Tris-HCl pH 7.5, 150 mM NaCl and 0.05% Tween® 20) and then were incubated in 3% bovine serum albumin (BSA) overnight at 4°C. After washing out the primary antibodies in TBS-T, the PVDF membranes were incubated with secondary antibodies diluted in 3-5% skim milk (or 3% BSA for anti-phosphorylation antibodies) at room temperature for 1 hr. The membranes were washed again in TBS-T and the imaging was done by a ChemiDoc MP imaging system (Bio-rad Laboratories, Hercules, CA) using a Clarity™ Western ECL Substrate (1705060, Bio-Rad Laboratories). Followings are the antibodies used for Western blot:

Primary antibodies – Anti-puromycin (Clone 12D10, Merck Millipore, Burlington, MA), anti-β-ACTIN (GTX109639, GeneTex, California), monoclonal mouse anti-MAT2A (Produced in

this study in lab, the production procedure is discussed under heading of "Monoclonal mouse anti-MAT2A antibody production"), polyclonal rabbit anti-MAT2B (Produced in lab by using six histidine-tagged mouse MAT2B recombinant protein as an antigen) [77], anti-GAPDH (ab8245, Abcam, Cambridge, UK), anti-histone H3K4me3 (ab8580, Abcam), anti-histone H3K9me3 (ab8898, Abcam), anti-histone H3K27me3 (07449, Merck Millipore), anti-histone H3 (ab1791, Abcam), anti-mTOR (2972, Cell Signaling Technology, Danvers, MA), anti-phospho-mTOR (S2448) (2971, Cell Signaling Technology), anti-p70 S6 kinase (9202, Cell Signaling Technology), anti-phospho-p70 S6 kinase (T389) (9205, Cell Signaling Technology), anti-p44/42 MAPK (9102, Cell Signaling Technology), anti- phospho-p44/42 MAPK (T202/Y204) (9102, Cell Signaling Technology), anti-eIF4E (9742, Cell Signaling Technology), anti-phospho-eIF4E (S209) (9741, Cell Signaling Technology), anti-AKT (9272, Cell Signaling Technology), anti-phospho-AKT (S473) (9271, Cell Signaling Technology), anti-RPL23A (sc-517097, Santa Cruz, Texas), anti-RPS3 (sc-376008, Santa Cruz) and anti-DDDDK-tag (M185-3L, MBL, Tokyo, Japan), anti-DiMethyl-eEF1A-K55 (A17987, ABclonal, Tokyo, Japan). All the primary antibodies were used with a 1000-fold dilution in skim milk or BSA except that the anti-GAPDH and anti-DDDDK-tag antibodies were used with a 4000-fold dilution.

Secondary antibodies – HRP linked anti-mouse IgG (NA931, GE healthcare, Chicago, IL) and anti-rabbit IgG (NA934, GE healthcare). Secondary antibodies were used with a 4000-fold dilution.

5. Monoclonal mouse anti-MAT2A antibody production

Two Balb/c mice were immunized with purified MAT2A (100 μg/mouse) by the intraperitoneal route together with the Imject Alum (Thermo Fisher Scientific). The procedure included two additional immunizations followed by a final booster intraperitoneal injection

administered two days prior to the harvest of spleen cells. Harvested spleen cells were subsequently fused with P3U1 cells using PEG1500 (Roche), and the hybridomas were grown in an RPMI medium supplemented with hypoxanthine, aminopterin, and thymidine for selection (Thermo Fisher Scientific). Culture supernatants were screened by enzyme-linked immunosorbent assay (ELISA). Clone M2aMab-4 (IgG2b, kappa) was established.

6. Translation assay

The rate of translation was examined by the SUnSET method[81]. Cells were seeded in 12- or 6-well plates or 6-cm dishes and were cultured for at least 24 hr to attain 70-80% confluency. The cells were then pulse-labeled with 20 mg/ml puromycin (P8833, Puromycin dihydrochloride, Sigma-Aldrich) for a period of 30 minutes at 37°C in a cell culture incubator. In serum stimulation, cells were grown in serum-free DMEM containing 4.5 g/l glucose (D5796, Sigma-Aldrich) for a period of 24 hr followed by the medium supplemented with 10% FBS for 1 or 3 hr before pulse-labeling with puromycin. After puromycin labeling, cells were washed 3 times with ice-cold PBS and were lysed with RIPA buffer supplemented with the protease and phosphatase inhibitors. The cleared lysate containing around 1-1.5 μg of protein was loaded in a lane for SDS-PAGE and subsequent Western blot detection was done by using the anti-puromycin antibody.

7. RNA interference

The knockdown of *Mat2a* was performed by using a Lipofectamine® RNAiMAX transfection reagent (13778150, Thermo Fisher Scientific). About 2×10^5 or 1×10^5 Hepa1 cells were seeded, respectively, in 6-well pate or 12-well plates. After 24 hr of culture, the cells were transfected with 10 pmol of a control or *Mat2a*-targeting siRNA. After 24 hr of transfection, the medium was refreshed, and RNA or protein sample was prepared after 48 hr

of transfection for quantification. The control and *Mat2a*-targeting siRNAs used in this experiment were previously described in other researches from our lab[77,82]. The sequences of the siRNAs are given below:

Control siRNA: 5′-AGGAGGAUAUUACCAUGAAGAAGAC-3′

siMAT2A (911): 5′-AGGAAAGGAUUAUACCAAAGUGGAC-3′

8. RNA extraction

Total RNA was extracted using an RNeasy Plus Mini kit (74134, Qiagen, Hilden, Germany) following the protocol supplied by the manufacturer. From the sucrose fractions in polysome analysis, RNA was extracted by ethanol precipitation in the presence of protein denaturing agent guanidine hydrochloride (Guanidine-HCl)[83]. Briefly, 500 µl of 8 M Guanidine-HCl was added to 226 µl of fractionated sample in an RNase free 1.5-ml centrifuge tube. After mixing well, 750 µl of cold ethanol was added. Then, after a brief mixing, the tube was chilled at -20°C for 20 minutes. The content was then centrifuged at 20,000 × *g* for 15 minutes at 4°C. The supernatant was removed and after the addition of 250 µl of 75% cold ethanol to the pellet, the tubes were centrifuged at 20,000 × *g* for 15 minutes. Two hundred microliter of RNA buffer, 20 µl of 3 M sodium acetate and 600 µl of 100% cold ethanol were added. The tubes were then chilled at -20°C for 1 hr. After incubation, the tubes were centrifuged at 20,000 × *g* for 15 minutes at 4°C. Finally, the pelleted RNA was washed with 75% ethanol, was dried, and was dissolved in RNase free water.

9. RNA quantification by RT-qPCR

cDNA was synthesized usually from 1 µg of total RNA using a SuperScript™ III Reverse Transcriptase (18080044, Thermo Fisher Scientific) or High-Capacity cDNA Reverse Transcription Kit (4374966, Thermo Fisher Scientific) using random primer. The synthesized

cDNA was amplified and was quantified by using a FastStart Essential DNA Green Master reaction mix (06924204001, Roche) in a LightCycler® 96 instrument (Roche). *Mat2a* was quantified using a primer pair targeting the coding sequence[77,82] and the 47S pre-rRNA was quantified using the one targeting the 5′ ETS sequence (Figure 10A)[84]. The primer sequences are as follows:

Species	Gene name	Direction	Sequence
Mouse	*Mat2a*	Forward (478)	5′- GGTGTTCATCTTGACCGGAATG - 3′
		Reverse (627)	5′- GCGGCGTAGTTCAGCCAATT - 3′
Mouse	*5′ ETS*	Forward	5′- GCTGTTTTGCTTGTCCAGCC - 3′
		Reverse	5′- AACGACACCTCGGGGAAATC - 3′

10. Polysome analysis

Approximately 5 × 10^6 cells were seeded in 25 ml of medium in 15-cm cell culture dishes and were grown for 18 hr. The cells were treated with either 10%-FBS-supplemented media (Control) or 30 mM cLEU (A48105, Sigma-Aldrich) dissolved in media supplemented with 10% FBS. After 6 hr of treatment, at 24 hr of culture, cells were treated with 100 μg/ml cycloheximide (06741–04, Nacalai Tesque) for 10 minutes. Cells were then harvested and were washed with ice-cold PBS supplemented with 100 μg/ml cycloheximide. After centrifugation, the cells were suspended in 550 μl of hypotonic lysis buffer (10 mM HEPES-KOH pH 7.9, 1.5 mM $MgCl_2$, 10 mM KCl, 0.5 mM DTT, 1% Triton™ X-100, 100 μg/mL of cycloheximide, 40 U/mL RNAsin® and cOmplete® Mini EDTA free protease inhibitor Cocktail) by pipetting and were mechanically lysed by 10 times through passing 25-gauge needle. After incubation on ice for 10 minutes, the insoluble fractions were removed by centrifugation at 15,000 × *g* for 10 minutes. The absorbance of 260 nm of the clarified lysate was measured using a Thermo Scientific™ NanoDrop™ One Spectrophotometer (Thermo Fisher Scientific). The absorbance

of control and treatment groups were equalized by adding lysis buffer. A 10-50% sucrose gradient was prepared in 14×89 mm open-top poly-clear centrifuge tube (7030, Seton Scientific, Petaluma, CA) in polysome buffer (20 mM HEPES-KOH pH 7.6, 5 mM $MgCl_2$, 100 mM KCl, 1 mM DTT and 100 µg/ml cycloheximide) using Gradient Master (Cosmo Bio, Tokyo, Japan). A total of 500 µL of lysate containing around 150 µg of total RNA was loaded on sucrose gradient. The gradient with lysate on top was then centrifuged at 40,000 rpm for 1.5 hr at 4°C with the maximum acceleration and deacceleration using an SW41Ti rotor (331362, Beckman Coulter, CA) in a Beckmam XL90 ultracentrifuge (Beckman Coulter). The fractions collection and polysome profile generation were done using a Piston Gradient Fractionator (Biocomb, Fredericton, Canada) equipped with a single path UV-1 optical unit (Biomini UV-monitor, ATTO, Tokyo Japan) and a chart recorder (Digital mini recorder, ATTO) as previously described[85].

11. RNA sequencing

Total RNA concentration was measured with a Quantus Fluorometer using a QuantiFluor RNA system (Promega, Wisconsin, USA), and the quality was confirmed by a 5200 Fragment Analyzer System using the Agilent HS RNA Kit (Agilent Technologies, CA). The library was prepared from 300 ng of total RNA using an MGIEasy RNA Directional Library Prep Set (MGI Tech Co., Ltd. Shenzhen Shi, China) with the protocol described in the manufacturer's manual. The dsDNA concentration of the library was measured by a Qubit 3.0 Fluorometer using a dsDNA HS Assay Kit (Thermo Fisher Scientific). The library quality was confirmed with Fragment Analyzer using a dsDNA 915 Reagent Kit (Advanced Analytical Technologies, Ankeny, IA). The circularized DNA was prepared using an MGIEasy Circularization Kit (MGI Tech Co., Ltd.) with the manufacturer's guideline. DNA nanoball (DNB) was made manually by using the DNBSEQ-G400RS High-throughput Sequencing Kit

(MGI Tech Co., Ltd.). The sequencing of the prepared DNBs at 2 × 100 bp was performed using DNBSEQ-G400. The following adapter sequences were removed by cutadapt (ver. 1.9.1).

Read 1 side: AAGTCGGAGGCCAAGCGGTCTTAGGAAGACAA and

Read 2 side: AAGTCGGATCGTAGCCATGTCGTTCTGTGAGCCAAGGAGTTG)

The low-quality reads (less than 20 quality score or less than 40 bases) were removed by sickle (ver. 1.33). The high-quality reads were then aligned to the GRCh38 human reference genome to provide mapped reads in a Sam format. Samtools (ver. 1.10) was used to convert the Sam format to Bam format. The reads mapped to genes were counted using featureCounts (ver. 2.0.0). The differential gene expression analysis was performed for transcripts aligned to more than 10 reads using estimateSizeFactors function, estimateDispersions function and nbinomWaldTest function in R package DESeq2.

12. Establishment of FB-MAT2A stable expressing HeLa cell line

A protocol modified from the one of Katoh et al.[77] was used to establish the stable cell line. About 6×10^5 HeLa cells were seeded and grew overnight in a 6-cm cell culture dish with 3 ml of the medium. Four micrograms of the FB-BirA plasmid was co-transfected with either 4 μg of FB-EV or FB-MAT2A using a Genejuice® transfection reagent (709674, EMD Millipore, Billerica, MA). After 24 hr of transfection, the medium was replaced with the one containing 4 μg/ml G418 (345810, EMD Millipore) and 4 μg/ml puromycin (8833, Puromycin dihydrochloride, Sigma-Aldrich). The cells were then sub-cultured and were maintained for the next 2 weeks in the presence of the antibiotics. The antibiotic resistant cells were used for the purification and LC-MS/MS analysis of FB-MAT2A (related to Figure 9). From this FB-MAT2A stable expressing cell line, a single clone expressing a high amount of FB-MAT2A was isolated by a limiting dilution and culture method. In this method, cells were diluted to 0.5 cell/100 μl of media and 100 μl of the cell suspension was dispensed to each well of a 96-well

flat-bottom culture plate. Therefore, around 50% of the wells contained a single cell. The wells containing a single cell were marked and the cells were grown to confluent. The cells derived from every single cell were then cultured in a 24-well plate to find high FB-MAT2A expressing clones by Western blot. The single clone with high FB-MAT2A expression was used for the experiment shown in Figure 2G and H.

13. Purification of FB-MAT2A and LC-MS/MS analysis

Two million stable expression cells were seeded in four 10-cm dishes 24 hr before the cell harvest. Cells were harvested by scrapping in ice-cold PBS, were washed, and were pelleted in a 15-ml centrifuge tube by centrifugation at 300 × *g* for 5 minutes. The cells were then transferred to protein-low-bind 1.5-ml tubes (0030108116, Eppendorf, Hamburg, Germany). The cell pellet was lysed by 1 ml of immunoprecipitation (IP) buffer (10 mM Tris-HCL pH 7.4, 150 mM NaCl, 1 mM EDTA, 0.3% NP-40, 2 mM DDT, protease (cOmplete®), and phosphatase (PhosSTOP®) inhibitor. The clarified supernatant obtained by centrifugation at 200 × g for 10 minutes was used for affinity purification with streptavidin-conjugated magnetic beads [78,80] (Dynabeads™ M-280 Streptavidin, Thermo Fisher Scientific). Briefly, 20 µl of Dynabeads™ slurry was equilibrated by washing with ice-cold IP wash buffer (10 mM Tris-HCL pH 7.4, 150 mM NaCl, 1 mM EDTA, 0.3% NP-40 and 2 mM DDT) twice on a magnetic stand. The clarified cell lysate was then added to the beads and the beads were incubated with an end-over-end rotation (10 rpm/min) at 4°C for 2 hr. The protein-bound beads were washed with 1 ml of ice-cold IP wash buffer five times on a magnetic stand. Competitive elution of proteins was performed by incubating the beads in the biotin elution buffer at 70°C for 15 minutes. The eluted proteins were processed for mass spectrometry analysis according to the previously described protocol[86,87]. Briefly, the purified proteins were separated in a 5-20% gradient gel (HON-052013; Oriental Instruments Co. Ltd. Kanagawa, Japan) and were

stained with CBB for visualization. Every lane was divided into small gel pieces and the pieces were treated with acetonitrile (ACN) for destaining. The samples were then reduced in an aqueous solution of 10 mM DTT and 25 mM ammonium bicarbonate (ABC) at 56°C for 1.5 hr. Alkylation of cysteine side chains was performed in a 55 mM acrylamide and 25 mM ABC solution. After dehydration in acetonitrile and drying in a SpeedVac, the samples were digested with 10-30 ng of trypsin in digestion buffer (50 mM ABC and 10% ACN) overnight at 37°C. The digested peptides were eluted by shaking in 75% ACN 1 % formic acid solution. The eluates were then concentrated in a SpeedVac and were analyzed in an Orbitrap Fusion mass spectrometer connected with an Easy-nLC 1000 HPLC (Thermo Fisher Scientific). The obtained raw MS/MS data were then converted to mgf files using a Proteome discoverer software (version 1.3.0.339, Thermo Fisher Scientific). To identify peptides, the converted files were used for the database search using a Mascot search engine (Matrix Science, London, UK) considering propionamide (Cys) as a fixed modification and acetyl (Protein N-term) and oxidation (Met) as variable modifications with an MS/MS tolerance of 0.5 Da.

14. Immunofluorescence microscopy

Immunostaining of cells was performed by methods slightly modified from that of Katoh et. al.[77]. A 12-well cell culture plate was prepared by placing sterile micro coverslips (C015001; 15 mm, Matsunami Glass Industry, Osaka, Japan) on the bottom of each well. HeLa cells stably expressing FB-EV or FB-MAT2A were cultured (8×10^4 cells/well in 1 ml media) on the micro coverslips for 24 hr. The cells in the coverslips were then fixed with 4% paraformaldehyde (1040051000, Merck KGaA, Darmstadt, Germany) in PBS for 10 minutes at room temperature. After washing with PBS, the cells were permeabilized with 0.5% Triton® X-100 in PBS at room temperature with gentle shaking for 5 minutes. The cells were then washed with PBS and were blocked with 3% bovine serum albumin (BSA) in PBS for 1 hr at

room temperature with gentle shaking. After blocking, cells were incubated with the anti-DDDDK-tag antibody (M185-3L, MBL) diluted 1000 times in 3% BSA in PBS at 37°C for 1 hr. After washing with PBS, the cells were incubated with an FITC-labeled anti-mouse IgG from sheep (F3008, Sigma-Aldrich) diluted 2000 times in 3% BSA in PBS. The nuclei were stained with 0.01 mg/ml Hoechst 33342 dissolved in PBS. The coverslips were then mounted on microscopic slides using VECTASHILD® (H-1000-10, Vector Laboratories, Burlingame) and the images were taken by an inverted fluorescence microscope (Leica AF6500, Wetzlar, Germany).

15. Quantification of rRNA

Ribosomal RNA was quantified by a 2100 Bioanalyzer Instrument (Agilent) using an Agilent RNA 6000 Pico kit (5067-1513, Agilent) following the manufacturer's instruction. Briefly, the gel matrix was prepared, was mixed with an RNA dye, and loaded into a cassette according to the manual. RNA makers were loaded to every well. An RNA ladder was loaded into the designated well. Total RNA from each sample was diluted to 5 ng/μl and was loaded into each well. RNA was quantified by the "Total eukaryotic RNA Pico-series-II program" of a Bioanalyzer instrument.

16. Heavy-methyl SILAC experiment

The heavy methyl-SILAC experiment was conducted based on the principles and procedure described in earlier researches[88–90]. The SILAC labeling media were prepared by reconstituting a commercially available DMEM high glucose media depleted for glutamine, methionine, and cysteine (21013024; DMEM high glucose, no glutamine, no methionine, no cysteine cell culture media, Thermo Fisher Scientific). For reconstitution, we added 4 mM glutamine (25030-081, Thermo Fisher Scientific), 200 μM cysteine (1001527621, L-cysteine

dihydrochloride, Sigma Aldrich) and either normal methionine (1001818815; L-Methionine, Sigma Aldrich) at 200 μM for the light medium, or heavy methionine (CDLM9289025, L-methionine, Methyl-13C 99%, Methyl-D3 98%, Cambridge Isotope Laboratories, Tewksbury, MA) at 200 μM for the heavy medium. After reconstitution, we added 10% dialyzed FBS (F0392, Sigma Aldrich) and a combination of 100 U/ml penicillin and 100 μg/ml streptomycin (15140-122, Penicillin-Streptomycin, Thermo Fisher Scientific). HeLa cells were cultured in either the light or heavy SILAC medium for at least 6 generations. Treatment with 30 mM of cLEU was performed for 6 hr before harvest. Ribosome was purified as follows:

Method 1 (Purification by immunoprecipitation): Light- and heavy-labeled cells were transfected with 15 μg of either the FL-EV or FL-RPL23A expression plasmids and were grown for 24 hr before harvest. After cell harvest by trypsinization, an equal number of light- and heavy-labeled cells were mixed and were lysed by 700 μl of lysis buffer (10 mM HEPES-KOH pH 7.4, 100 mM NaCl, 10 mM MgCl2, 10% glycerol, 2 mM DTT, 1 mM PMSF, 2% NP-40 and cOmplete® protease inhibitor). The cleared lysate was then used for ribosome purification by an anti-DDDDK antibody bound to magnetic beads (M185-11R, anti-DDDDK-tag mAb- magnetic beads, MBL) at 4°C for 2 hr in tubes with end-over-end rotation. The ribosomes were then heat-eluted by denaturation at 95°C for 5 minutes in the presence of SDS-sample buffer.

Method 2 (Purification by pelleting on sucrose cushion): 5×10^6 of light- and heavy-labeled cells were mixed in 1:1 ratio and were lysed in 350 μl of lysis buffer (20 mM Tris-HCL 7.5, 150 mM NaCl, 5 mM MgCl, 1 mM DTT, 1% Triton-X100, cOmplete® protease inhibitor and 100 μg/ml cycloheximide). The lysate was clarified by centrifugation at 2000 × *g* for 20 minutes at 4°C. One-molar sucrose cushion was prepared in a buffer containing 20 mM Tris-HCL 7.5, 150 mM NaCl, 5 mM MgCl, 1 mM DTT and 100 μg/ml cycloheximide). The cleared lysate was then layered on 900 μl of 1 M sucrose cushion in a 13 × 56 mm 3.2-ml capacity

thick wall polycarbonate ultracentrifuge tube (362305; Beckman Coulter). The tubes were then centrifuged in a TLA-110 fixed angle rotor (366735, Beckman Coulter) at 100,000 rpm for 1 hr at 4°C in an Optima™ MAX-XP Benchtop Ultracentrifuge (Beckman Coulter). The resulting ribosome pellet was washed with ice-cold PBS and was dissolved in SDS-sample buffer. The samples were denatured at 95°C for 5 minutes before SDS-PAGE.

After purification of ribosome by either method, the LC-MS/MS sample preparation and analysis were performed as described in "Purification of FB-MAT2A and LC-MS/MS analysis".

After obtaining the LC-MS/MS data, identification of light-labeled proteins was done using a Mascot search engine considering propionamidation of Cys as a fixed modification as well as acetylation at protein N-ter, methylation at Lys and Arg, dimethylation at Lys and Arg, and trimethylation at Lys as variable modifications. For every identified methylated peptide, the *m*/*z* value of the corresponding heavy-methyl peptide was calculated as follows:

Observed light peptide $m/z = \frac{M + (z \times 1.0078)}{z}$

Expected heavy peptide $m/z = \frac{M + \Delta M \times \mathrm{n} + (z \times 1.0078)}{z}$

Where, M = observed mass, z = charge and 1.0078 is the mass of H^+, ΔM = mass difference given by addition of one heavy-methyl group = 4.0186. n = sum of the number of methyl group added to Lys/Arg and the number of methionine residues in the peptide.

The Thermo scientific qual browser was then used to calculate heavy-to-light ratios by obtaining peak area values in extracted ion chromatograms of light and heavy peptides. The heavy-to-light ratios of the methylated peptides were normalized to those of methionine-containing non-methylated peptide(s). When methionine-containing peptides were not

available, the normalization was done by methionine containing peptide(s) of either RPL23A (in method 1) or PABPC1 (in method 2).

17. Statistical analysis and software

Welch two-sample t-test was performed using an R program (Version 4.0.2) for comparison of *Mat2a* mRNA (Figure 1B) and rRNA ratio (Figure 10D). The relative intensity values were analyzed by one way analysis of variance (ANOVA) assuming equal variance followed by Tukey's honest significance (HSD) test for the comparison of multiple means (Figure 4A). The GO analysis for protein complex (Figure 9D, E and F) or genes (Figure 7B) were performed by using package "Go.db" with "enrichGo" function in R. The protein complex network (Figure 9G) was generated by cytoscape (version 3.8.0). The intensity of proteins in Western blot was measured by ImageJ software (Version 1.53i). The online tool Heatmaper (http://heatmapper.ca/) was used to generate heatmap in Figure 7C. Pearson's correlation analysis was performed to find the correlation between the abundance of light and heavy unmethylated methionine-containing peptides (Figure 13B and C) using package "ggpmisc" with "stat(eq.label)" function in R. Figures were prepared with the aid of photoshop creative cloud (2019 version).

Results

1. MAT2A depletion reduced protein synthesis in Hepa 1 cells

We examined the influence of MAT2A on global protein synthesis rate in a mouse hepatocellular carcinoma cell line (Hepa1) by surface sensing of translation (SUnSET) method[81]. In this method, the cultured cells were pulse-labeled for 30 minutes with the aminoglycoside antibiotic puromycin. Because of its structural similarity to tyrosyl-tRNA, puromycin enters elongating peptides from ribosomal A site. Once puromycin is incorporated in elongating peptides (Puromycilation)[91], the translation is terminated with release of puromycin-labeled short peptides (Figure 1A). These peptides can be detected using an antibody against puromycin in immunoblot and their amount directly reflects the rate of translation. To see the effect of MAT2A depletion on protein synthesis, we knocked down *Mat2a* in Hepa1 by siRNA against *Mat2a* (Figure 1B) and observed that the global translation was reduced (Figures 1C, lanes 3, 4) compared to the control siRNA (Lanes 1 and 2). This observation suggests that MAT2A contributes to translation in these cells. We inhibited translation by using the translation inhibitor cycloheximide (CHX), which greatly diminished the puromycin signals on the blot membrane, indicating that puromycin specifically labeled the nascent peptides (Figure 1C, lanes 5 and 6) and antibody against puromycin worked properly in Western blot.

2. MAT2A overexpression induced protein synthesis in HeLa cells

Postulating that the amount of MAT2A in proliferating cells is insufficient for the maximum stimulation of protein synthesis, we examined the effect of MAT2A overexpression on protein synthesis. First, we transiently overexpressed MAT2A in HeLa cells and measured the protein synthesis by SUnSET. As expected, we observed that protein synthesis was induced

in MAT2A overexpressing cells compared to cells transfected with empty vector (EV) (Figure 2A). To know the long-term effect of MAT2A overexpression on translation, we established HeLa cells with stable expression of ectopic FLAG-Bio-tagged MAT2A (FB-MAT2A) (Figure 2B). HeLa cells were transfected with the FB-MAT2A expressing vector and were selected with puromycin. The expression of FB-MAT2A was examined by Western blot (Figure 2C). To ensure that the exogenously expressed FB-MAT2A protein is functional, the interaction of FB-MAT2A with MAT2B was confirmed by co-purification of MAT2B with FB-MAT2A[58,92] in streptavidin affinity purification (Figure 2D). Moreover, we performed immunostaining with an anti-FLAG antibody and confirmed nuclear localization of the FB-MAT2A protein[77] (Figure 2E). Since the overexpression of exogenous FB-MAT2A was low compared to the endogenous protein (Figure 2C), we isolated a single clone of the cells which produce a higher amount of FB-MAT2A by limiting dilution technique. The high FB-MAT2A producing clone (Figure 2F, clone 9) was selected for the experiment. We observed that this high FB-MAT2A expressing clone suppress the endogenous MAT2A (Endo-MAT2A). Therefore, we judged the extend of functional capabilities of FB-MAT2A in this clone by quantifying histone 3 trimethylation at various positions. The FB-MAT2A overexpressing cells showed a selective increase in H3K27 trimethylation (H3K27me3) compared to that of the cells expressing only FLAG-Bio-empty vector (FB-EV) (Figure 2G), suggesting stably expressing ectopic FB-MAT2A is functionally more efficient compared to endogenous MAT2A to dynamic methylation of H3K27me3. Cells derived from single clone were cultured normally or were starved under 0% serum and then re-stimulated with 10% serum. Serum starvation or rapamycin treatment reduced, and serum stimulation induced mTORC1 activity judged by the amount of phosphorylated S6 kinase (Phos-S6K) in both control (FB-EV) and FB-MAT2A expressing cells. Interestingly, under all conditions, FB-MAT2A expressing cells showed higher protein synthesis compared to control cells with FB-EV (Figure 2H). These results

suggested that MAT2A fosters global protein synthesis in the cell independent of growth factor signals from serum.

3. MAT2A catalytic activity is essential for protein synthesis

The enzyme MAT catalyzes the synthesis of SAM from methionine and ATP. The synthetic cyclic analogue of methionine named cycloleucine (L-aminoacyclopentane-1-catboxilic acid) is a competitive catalytic inhibitor of MATs for the synthesis of SAM. cLEU competes with methionine to bind MAT2 and thereby reduce SAM synthesis[93,94] (Figure 3A). To reveal the requirements of the catalytic activity of MAT2A in protein synthesis, we added cLEU in the cell culture media. In line with knockdown of *Mat2a*, chemical inhibition by cLEU reduced protein synthesis in Hepa 1 (Figure 3B) and HeLa (Figure 4A) cells. Notably, the protein synthesis reduction was also observed as early as 1 hr of treatment with cLEU (Figure 4B). These observations suggest that MAT2A catalytic activity for the synthesis of SAM is essential for protein synthesis and reduction of protein synthesis is an acute response to SAM depletion.

4. MAT2A-regulated protein synthesis is not contingent on mTORC1 activity

Protein synthesis in the mammalian cells can be altered by the activity of PI3K–AKT and MAPK/ERK pathways. These pathways are activated by various stimuli including growth factors and nutrients such as amino acids, exerting effects on translation machineries through mTORC1 (Figure 5A). Since MAT2A stimulates protein synthesis, we examined whether MAT2A affects the mTOR1 signaling pathway. P70 S6 Kinase (S6K) is the direct downstream target of mTORC1 and the amount of Phos-S6K directly reflects the activity of mTORC1 signaling[95]. We measured the amount of Phos-S6K by immunoblot after MAT2A perturbations. Although having a high protein synthesis capability, FB-MAT2A stable expressing cells did

not show any appreciable alteration in Phos-S6K compared to the control cells under the normal conditions or when the cells were starved and re-stimulated with serum (Figure 2H). This observation depicts that MAT2A induced translation without affecting the activation status of mTORC1. Moreover, Phos-S6K was unchanged upon MAT2A inhibition by cLEU in both Hepa1 (Figure 5B) and HeLa (Figure 5C) cells whereas it was reduced in response to mTORC1 inhibitor rapamycin treatment. These results suggest that the effects of MAT2A on protein synthesis is independent of the activity of mTORC1.

5. Feedback activation of AKT and MAPK pathways upon MAT2A inhibition

The AKT and MAPK pathways are often activated upon mTOR inhibition in various cancers as a part of feedback mechanism[48,51,96–98]. We therefore examined the activation status of AKT and MAPK and observed that both AKT (Phosphorylation at S473/T308) and MAPK (Phosphorylation at T202/Y204) were activated in HeLa cells where MAT2A was inhibited by cLEU (Figure 6A and B). These observations suggest an mTORC1-independant feedback regulation in response to MAT2A inhibition.

6. MAT2A activity is required for the transcription of genes encoding proteins for ribosome biogenesis

MAT2A can influence mRNA transcription by methylation of DNA and histones. Therefore, we examined the mRNA expression by RNA sequencing upon MAT2A inhibition by cLEU. Compared to control in MAT2A inhibited cells, a total of 1147 and 328 transcripts, respectively, were up and down-regulated significantly ($q < 0.01$) (Figure 7A). Gene ontology (GO) analysis for biological process of transcriptionally down-repressed genes upon cLEU treatment revealed that the expression of genes involved in ribosome biogenesis was hampered (Figure 7B). The normalized expression of these genes is presented as a heatmap (Figure 7C).

These data suggest that MAT2A may contribute to ribosome biogenesis by promoting expression of proteins involved in ribosome biogenesis.

7. MAT2A and SAM are essential for maintaining active translation

To elucidate the features of MAT2A-regulated protein synthesis, we carried out polysome profiling of HeLa cells upon MAT2A inhibition by cLEU. Ribosome was fractionated by a sucrose density gradient fractionation method (Figure 8A). We found that the formation of heavy polysome/active polysome (polysome bearing more than 3 monosomes) was impaired upon MAT2A inhibition with a concomitant increase of monosome (80S) and its subunits (40S and 60S) (Figure 8B). These characteristics of polysome profile suggest that translation initiation to form monosomes was hampered, and only a smaller fraction of successfully formed monosomes proceeded to active polysome formation.

To investigate MAT2A-regulated translational control, we isolated translating mRNA from the polysome fractions and performed RNA sequencing. We found that after MAT2A inhibition, 507 transcripts were up-regulated and 193 were down-regulated in polysome occupancy (Figure 8C). The TE of each mRNA was calculated by a ratio of reads number between polysome fraction and total RNA, which showed that the number of transcripts with decreased TE (135) by MAT2A inhibition was greater than that of transcripts with increased TE (120) (Figure 8D and Table 1 and 2). These results strongly suggest, in addition to transcriptional regulation, the presence of a translational regulation by MAT2A and SAM, which concerns the expression of a specific subset of mRNA through the altered formation of polysome.

8. MAT2A interacts with proteins involved in ribosome biogenesis and translation

In living cells proteins form a network of functional interactions. These interactions can positively or negatively regulate the functions of other proteins. Therefore, to understand the mechanism of the regulation of protein synthesis by MAT2A, we aimed to elucidate the MAT2A-interacting protein network. We purified FB-MAT2A by affinity purification with streptavidin from HeLa cells stably expressing FB-MAT2A. The purified proteins were then separated by sodium dodecyl sulphate-polyacrylamide gel electrophoresis (SDS-PAGE), were in-gel trypsin digested and were analyzed by liquid chromatography with tandem mass spectrometry (LC-MS/MS) (Figure 9A). Coomassie Brilliant Blue (CBB) staining (Figure 9B) and immunoblot (Figure 9C) of the purified protein showed that both endogenous MAT2A and FB-MAT2A were specifically enriched compared to the mock purification. We found that 81 proteins were specifically co-purified with FB-MAT2A (Table 3). To elucidate the biological significance of the interaction of MAT2A with a wide range of proteins, we employed GO analysis. The top enriched terms were related to ribosome biogenesis and/or functions such as ribonucleoprotein complex biogenesis, rRNA processing, rRNA metabolic process, preribosome, small nucleolar ribonucleoprotein complex and snoRNA binding (Figure 9D, E and F), suggesting an involvement of MAT2A in ribosome biogenesis and/or function. Notably, the 81 purified proteins contained the core protein components of the snoRNP complex (NOP56, NOP58 and SNU13) except for FBL (Fibrillarin) (Figure 9G). The snoRNP complex plays an important role in ribosome biogenesis by 2′-O-methylation of rRNA, and this methylation also enhances the translation capability of ribosome[99]. These results strongly support the imperativeness of MAT2A in the ribosome function.

9. MAT2A is not essential for rRNA transcription

The interaction of MAT2A with the ribosome biogenesis factors inspired us to investigate the involvement of MAT2A in the rRNA biogenesis. Ribosomal RNA is transcribed by RNA polymerase I from the genomic rDNA repeat as a large single transcript, which is called the 47S pre-rRNA in mammals. This pre-rRNA bears external and internal transcribed spaces, which must be removed by complex steps of endo and exonucleolytic cleavages[100] to produce the mature 18S, 5.8S and 28S rRNAs (Figure 10A). To elucidate whether MAT2A is required for the pre-rRNA transcription, we quantified the pre-rRNA content in *Mat2a*-knocked-down Hepa1 cells by qPCR using a primer pair targeting the 5′ external transcribed spacer sequence (Figure 10A)[84]. We observed that *Mat2a* knockdown did not alter the rRNA transcription in Hepa1 cells (Figure 10B), suggesting that MAT2A is dispensable for rRNA transcription.

10. MAT2A depletion or inhibition reduced 18S rRNA abundance

The sno-RNP complex plays a significant role in rRNA production through methylation[73,101,102]. Since MAT2A interacted with the snoRNP complex (Figure 9G), we hypothesized that MAT2A might be present at the site of rRNA methylation for local SAM synthesis. Indeed, *Mat2a* knock down decreased the 18S/28S rRNA ratio in Hepa1 cells with reduced abundance of the 18S rRNA (Figure 10C and D). Chemical inhibition of MAT2A by cLEU in HeLa cells also reduced the quantity of 18S rRNA (Figure 11A) with changing the 18S/28S ratio in a concentration-dependent manner (Figure 11B). Considering that rRNA transcription was not affected by MAT2A knockdown, the reduced 18S rRNA production could be a result of disturbed rRNA processing and or impairment of stability. The reduction of 18S rRNA might be one of the contributing factors for the reduction of protein synthesis in MAT2A depletion or inhibition.

11. MAT2A contributes to dynamic methylation of proteins involved in translation

Many proteins involved in translation were found to be methylated in *E. coli*, yeast and mammals[74,76,103–106]. Even though some of these methylations appeared important for translation[75,76,107], the biological significance of the majority is unclear. Therefore, we hypothesized that a reduction of dynamic methylation of proteins involved in translation might cause the protein synthesis reduction upon MAT2A inhibition. To compare methylation of proteins under a MAT2A-inhibition condition, we employed a variant approach of stable isotope labeling by amino acid in cell culture (SILAC) named heavy methyl SILAC[90] followed by identification and quantification of methylated peptides using LC-MS/MS. In this approach, HeLa cells were labeled with either light methionine (standard methionine) containing protium isotope of hydrogen (mass: 1.0078) in the methyl group or heavy methionine containing deuterium isotope (mass: 2.014). The methionine is then converted to SAM containing either light or heavy methyl group. Since SAM is the methyl donor for protein methylation, these light and heavy methyl groups are transferred to protein by various methyltransferases. In our study, we cultured the cells either light or heavy methionine containing media (light and heavy media, respectively) for six generations. The heavy-labeled cells were treated with 30 mM cLEU for 6 hr. Light and heavy-labeled cells were then mixed in a ratio of 1:1 and, for the maximum coverage, ribosomes were purified by two methods (Figure 12A): by immunoprecipitation (IP) (method 1) or ultracentrifugation in sucrose cushion (method 2). In method 1, the 3×FLAG-tagged RPL23A protein (FL-RPL23A) was expressed and was purified by using an ani-DDDDK antibody conjugated to magnetic beads. For comparison, a mock purification was also performed in parallel using cells transfected with the empty vector (Figure 12B). In the method 2, ribosome was pelleted by passing the cleared lysate through 1M sucrose cushion in ultracentrifugation (Figure 12C and D).

With mass spec analysis, we identified many ribosomal proteins purified in both methods. By combining the data obtained from the two methods, we identified 29 methylated peptides. The heavy/light ratio was calculated from the relative abundance of methylated peptides normalized to unmethylated methionine-containing peptides derived from the same protein or other proteins depending on the availability (see materials and methods for detail) (Table 4). By taking average abundance values of peptides purified twice, we finally identified 17 unique peptides (Table 5). Among the unique peptides, 13 peptides were derived from proteins involved in translation and six of them showed a reduction by 50% or more in methylation upon MAT2A inhibition by the cLEU treatment for 6 hr (Figure 13A). The relative abundance of light and heavy methionine containing peptides used for normalization showed a linear correlation in both method 1 (Figure 13B) and method 2 (Figure 13C), indicating that the similar amounts of proteins was purified from the control and treatment samples. These results suggest that MAT2A contribute to dynamic methylation of a specific set of proteins involve in translation. The highest methylation reduction was observed in eEF1A1/2K55me2. The chromatogram and mass spectrum of eEF1A1/2K55me2 light and heavy peptides are presented in Figure 14A. Next, we further validated the effect of MAT2A on eEF1A1/2K55me2 by Western blot using specific antibody for this methylation. For convenience of transfection, we selected HEK293T cells for this experiment. Considering that the principal form of eEF1A in HEK293T cells is eEF1A1, we examined the methylation status of eEF1A1K55me2 in HEK293T cells upon MAT2A transient overexpression. First, we validated the specific reactivity of commercially available DiMethyl-eEF1A-K55 (anti-eEF1AK55me2) antibody by overexpressing either wild type FB-eEF1A1 or mutant FB-eEF1A1K55R (Lysine was mutated to Arginine) in HEK293T cells followed by immunoprecipitation and immunoblotting. We observed that, anti-eEF1AK55me2 detected wild type FB-eEF1A1 both in input (Figure 14B, lane 2) and IP (Figure 14B, lane 5) samples

but failed to detect the proteins where methylation site was mutated (FB-eEF1A1K55R) (Figure 14B, Lanes 3 and 6) suggesting that this antibody specifically detects the eEF1A1K55me2. Next, we co-expressed either wild type FB-eEF1A1 or mutant FB-eEF1A1K55R with MAT2A in HEK293T cells. As expected, we observed that expression of MAT2A induced eEF1K55me2 (Figure 14C, lane 5). This data further validates the eEF1K55me2 methylation reduction observed in heavy methyl-SILAC upon MAT2 inhibition.

Discussion

In this research, we discovered an intimate relationship between methionine metabolism and translation. MATs are the enzymes for the first reaction of methionine metabolism where methionine and ATP react to form SAM[52]. We examined the effects of MAT2A and SAM on protein synthesis in mammalian cells. With SUnSET assay, we revealed that MAT2A and SAM are essential to maintain global protein synthesis independently of the mTORC1 signaling. In the polysome profiling experiment, we observed that inhibition of the MAT2A activity impaired the active polysome formation and altered the TE of a subset of mRNA. In addition, the MAT2A inhibition reduced the transcription of genes encoding proteins involved in translation (Figure 7B and C). To understand the mechanistic aspects, we studied MAT2A interactomes by mass spectrometry. We observed that MAT2A interacts with many rRNA processing and ribosome biogenesis factors (Figure 9). By the quantification of mature rRNA, we revealed that the 18S rRNA abundance was severely affected by MAT2A depletion and inhibition (Figure 10 and 11). With the aid of quantitative mass spectrometry, we revealed a drastic reduction of methylation of translation factors in MAT2A-inhibited cells (Figure 13). To sum up, MAT2A and SAM promote translation in mammalian cells by: (i) maintaining rRNA abundance, (ii) promoting active polysome formation and (iii) regulating the methylation of translation factors (Figure 15). Importantly, the effect of MAT2A and SAM on translation is independent of the mTORC1 signaling.

Among the MAT isozymes, MAT2A is the principal form in adult extrahepatic tissues and cancerous hepatic tissues[108] in that in these tissues SAM is synthesize by the catalytic activity of MAT2A. We observed reduction in protein synthesis upon not only MAT2A depletion but also chemical inhibition, indicating that MAT2A relies on SAM for promoting protein synthesis in the cells. It has been reported that SAM and its precursor methionine are necessary for proliferation of cancer cells[109–111] and stem cells[12–114]. Moreover, SAM scarcity

in cancer leads to cell cycle arrest in G1 and G2 phases where cells synthesize proteins, lipids and other biomolecules[60,115]. In addition, cell proliferation requires the synthesis of a copious amount of protein. Therefore, our data suggest that MAT2A and SAM contribute to cell proliferation by maintaining protein synthesis. On the other hand, several studies depicted that an excess of exogenous SAM supplementation can be toxic and suppresses proliferation of cells from various cancers including uterine cervix[80], colon[116], colorectal[117] and breast[118] by arresting cell cycle in S phase[117,119]. Therefore, an optimum amount of SAM is necessary for protein synthesis in the cells.

In our SUnSET data in Figure 2H, we observed induction of small molecular weight proteins upon MAT2A overexpression. This phenomenon might be due to the nature of the protein synthesis assay employed. SUnSET works with puromycin labeling in peptides. Upon incorporation of puromycin to elongating peptides, the translation is terminated. Therefore, truncated short peptides were formed even in presence of long coding sequences. As MAT2A overexpression induced protein synthesis, the probability of generating of these puromycin labeled short peptides is much higher in MAT2A overexpressing cells which may contribute to the concentrated small protein signals in Western blot membrane. Since truncated peptides are form from long coding proteins, it is likely that the larger size protein synthesis will be hampered during puromycin labeling. Again, due to high protein synthesis rate, in FB-MAT2A expressing cells may produce more truncated form of large size protein compared to FB-EV leading to reduced larger protein signals in the blot membrane. Therefore, reduction of large protein signals in MAT2A overexpression might be a compensation for the formation of much higher number of truncated peptides from long coding sequence compared to cells expressing FB-EV.

We observed that protein synthesis was not reduced in response to mTOR inhibition by rapamycin (Figure 2H, Lanes 1, 2). This might be due to the short duration of rapamycin

treatment in our experiment in which we treated cells with rapamycin for 1 hr. Another possibility is that, upon mTOR inhibition feedback activation of MAPK, as observed in Figure 6, can induce translation of oncogenes independent of mTORC1 through activation of MAPK-interacting kinases 1 and 2 (MNK1/2)[29]. Moreover, mTORC1 inhibition can activate cap-independent translation[120] which may contributes for the maintenance of translation upon mTORC1 inhibition.

In Figure 2H, we also observed that MAT2A overexpression suppressed the endogenous MAT2A expression, and the total amount of expression seems to be same between FB-EV and FB-MAT2A. Although the expression is same, ectopic MAT2A expressing cells showed higher functional capabilities in terms of H3K27me3 (Figure 2G). The H3K27me3 is known to be induced by MAT2A overexpression[121]. From our previous experience, we noticed that it is difficult to maintain high amount of MAT2A in stable expressing cells. One of the possibilities of this phenomena is that MAT2A negatively regulates by its catalytic product SAM. When cellular SAM concentration is high the MAT2A mRNA is destabilized by N^6-Adenosine methylation (m^6A) at 3′ UTR leading to degradation by YTHDC1-dependent manner[80]. In this study, since we have found that induction of protein synthesis is mediated by SAM (Figure 3), FB-MAT2A expressing cells might produce higher amount of SAM compared to FB-EV and expression of FB-MAT2A is continuously regulated depending cellular SAM concentration. Therefore, we might harvest the cells when FB-MAT2A was downregulated by pre-existing high SAM concentration.

In this study, we found that the MAT2A-mediated translation control is independent of the mTORC1 activity. Contrary to these findings, a previous study showed that the activity of mTORC1 is highly dependent on cellular SAM concentration. In HEK293T cells, it was reported that when SAM is low, SAMTOR inhibits the mTORC1 activity by forming a stable dimer with GATOR1 (SAMTOR-GATOR dimer). Under a sufficient SAM condition, SAM

binds to SAMTOR to disrupt the SAMTOR-GATOR1 complex, thereby activating mTORC1 and translation[70]. Our findings are contradictory to this report, the difference may be caused by SAM depletion techniques employed. They carried out methionine restriction for 2 hr in their experiment. The activation of mTORC1 requires its localization on the lysosomal surface, where the activator RHEB resides, and the localization is stimulated by an amino acid signaling[48,122]. Therefore, the observation by Gu et al. might be confounded by a compromised amino acid signaling rather than solely depending on SAM concentration. Further studies are required to clarify these possibilities. This contradictory observation might also be arising from differences in cell types between the experiments.

The feedback activation of AKT and MAPK pathways is often seen upon mTOR inhibition[96,123,124]. In our data, upon MAT2A inhibition, we observed a sharp activation of AKT and MAPK (Figure 6A and B) without affecting the mTORC1 activity. It has been reported that AKT was activated by protein synthesis inhibition with cycloheximide treatment in a human embryonic kidney cell line[125]. Similarly, the MAPK was also activated by protein synthesis inhibition with anisomycin and cycloheximide treatment in HeLa cells[126]. Therefore, feedback loop is a more general phenomenon responsive to protein synthesis inhibition rather than only specific to mTORC1 inhibition.

As a transcriptional regulation, we observed that MAT2A inhibition by cycloleucine reduced expression of genes related to ribosome biogenesis. This kind of regulation may be generated from reduced methylation of DNA, histone or mRNA itself by SAM depletion. The m^6A has been shown to be required for maintenance of mRNA stability[127]. Therefore, this reduction of gene related to ribosome biogenesis might be resulting from reduced stability by reduction of methylation.

Paradoxically to the drastic protein synthesis reduction, only a small number of mRNAs

showed a reduction TE in MAT2A inhibited cells. This observation can be explained by the fact that MAT2A is important for global translation rather than that of specific mRNA. Therefore, a small reduction of TE, which was not considered in the TE calculation in Figure 8D, for many genes combinedly might lead to the huge protein synthesis reduction. In addition, we examined the protein synthesis for a short time by labeling with puromycin for 30 minutes. Therefore, the protein synthesis reduction observed in SUnSET assay is reflecting to rapidly translating proteins.

We found the existence of many rRNA and ribosome biogenesis factors as MAT2A interactome (Figure 9G). Using the similar purification technique, one of our previous colleagues identified MAT2B complex from Hepa1 cells, where the top enriched proteins were related to rRNA processing and ribosome biogenies factors (Unpublished). Since in mammalian cells MAT2A always found with MAT2B as heteromer, this data may support our MAT2A interactomes. However, our MAT2A interactome is completely different from that of MAT2A interactome identified from mouse erythroleukemia (MEL) cell line by our another colleague[77]. Since similar purification techniques were used, the differences might arise from differences in cells lines. Compared to regular epithelial cell lines, MEL cells are specialized in that it is one of the developing stages of erythroid cell. During erythrocytes development DNA and histone methylation occurs in a stereotypic manner[128,129]. Moreover, we observed negative feedback regulation of MAT2A by cellular SAM concentration[80] is not exist in MEL cells (Unpublished). Therefore, regulation of MAT2A may be different in MEL cells compered to HeLa cells and MAT2A may form separate complex in MEL cells. Another possibility for this difference might be the cell fractions used for MAT2A complex purification. Kotoh et al. used nuclear fraction whereas we used whole cell lysate for MAT2A complex purification. The difference might also be generated from the control used to compare with purification. We use FB-EV expressing cells whereas experiment in Katoh et al. used only biotin ligase (BirA)

expressing cells. Although we used appropriate control in our experiment and we considered successful purification of protein as MAT2A interactant when the ratio to its control purification is greater than five, these data need to be further validated using co-immunoprecipitation. In our data, MAT2A was co-purified with the components of the sno-RNP complex (Figure 9G). The snoRNP complex consists of three structural proteins (NOP56, NOP58 and SNU13) and one methyltransferase (FBL). The sno-RNA complex methylates rRNA at 106 different sites. It has been reported that the snoRNP complex is necessary for cancer progression. Moreover, depletion of FTSJ3, a methyltransferase for different RNAs including rRNA, reduced 18S rRNA biogenesis by interfering site specific cleavage[72]. Therefore, the necessity of rRNA methylation for its biogenesis [114] suggests that the 18S rRNA defects observed upon MAT2A depletion or inhibition (Figure 10 and 11) is explained by impaired methylation of rRNA precursor. Since methylation is important for RNA stability, the reduced amount of 18S rRNA might also resulting from reduced methylation of 18S rRNA by SAM depletion. The interaction of MAT2A with the snoRNP complex may expand the idea of the local SAM synthesis and consumption model of chromatin methylation in which SAM is produced on chromatin for local histone methylation[77,82]. MAT2A may produce SAM for rRNA methylation along with its processing. Further studies are necessary to draw an absolute conclusion

Post-translational modifications are important for efficient functioning and stability of proteins. Methylation is one of the most common post-translational modifications found in a wide range of histone and non-histone proteins. Many of the proteins related to translation are known to be methylated including ribosomal proteins and translation initiation, elongation and termination factors [74]. Many studies explored the roles of histone methylation on chromatin regulations and gene expression. However, studies on methylation of proteins involved in translation and their importance in gene expression are scarce. Given that translation is one of

the key control steps of gene expression, methyl-modification of ribosomal proteins and translation factors might be crucial for the translational regulation of gene expression. With the aid of quantitative mass spectrometry, we revealed that methylation of some translation factors, such as eEF1AK55me2, PABPC3K104me1, PABPC1LK361me1, eEF2K525me3 and PABPC4R534me2, were reduced by more than 50% upon MAT2A inhibition (Figure 13A). These observations suggest that methylations of these proteins are dynamically regulated by intracellular SAM concentration. We further validate the effect of MAT2A on eEF1AK55me2 by specific antibody (Figure 14B and C). In our data we found transient overexpression MAT2A induced eEF1AK55me2. We observed methylation induction only in the ectopically expressed eEF1A but not the endogenous proteins. This may be probably because of high abundance of methylated form in normal condition. Therefore, ectopically expressing eEF1A1 was preferentially methylated upon MAT2A overexpression. It has been reported that eEF1AK55me2 is required for protein synthesis and tumorigenesis in lung cancer[76], and cell proliferation in acute myeloid leukemia[132]. It is also reported that eEF1AK55me2 has a more specific function to enhance the translation of codons for tryptophan and alanine[133]. Therefore, MAT2A may at least partially rely on eEF1AK55me2 to stimulate protein synthesis. eEF2K509me3 (corresponding residue in human is K525) is essential for maintaining translation frame in yeast and translation frameshifting in the absence of this methylation render yeast cells sensitive to translation inhibitor sordarin[107]. Although there is no report of PABPC1L methylation as far as we know, upregulation of PABPC1L is associated with proliferation and migration of prostrate and colorectal cancers[134,135]. Therefore, it would be promising to investigate the importance of PABPC1LK361me1 in translation. PABPC3 and PABPC4 are known to be methylated at several lysine and arginine residues[136,137]. However, the biological significance of these methylations is still unknown. PABPCs are extensively studied for their translation stimulating capabilities by diverse mechanisms including co-

binding to poly(A) tail of mRNA and translation initiation factors [138–140], enhancing the recruitment of small ribosomal subunits (40S), recycling of initiation factors and boosting translation termination[141,142]. However, the roles of post-translational methylation in their functions on translational regulation are still elusive. Therefore, the biological significance of their methylations would be promising to be explored in future.

In this study, we focused on methylation of translation-related proteins to explain the contribution of MAT2A to translation. However, we overlooked tRNA which is also highly modified by methylation at different positions and some of them have already been proven important for different aspects of translation control[143–145]. Therefore, in future, it will be propitious to investigate whether and how MAT2A and SAM contribute to tRNA-modification.

Conclusions and significance of the study

By utilizing SUnSET for examination of global translation efficiency under the condition of suppression of the MAT2A activity using RNAi or chemical inhibition by cLEU, or overexpression of MAT2A, we found that MAT2A stimulates protein synthesis in mammalian cells in an mTORC1-independent manner. By combining polysome profiling and RNA sequencing, we revealed that MAT2A is required for the formation of active polysome and maintenance of translation efficiencies of mRNAs. Moreover, we found that MAT2A interacts with ribosome biogenesis factors and contributes to the 18S rRNA abundance and dynamic methylation of translation factors.

Due to the complex nature of the mTOR signaling, the cancer chemotherapy targeting the mTOR signaling pathways for translation control is often compromised by different mechanisms including mutations of inhibitor binding sites[146,147], activation of co-stimulatory molecules[148], induced expression of growth factor receptors[149] and reduced expression of inhibitory molecules[150]. Furthermore, the mTOR inhibitors compromise cancer therapy with their potent immunosuppressive properties[151]. Under these circumstances, a therapy targeting MAT2A could be an alternative to suppress the translation for cancer therapy. In addition, some cancer cells do not respond to methionine restriction therapy because of a high concentration of intracellular SAM[60,60,61]. In that case, suppression of MAT2A activity by depletion or inhibition may revert the methionine-dependency for the success of methionine restriction cancer therapy.

Figure legends

Figure 1: MAT2A depletion reduced protein synthesis in Hepa1 cells

A. The schematic diagram showing the mechanism of surface sensing of translation (SUnSET). Puromycin is structurally like tyrosyl-tRNA. Upon incorporation of puromycin by entering through the A site of ribosome, the translation is terminated due to a failure of subsequent peptide bond formation. The immature termination of translation generates short peptides labeled with puromycin. These short peptides can be detected by Western blot using an anti-puromycin antibody and the amount of these short peptides directly reflects the rate of translation.
B. A bar plot showing relative mRNA expression of *Mat2a* in Hepa1 cells after 48-hr knock down by the indicated stealth siRNA (n = 3, number of samples).
C. Reduction of global translation upon MAT2A knock down in Hepa1 cells examined by SUnSET (lanes 1-4). The cells were harvested 48 hr after siRNA transfection. Before harvest, the cells were treated with puromycin (20 μg/ml) for 30 minutes. The addition of cycloheximide (CHX, at 50 μg/ml for 4 hr) to inhibit protein synthesis ensured the specificity of the anti-puromycin antibody (lanes 5 and 6).

Figure 2: Overexpression of MAT2A induced protein synthesis in HeLa cells

A. Transient overexpression of MAT2A and corresponding empty vector (EV) for 24-hr in HeLa cells followed by quantification of protein synthesis by SUnSET.
B. Schematic presentation of FLAG-Bio tag MAT2A (FB-MAT2A) overexpression cell line establishment.
C. Immunoblot showing stable expression of FB-MAT2A in HeLa cells. The protein was detected with a mouse monoclonal anti-MAT2A antibody.

D. Immunoblot showing co-purification of MAT2B with FB-MAT2A in a streptavidin purification. The blot was detected with mouse monoclonal MAT2A and rabbit polyclonal MAT2B antibodies.

E. Immunostaining of FB-MAT2A stably expressing HeLa cells showing the nuclear-dominant localization of the FB-MAT2A protein. The cells carrying the FLAG-Bio tag empty vector (FB-EV) are shown as a negative control. The nucleus was stained with Hoechst. FB-MAT2A was detected with a mouse anti-DDDDK-tag (M185-3L, MBL) primary antibody followed by FITC-labeled anti-mouse IgG (F3008, Anti-Mouse IgG–FITC antibody produced in sheep, Sigma Aldrich). Scale bar = 10 μm.

F. The Western blot detecting the FB-MAT2A protein in different single clones isolated from the FB-MAT2A stable expression cells. Single cell clones were isolated by limiting dilution technique. Among the 10 clones, clone number 9 showed the highest expression.

G. Immunoblot showing various histone methylation in FB-EV and FB-MAT2A stably expressing HeLa cells.

H. SUnSET assay was performed with HeLa cells stably expressing FB-MAT2A in different treatment conditions. Lanes 1 and 2: the cells were treated with 400 nM rapamycin for 1 hr. For serum stimulation, cells were first cultured in serum-free media for 24 hr (serum starvation) and then cultured in 10%-FBS-containing media for either 1 or 3 hr (serum stimulation). Phos-S6K (T389): Phosphorylated S6 kinase (S6K) at threonine 389, Endo-MAT2A: Endogenous MAT2A.

Figure 3: MAT2A catalytic activity is essential for protein synthesis in Hepa 1 cells

A. SAM is synthesized from methionine and ATP by the catalytic activity of methionine adenosyltransferase (MAT). Cycloleucine (cLEU) is a competitive inhibitor of MAT.

cLEU competes with methionine for binding to MAT thereby inhibits the MAT catalytic activity, which reduces intracellular SAM concentration.

B. MAT2A inhibition by cLEU reduced protein synthesis in Hepa1 cells. Cells were treated with cLEU at the indicated concentrations for 6 hr (Left panel). The intensity of puromycin-labeled peptides on the blot was quantified and was normalized to that of β-ACTIN (Right panel).

Figure 4: MAT2A catalytic activity is essential for protein synthesis in HeLa cells

A. MAT2A inhibition by cLEU reduced protein synthesis in HeLa cells. Cells were treated with cLEU at the indicated concentrations for 6 hr (Left panel). The intensity of puromycin-labeled peptides on the blot was quantified and was normalized to that of β-ACTIN (Right panel). Mean values ± SD are shown (n = 4 biological replicates of the experiment).

B. Assessment of global protein synthesis in HeLa cells upon MAT2A inhibition by cLEU at various concentrations (10, 20 and 30 mM) and timepoints (6, 3 and 1 hr).

Figure 5: MAT2A-regulated protein synthesis is not contingent to mTORC1 activity

A. Schematic presentation of mTORC1 activation and effects on translation machinery.

B. Western blot analysis for the mTOR pathway proteins after treating Hepa1 cells with the indicated concentrations of cLEU for 6 hr. In lane 2, cells were treated with 400 nM of rapamycin for 1 hr. cLEU did not alter the mTORC1 activity indicated by Phos-S6K.

C. Western blot analysis for the mTOR pathway proteins after treating HeLa cells with the indicated concentrations of cLEU for 6 hr. In lane 2, cells were treated with 400 nM of rapamycin for 1 hr. cLEU did not alter the mTORC1 activity measured by Phos-S6K.

Figure 6: Feedback activation of AKT and MAPK pathways upon MAT2A inhibition

A. Western blot analysis for the AKT pathway proteins after treating HeLa cells with the indicated concentrations of cLEU for 6 hr. In lane 2, cells were treated with 400 nM of rapamycin for 1 hr.
B. Western blot analysis for the MAPK pathway proteins after treating HeLa cells with the indicated concentrations of cLEU for 6 hr. In lane 2, cells were treated with 400 nM of rapamycin for 1 hr.

Figure 7: MAT2A activity is required for transcription of genes encoding proteins for ribosome biogenesis

A. RNA sequencing was performed using the total cytoplasmic mRNA from the control cells and cells treated with cLEU for 6 hr. Differential expression analysis was performed for the genes exhibiting 10 or more read counts. The genes significantly altered upon the treatment are indicated in dark gray. Differences between the control and treated group were considered significant when q value was smaller than 0.01 (n = 2 replicates of sample).
B. Gene ontology (GO) analysis for the term "biological process" of the transcriptionally downregulated genes from (A). MAT2A inhibition reduced transcription of genes involved in ribosome biogenesis (n = 2 replicates of sample).
C. The normalized expression of genes belonging to the term 'Ribosome biogenesis' in the Figure (B) is presented as heatmap (n = 2 replicates of sample).

Figure 8: MAT2A and SAM are essential for maintaining active translation

A. Schematic presentation of polysome analysis. HeLa cells were cultured for 18 hr. The cells were then treated with cLEU and cultured for another 6 hr. After cell lysis, the nuclei

were removed, and the cleared lysate was fractionated in a sucrose density gradient. The A260 of fractions were used for the generation of polysome analysis curve.

B. Representative merge of polysome curve derived from the control and cLEU-treated cells. HeLa cells showed decreased active polysome formation (consisting of more than 3 translating ribosomes on a particular transcript) with shifting the spare ribosome from the polysome to monosome and their subunits. The experiment was repeated three times, which resulted in similar polysome curves.

C. RNA sequencing was performed using mRNA extracted from the sucrose gradient of polysome fractions shown in (B). Differential expression analysis was performed for the polysome-bound transcripts exhibiting 10 or more read counts. Differences between the control and treated group were considered significant when *q* value was smaller than 0.01. (n = 2 replicates of sample).

D. Translation efficiency (TE) of each transcript was calculated by using a ratio of reads number between polysome fraction (From B) and total RNA. Transcripts with more than 2-fold increment, and decrement in TE are colored red and blue, respectively. (n = 2 replicates of sample)

Figure 9: MAT2A interacts with proteins involved in ribosome biogenesis and translation

A. Schematic representation of the workflow for ectopic expression and purification of FB-MAT2A for LC-MS/MS analysis. FB-MAT2A was stably expressed in HeLa cells and was purified by biotin-streptavidin affinity purification using streptavidin-bound magnetic beads. In parallel, we also did mock purification as a control from HeLa cells carrying FB-EV to eliminate non-specifically binding proteins. The purified proteins were separated in SDS-PAGE and were in-gel trypsin digested into peptides. The extracted peptides were prepared for LC-MS/MS analysis.

B. The FB-MAT2A protein was purified from FB-MAT2A stable expression HeLa cells using streptavidin beads. HeLa cells carrying the FB-EV served as a negative control. FB-MAT2A and its interacting proteins were visualized by Coomassie Brilliant Blue (CBB) staining following separation by SDS-PAGE.

C. Confirmation of purification of FB-MAT2A by Western blot using mouse monoclonal MAT2A antibody.

D. GO analysis for the GO-Term biological process showing the ribosome biogenesis factors were co-purified as FB-MAT2A interacting proteins. Top seven enriched terms are presented in a horizontal bar blot. An adjusted *p*-value <0.05 was considered for significant enrichment of a term.

E. GO analysis for the GO-Term molecular function as in D.

F. GO analysis for the GO-Term cellular contents as in D.

G. All the FB-MAT2A interactant proteins are presented as a network. The color grade indicates the fold change of protein score over control purification. The proteins in the left rectangular area are related to ribosome biogenesis or function. Proteins inside the dashed black circle are the components of snoRNP complex.

Figure 10: MAT2A is required for rRNA processing

A. Ribosomal RNA is transcribed as the single large 47S pre-rRNA containing the sequences for the 18S, 5.8S and 28S rRNA which are separated by the internal transcribed spacer sequences (ITS1 and 2) and are flanked by the external transcribed spacer sequences (5′ and 3′ ETS). During the generation of mature rRNA, the transcribed spacer sequences (TSs) are removed by endo and exonucleolytic cleavages.

B. The 47S pre-rRNA from Hepa1 cells was quantified by qPCR after MAT2A knock-down for 48 hr. The primers targeted to the 5′ ETS so that only the pre-rRNAs can specifically be detected. The primer positions are shown in (A).

C. The mature 18S and 28S rRNAs in Hepa1 cells was quantified after 48-hr knock-down of MAT2A. The representative electropherogram from triplicates measurements showed that the 18S rRNA production was reduced markedly.

D. A bar plot derived from the experiment representing in (C) showed a significant reduction of the 18S/28S rRNA ratio. Mean ± SD are shown (n = 3 replicates of sample).

Figure 11: MAT2A catalytic activity is required for rRNA processing

A. The representative electropherogram of rRNA measurement showed that 18S rRNA production was reduced upon MAT2A inhibition by cLEU in HeLa cells.

B. A par plot derived from data of Figure (A). The decreased 18S/28S rRNA ratio was observed after chemical inhibition of MAT2A by cLEU for 6 hr in HeLa cells.

Figure 12: Heavy methyl SILAC experiment

A. Schematic diagram of heavy methyl-SILAC. HeLa cells were grown in the light and heavy methionine for 6 generations. Transfection using the FLAG-tagged ribosomal protein (FL-RPL23A) expression vector was performed 24 hr before cell harvest in method 1. Six hours before cell harvest, the heavy-labeled cells were treated with 30 mM cLEU. After cell harvest, the heavy- and light-labeled cells were mixed in equal numbers and ribosome was purified either by immunoprecipitation using an anti-DDDDK antibody bound to magnetic beads (method 1) or by pelleting in ultracentrifugation by passing through 1 M sucrose cushion (method 2). The purified ribosomes were then analyzed by LC-MS/MS.

B. CBB-stained gel loaded with the ribosome proteins purified by anti-FLAG immunoprecipitation. FL-RPS2 and FL-RPL23A are indicated by the arrows. Many different protein bands in a molecular mass range between 10 to 35 kDa, which is the migration range of most of the ribosomal proteins, in the IP lane compared to mock

purification suggests other ribosomal proteins were co-precipitated along with FL-RPL23A.

C. CBB-stained gel loaded with the ribosomal protein purified by ultracentrifugation in a sucrose cushion. Samples from duplicate purification are loaded. Compact protein bands were observed between 10 to 35 kDa which is the mass range of the ribosomal proteins.

D. Western-blot analysis of ribosome purified by method 2 showed the enrichment of the ribosomal protein RPL3 over β-ACTIN, which suggests a successful purification of ribosome. About 3.3 % of the lysate was loaded as input.

Figure 13: Attributes of methylated peptides identified in Heavy methyl SILAC experiment

A. The identified methylated peptides derived from proteins involved in translation are shown. The methylated residues are shown in magenta. The horizontal bar plot indicates the heavy/light ratio of every peptide. A ratio smaller than 1 indicate reduced methylation in the peptides by cLEU treatment and those greater than 1 depicts increased methylation. The bars of peptides whose methylation reduced by 50% or more (ratio <0.5) are presented in blue. The types of modification are labeled at the tip of each bar. Kme1: monomethylated lysine, Kme2: dimethylated lysine, Kme3: trimethylated lysine, Rme1: monomethylated arginine, Rme2: dimethylated arginine.

B. Correlation analysis between relative abundance of light and heavy unmethylated methionine-containing peptides used to normalize the values of methylated peptides form ribosome purified in IP (method 1) (two peptides from PABPC1, two from RPL23A and one from DDX17) is presented in plot. The values of light and heavy peptides showed a strong positive correlation (R^2_{adj} = 0.94) suggesting equal amount of light and heavy labeled proteins were purified and considered for the experiment. The gray zone indicates the 95% confidence level interval predicted from a linear model ("lm") in R.

C. Correlation analysis between relative abundance of light and heavy unmethylated methionine-containing peptides used to normalize the values of methylated peptides form ribosome purified by sucrose cushion (method 2) (one peptide from eEF1A1/2, three from eEF2, three from PABPC1, two from PABPC3 and two from PABPC4) is presented in plot. The abundance of light and heavy peptides showed a strong positive correlation (R^2_{adj} = 0.99) suggesting an equal amount of light and heavy labeled proteins were purified and considered for the experiment. The gray zone indicates the 95% confidence level interval predicted from a linear model ("lm") in R.

Figure 14: Chromatogram and mass spectrum of eEF1A1/2K55me2 and validation of eEF1A1K55me2 by western blot.

A. The chromatogram (Upper panels) and mass spectrum (Lower panels) of light and heavy eEF1A1/2K55me2 peptides are presented. The RT, AA, mass/charge of this peptide are presented in blue (Light peptide) and magenta (Heavy peptide) colored text. RT, retention time, AA, area.
B. The specific reactivity of anti-eEF1AK55me2 antibody was determined by overexpression of eEF1A1 WT and methylation mutant plasmid in HEK293T cells for 24 hr followed by immunoprecipitation and immunoblotting with indicating antibodies. The magenta-colored arrows indicate ectopic FB-eEF1A1.
C. eEF1A1 WT and methylation mutant plasmid were co-expressed with MAT2A in HEK293T cells for 24 hr followed by immunoblotting with indicated antibodies. The magenta-colored arrows indicate ectopic FB-eEF1A1.

Figure 15: MAT2A contributes to mammalian translation by multi-pronged strategies

Firstly, in the nucleolus it promotes the 18S rRNA processing or maintain its stability. In the cytoplasm, MAT2A promotes translation initiation and active polysome formation

during translation. Moreover, MAT2A dynamically regulates methylation of some translation factors.

Table legends

Table 1: Different attributes of the transcripts with increased TE by greater than 2-fold (log2) upon MAT2A inhibition by cycloleucine are listed (related to Figure 8D).

Table 2: Different attributes of the transcripts with decreased TE by greater than 2-fold (log2) upon MAT2A inhibition by cycloleucine are listed (related to Figure 8D).

Table 3: Different attributes of proteins purified as FB-MAT2A complex are presented (related to Figure 9). The text of the proteins related to ribosome biogenesis or functions are colored in magenta and among them those are component of snoRNP complex are highlighted in light blue.

Table 4: Different attributes of all 29 identified methylated peptides in two different ribosome purification methods are listed. The methylated residues are presented in magenta color.

Table 5: Different attributes of the identified methylated peptides are listed (related to Figure 12A). Whenever applicable, the values are generated by taking average of peptides purified twice in either method of purification. The methylated residues are presented in magenta color. The methylated peptides involved in translation are colored in light green except that of those methylations were reduced by more than 50% are highlighted in blue.

Acknowledgement

Foremost, I would like to pay my respect and my sincere gratitude to my advisor Professor Kazuhiko Igarashi for the continuous support during my doctoral studies. I must thank him for his patience, continuous motivations and too much gentle approach to me. I am lucky to find someone like Professor Igarashi because he teaches me to leading the project from the front as a researcher. I could not have imagined having a better advisor and mentor for my Ph.D study.

Besides my advisors, I would like to thank the lab members of Biochemistry Department. Particularly my mindful thanks and respect to Dr. Hiroki Shima for teaching me with fulltime support whenever needed. Many thanks to Dr. Mitsuyo Matsumoto for immense help in data analysis and figure preparation. My appreciation goes to Dr. Akihiko Muto for helping me organize the figures and preparing for different presentations.

My sincere thank also goes to my collaborative advisor Professor Tohifumi Inada form the Laboratory of Gene Regulation, Tohoku University Graduate School of Pharmaceutical Science for supporting to do some parts of experiments in his lab as well as advice.

I am grateful to lab member of Gene Regulation, for their support in various purposes. Particularly, I would like to address the contributions of Dr. Yoshitaka Matsuo for help in the experiment, advice and helping for RNA-seq data analysis.

Many thanks to Dr. Tadashi Nakagawa of the Department of Cell Proliferation, Tohoku University Graduate School of Medicine for the technical advice in the SUnSET experiment.

I thank my fellow lab mates in Biochemistry: Dr. Yusho Ishii, Dr. Long Chi Nguyen, Mr. Liu Liang and Dr. Stephanie Kaypee for various advice.

I am very much grateful to authority of Chattogram Veterinary and Animal Sciences University (CVASU), Bangladesh for providing me the study leave.

References

1. Abreu, R. de S., Penalva, L. O., Marcotte, E. M. & Vogel, C. Global signatures of protein and mRNA expression levels. *Mol Biosyst* **5**, 1512–1526 (2009).
2. de Sousa Abreu, R., Penalva, L. O., Marcotte, E. M. & Vogel, C. Global signatures of protein and mRNA expression levels. *Mol Biosyst* **5**, 1512–1526 (2009).
3. Maier, T., Güell, M. & Serrano, L. Correlation of mRNA and protein in complex biological samples. *FEBS Lett* **583**, 3966–3973 (2009).
4. Buccitelli, C. & Selbach, M. mRNAs, proteins and the emerging principles of gene expression control. *Nat Rev Genet* **21**, 630–644 (2020).
5. Emmott, E., Jovanovic, M. & Slavov, N. Ribosome Stoichiometry: From Form to Function. *Trends in Biochemical Sciences* **44**, 95–109 (2019).
6. Tahmasebi, S., Khoutorsky, A., Mathews, M. B. & Sonenberg, N. Translation deregulation in human disease. *Nat Rev Mol Cell Biol* **19**, 791–807 (2018).
7. Teixeira, F. K. & Lehmann, R. Translational Control during Developmental Transitions. *Cold Spring Harb Perspect Biol* **11**, a032987 (2019).
8. Zhao, B. S., Roundtree, I. A. & He, C. Post-transcriptional gene regulation by mRNA modifications. *Nat Rev Mol Cell Biol* **18**, 31–42 (2017).
9. Jansen, M., de Moor, C. H., Sussenbach, J. S. & van den Brande, J. L. Translational control of gene expression. *Pediatr Res* **37**, 681–686 (1995).
10. Topisirovic, I. & Sonenberg, N. mRNA translation and energy metabolism in cancer: the role of the MAPK and mTORC1 pathways. *Cold Spring Harb Symp Quant Biol* **76**, 355–367 (2011).
11. Kozak, M. Influence of mRNA secondary structure on binding and migration of 40S ribosomal subunits. *Cell* **19**, 79–90 (1980).

12. Pestova, T. V. & Kolupaeva, V. G. The roles of individual eukaryotic translation initiation factors in ribosomal scanning and initiation codon selection. *Genes Dev.* **16**, 2906–2922 (2002).

13. Macejak, D. G. & Sarnow, P. Internal initiation of translation mediated by the 5' leader of a cellular mRNA. *Nature* **353**, 90–94 (1991).

14. Beretta, L., Gingras, A. C., Svitkin, Y. V., Hall, M. N. & Sonenberg, N. Rapamycin blocks the phosphorylation of 4E-BP1 and inhibits cap-dependent initiation of translation. *EMBO J* **15**, 658–664 (1996).

15. Winter, J. N., Jefferson, L. S. & Kimball, S. R. ERK and Akt signaling pathways function through parallel mechanisms to promote mTORC1 signaling. *Am J Physiol Cell Physiol* **300**, C1172-1180 (2011).

16. Chung, J., Grammer, T. C., Lemon, K. P., Kazlauskas, A. & Blenis, J. PDGF- and insulin-dependent pp70S6k activation mediated by phosphatidylinositol-3-OH kinase. *Nature* **370**, 71–75 (1994).

17. Kim, D.-H. *et al.* mTOR interacts with raptor to form a nutrient-sensitive complex that signals to the cell growth machinery. *Cell* **110**, 163–175 (2002).

18. Kandel, E. S. & Hay, N. The regulation and activities of the multifunctional serine/threonine kinase Akt/PKB. *Exp Cell Res* **253**, 210–229 (1999).

19. Inoki, K., Li, Y., Zhu, T., Wu, J. & Guan, K.-L. TSC2 is phosphorylated and inhibited by Akt and suppresses mTOR signalling. *Nat Cell Biol* **4**, 648–657 (2002).

20. Castro, A. F., Rebhun, J. F., Clark, G. J. & Quilliam, L. A. Rheb binds tuberous sclerosis complex 2 (TSC2) and promotes S6 kinase activation in a rapamycin- and farnesylation-dependent manner. *J Biol Chem* **278**, 32493–32496 (2003).

21. Zhang, Y. *et al.* Rheb is a direct target of the tuberous sclerosis tumour suppressor proteins. *Nat Cell Biol* **5**, 578–581 (2003).

22. Li, Y., Inoki, K., Vacratsis, P. & Guan, K.-L. The p38 and MK2 Kinase Cascade Phosphorylates Tuberin, the Tuberous Sclerosis 2 Gene Product, and Enhances Its Interaction with 14-3-3 *. *Journal of Biological Chemistry* **278**, 13663–13671 (2003).

23. Holz, M. K., Ballif, B. A., Gygi, S. P. & Blenis, J. mTOR and S6K1 mediate assembly of the translation preinitiation complex through dynamic protein interchange and ordered phosphorylation events. *Cell* **123**, 569–580 (2005).

24. Roux, P. P. *et al.* RAS/ERK signaling promotes site-specific ribosomal protein S6 phosphorylation via RSK and stimulates cap-dependent translation. *J Biol Chem* **282**, 14056–14064 (2007).

25. Yang, H.-S. *et al.* The transformation suppressor Pdcd4 is a novel eukaryotic translation initiation factor 4A binding protein that inhibits translation. *Mol Cell Biol* **23**, 26–37 (2003).

26. Dorrello, N. V. *et al.* S6K1- and betaTRCP-mediated degradation of PDCD4 promotes protein translation and cell growth. *Science* **314**, 467–471 (2006).

27. Wang, X. *et al.* Regulation of elongation factor 2 kinase by p90RSK1 and p70 S6 kinase. *EMBO J* **20**, 4370–4379 (2001).

28. Burnett, P. E., Barrow, R. K., Cohen, N. A., Snyder, S. H. & Sabatini, D. M. RAFT1 phosphorylation of the translational regulators p70 S6 kinase and 4E-BP1. *Proc Natl Acad Sci U S A* **95**, 1432–1437 (1998).

29. Ueda, T., Watanabe-Fukunaga, R., Fukuyama, H., Nagata, S. & Fukunaga, R. Mnk2 and Mnk1 are essential for constitutive and inducible phosphorylation of eukaryotic initiation factor 4E but not for cell growth or development. *Mol Cell Biol* **24**, 6539–6549 (2004).

30. Zhu, J. & Thompson, C. B. Metabolic regulation of cell growth and proliferation. *Nat Rev Mol Cell Biol* **20**, 436–450 (2019).

31. Hershey, J. W. B. Regulation of protein synthesis and the role of eIF3 in cancer. *Braz J Med Biol Res* **43**, 920–930 (2010).

32. Bhat, M. *et al.* Targeting the translation machinery in cancer. *Nat Rev Drug Discov* **14**, 261–278 (2015).

33. de la Parra, C., Walters, B. A., Geter, P. & Schneider, R. J. Translation initiation factors and their relevance in cancer. *Current Opinion in Genetics & Development* **48**, 82–88 (2018).

34. Truitt, M. L. & Ruggero, D. New frontiers in translational control of the cancer genome. *Nat Rev Cancer* **16**, 288–304 (2016).

35. Boroughs, L. K. & DeBerardinis, R. J. Metabolic pathways promoting cancer cell survival and growth. *Nat Cell Biol* **17**, 351–359 (2015).

36. Vander Heiden, M. G., Cantley, L. C. & Thompson, C. B. Understanding the Warburg Effect: The Metabolic Requirements of Cell Proliferation. *Science* **324**, 1029–1033 (2009).

37. Ussowicz, M. *et al.* Analysis of the rRNA methylation complex components in pediatric B-cell precursor acute lymphoblastic leukemia: A pilot study. *Adv Clin Exp Med* **29**, 107–113 (2020).

38. Robichaud, N. *et al.* Phosphorylation of eIF4E promotes EMT and metastasis via translational control of SNAIL and MMP-3. *Oncogene* **34**, 2032–2042 (2015).

39. Ruggero, D. Translational control in cancer etiology. *Cold Spring Harb Perspect Biol* **5**, a012336 (2013).

40. Silvera, D., Formenti, S. C. & Schneider, R. J. Translational control in cancer. *Nat Rev Cancer* **10**, 254–266 (2010).

41. Martineau, Y. *et al.* Pancreatic tumours escape from translational control through 4E-BP1 loss. *Oncogene* **33**, 1367–1374 (2014).

42. Zhang, L., Pan, X. & Hershey, J. W. B. Individual overexpression of five subunits of human translation initiation factor eIF3 promotes malignant transformation of immortal fibroblast cells. *J Biol Chem* **282**, 5790–5800 (2007).

43. Tian, T., Li, X. & Zhang, J. mTOR Signaling in Cancer and mTOR Inhibitors in Solid Tumor Targeting Therapy. *Int J Mol Sci* **20**, 755 (2019).

44. Xie, J., Wang, X. & Proud, C. G. mTOR inhibitors in cancer therapy. *F1000Res* **5**, F1000 Faculty Rev-2078 (2016).

45. Zou, Z., Tao, T., Li, H. & Zhu, X. mTOR signaling pathway and mTOR inhibitors in cancer: progress and challenges. *Cell & Bioscience* **10**, 31 (2020).

46. Hua, H. *et al.* Targeting mTOR for cancer therapy. *J Hematol Oncol* **12**, 71 (2019).

47. Bozulic, L. & Hemmings, B. A. PIKKing on PKB: regulation of PKB activity by phosphorylation. *Curr Opin Cell Biol* **21**, 256–261 (2009).

48. Kim, E., Goraksha-Hicks, P., Li, L., Neufeld, T. P. & Guan, K.-L. Regulation of TORC1 by Rag GTPases in nutrient response. *Nat Cell Biol* **10**, 935–945 (2008).

49. PARK, E. *et al.* NVP-BKM120, a novel PI3K inhibitor, shows synergism with a STAT3 inhibitor in human gastric cancer cells harboring KRAS mutations. *Int J Oncol* **40**, 1259–1266 (2011).

50. Rastogi, R. *et al.* Rapamycin Induces Mitogen-activated Protein (MAP) Kinase Phosphatase-1 (MKP-1) Expression through Activation of Protein Kinase B and Mitogen-activated Protein Kinase Kinase Pathways. *J Biol Chem* **288**, 33966–33977 (2013).

51. Wang, X. *et al.* Overcoming mTOR inhibition-induced paradoxical activation of survival signaling pathways enhances mTOR inhibitors' anticancer efficacy. *Cancer Biol Ther* **7**, 1952–1958 (2008).

52. Cantoni, G. L. S-Adenosylmethionine; a new intermediate formed enzymatically from L-methionine and adenosinetriphosphate. *J Biol Chem* **204**, 403–416 (1953).

53. Sakata, S. F. *et al.* Effect of Fasting on Methionine Adenosyltransferase Expression and the Methionine Cycle in the Mouse Liver. *Journal of Nutritional Science and Vitaminology* **51**, 118–123 (2005).

54. Sakata, S. F., Shelly, L. L., Ruppert, S., Schutz, G. & Chou, J. Y. Cloning and expression of murine S-adenosylmethionine synthetase. *J Biol Chem* **268**, 13978–13986 (1993).

55. Halim, A. B., LeGros, L., Chamberlin, M. E., Geller, A. & Kotb, M. Regulation of the human MAT2A gene encoding the catalytic alpha 2 subunit of methionine adenosyltransferase, MAT II: gene organization, promoter characterization, and identification of a site in the proximal promoter that is essential for its activity. *J Biol Chem* **276**, 9784–9791 (2001).

56. Kotb, M. *et al.* Consensus nomenclature for the mammalian methionine adenosyltransferase genes and gene products. *Trends Genet* **13**, 51–52 (1997).

57. LeGros, L., Halim, A. B., Chamberlin, M. E., Geller, A. & Kotb, M. Regulation of the human MAT2B gene encoding the regulatory beta subunit of methionine adenosyltransferase, MAT II. *J Biol Chem* **276**, 24918–24924 (2001).

58. Murray, B. *et al.* Structure and function study of the complex that synthesizes S-adenosylmethionine. *IUCrJ* **1**, 240–249 (2014).

59. Kaiser, P. Methionine Dependence of Cancer. *Biomolecules* **10**, 568 (2020).

60. Booher, K., Lin, D.-W., Borrego, S. L. & Kaiser, P. Downregulation of Cdc6 and pre-replication complexes in response to methionine stress in breast cancer cells. *Cell Cycle* **11**, 4414–4423 (2012).

61. Lin, D.-W., Chung, B. P. & Kaiser, P. S-adenosylmethionine limitation induces p38 mitogen-activated protein kinase and triggers cell cycle arrest in G1. *J Cell Sci* **127**, 50–59 (2014).

62. Cai, J., Sun, W. M., Hwang, J. J., Stain, S. C. & Lu, S. C. Changes in S-adenosylmethionine synthetase in human liver cancer: molecular characterization and significance. *Hepatology* **24**, 1090–1097 (1996).

63. Huang, Z.-Z., Mao, Z., Cai, J. & Lu, S. C. Changes in methionine adenosyltransferase during liver regeneration in the rat. *American Journal of Physiology-Gastrointestinal and Liver Physiology* **275**, G14–G21 (1998).

64. Frau, M., Feo, F. & Pascale, R. M. Pleiotropic effects of methionine adenosyltransferases deregulation as determinants of liver cancer progression and prognosis. *Journal of Hepatology* **59**, 830–841 (2013).

65. Liu, T. *et al.* Mechanisms of MAFG Dysregulation in Cholestatic Liver Injury and Development of Liver Cancer. *Gastroenterology* **155**, 557-571.e14 (2018).

66. Chen, H. *et al.* Circular RNA hsa_circ_0007364 increases cervical cancer progression through activating methionine adenosyltransferase II alpha (MAT2A) expression by restraining microRNA-101-5p. *Bioengineered* **11**, 1269–1279 (2020).

67. Tomasi, M. L. *et al.* Polyamine and methionine adenosyltransferase 2A crosstalk in human colon and liver cancer. *Exp Cell Res* **319**, 1902–1911 (2013).

68. Phuong, N. T. T. *et al.* Induction of methionine adenosyltransferase 2A in tamoxifen-resistant breast cancer cells. *Oncotarget* **7**, 13902–13916 (2016).

69. Villa, E. *et al.* mTORC1 stimulates cell growth through SAM synthesis and m6A mRNA-dependent control of protein synthesis. *Molecular Cell* **81**, 2076-2093.e9 (2021).

70. Gu, X. *et al.* SAMTOR is an S-adenosylmethionine sensor for the mTORC1 pathway. *Science* **358**, 813–818 (2017).

71. Ringeard, M., Marchand, V., Decroly, E., Motorin, Y. & Bennasser, Y. FTSJ3 is an RNA 2′-O-methyltransferase recruited by HIV to avoid innate immune sensing. *Nature* **565**, 500–504 (2019).

72. Morello, L. G. *et al.* The Human Nucleolar Protein FTSJ3 Associates with NIP7 and Functions in Pre-rRNA Processing. *PLOS ONE* **6**, e29174 (2011).

73. Ishiguro, K., Arai, T. & Suzuki, T. Depletion of S-adenosylmethionine impacts on ribosome biogenesis through hypomodification of a single rRNA methylation. *Nucleic Acids Research* **47**, 4226–4239 (2019).

74. Polevoda, B. & Sherman, F. Methylation of proteins involved in translation. *Molecular Microbiology* **65**, 590–606 (2007).

75. Malecki, J. *et al.* The novel lysine specific methyltransferase METTL21B affects mRNA translation through inducible and dynamic methylation of Lys-165 in human eukaryotic elongation factor 1 alpha (eEF1A). *Nucleic Acids Res* **45**, 4370–4389 (2017).

76. Liu, S. *et al.* METTL13 Methylation of eEF1A Increases Translational Output to Promote Tumorigenesis. *Cell* **176**, 491-504.e21 (2019).

77. Katoh, Y. *et al.* Methionine adenosyltransferase II serves as a transcriptional corepressor of Maf oncoprotein. *Mol Cell* **41**, 554–566 (2011).

78. Boer, E. de *et al.* Efficient biotinylation and single-step purification of tagged transcription factors in mammalian cells and transgenic mice. *Proceedings of the National Academy of Sciences of the United States of America* (2003) doi:10.1073/pnas.1332608100.

79. Shechter, D., Dormann, H. L., Allis, C. D. & Hake, S. B. Extraction, purification and analysis of histones. *Nat Protoc* **2**, 1445–1457 (2007).

80. Shima, H. *et al.* S-Adenosylmethionine Synthesis Is Regulated by Selective N6-Adenosine Methylation and mRNA Degradation Involving METTL16 and YTHDC1. *Cell Reports* **21**, 3354–3363 (2017).

81. Schmidt, E. K., Clavarino, G., Ceppi, M. & Pierre, P. SUnSET, a nonradioactive method to monitor protein synthesis. *Nature methods* **6**, 275–277 (2009).

82. Kera, Y. *et al.* Methionine Adenosyltransferase II-dependent Histone H3K9 Methylation at the COX-2 Gene Locus. *J Biol Chem* **288**, 13592–13601 (2013).

83. Frazier, M. L., Mars, W., Florine, D. L., Montagna, R. A. & Saunders, G. F. Efficient extraction of RNA from mammalian tissue. *Mol Cell Biochem* **56**, 113–122 (1983).

84. Corsini, N. S. *et al.* Coordinated Control of mRNA and rRNA Processing Controls Embryonic Stem Cell Pluripotency and Differentiation. *Cell Stem Cell* **22**, 543-558.e12 (2018).

85. Matsuo, Y. *et al.* Ubiquitination of stalled ribosome triggers ribosome-associated quality control. *Nat Commun* **8**, 159 (2017).

86. Ochiai, K. *et al.* Protocol for in vitro BCR-mediated plasma cell differentiation and purification of chromatin-associated proteins. *STAR Protocols* **2**, 100633 (2021).

87. Tanaka, H. *et al.* Epigenetic Regulation of the Blimp-1 Gene (Prdm1) in B Cells Involves Bach2 and Histone Deacetylase 3. *J Biol Chem* **291**, 6316–6330 (2016).

88. Cao, X.-J., Zee, B. M. & Garcia, B. A. Heavy methyl-SILAC labeling coupled with liquid chromatography and high-resolution mass spectrometry to study the dynamics of site-specific histone methylation. *Methods Mol Biol* **977**, 299–313 (2013).

89. Musiani, D. *et al.* Proteomics profiling of arginine methylation defines PRMT5 substrate specificity. *Sci Signal* **12**, eaat8388 (2019).

90. Ong, S.-E., Mittler, G. & Mann, M. Identifying and quantifying in vivo methylation sites by heavy methyl SILAC. *Nature Methods* **1**, 119–126 (2004).

91. Azzam, M. E. & Algranati, I. D. Mechanism of puromycin action: fate of ribosomes after release of nascent protein chains from polysomes. *Proc Natl Acad Sci U S A* **70**, 3866–3869 (1973).

92. Shafqat, N. *et al.* Insight into S-adenosylmethionine biosynthesis from the crystal structures of the human methionine adenosyltransferase catalytic and regulatory subunits. *Biochem J* **452**, 27–36 (2013).

93. Jani, T. S. *et al.* Inhibition of methionine adenosyltransferase II induces FasL expression, Fas-DISC formation and caspase-8-dependent apoptotic death in T leukemic cells. *Cell Res* **19**, 358–369 (2009).

94. Sufrin, J. R., Coulter, A. W. & Talalay, P. Structural and conformational analogues of L-methionine as inhibitors of the enzymatic synthesis of S-adenosyl-L-methionine. IV. Further mono-, bi- and tricyclic amino acids. *Mol Pharmacol* **15**, 661–677 (1979).

95. Gingras, A. C., Raught, B. & Sonenberg, N. eIF4 initiation factors: effectors of mRNA recruitment to ribosomes and regulators of translation. *Annu Rev Biochem* **68**, 913–963 (1999).

96. Carracedo, A. *et al.* Inhibition of mTORC1 leads to MAPK pathway activation through a PI3K-dependent feedback loop in human cancer. *J Clin Invest* **118**, 3065–3074 (2008).

97. Li, Y. *et al.* Protein phosphatase 2A and DNA-dependent protein kinase are involved in mediating rapamycin-induced Akt phosphorylation. *J Biol Chem* **288**, 13215–13224 (2013).

98. Sancak, Y. *et al.* The Rag GTPases bind raptor and mediate amino acid signaling to mTORC1. *Science* **320**, 1496–1501 (2008).

99. Monaco, P. L., Marcel, V., Diaz, J.-J. & Catez, F. 2'-O-Methylation of Ribosomal RNA: Towards an Epitranscriptomic Control of Translation? *Biomolecules* **8**, E106 (2018).

100. Henras, A. K., Plisson-Chastang, C., O'Donohue, M.-F., Chakraborty, A. & Gleizes, P.-E. An overview of pre-ribosomal RNA processing in eukaryotes. *Wiley Interdiscip Rev RNA* **6**, 225–242 (2015).

101. Figaro, S. *et al.* Trm112 is required for Bud23-mediated methylation of the 18S rRNA at position G1575. *Mol Cell Biol* **32**, 2254–2267 (2012).

102. Shubina, M. Y., Musinova, Y. R. & Sheval, E. V. Nucleolar Methyltransferase Fibrillarin: Evolution of Structure and Functions. *Biochemistry (Mosc)* **81**, 941–950 (2016).

103. Hamey, J. J. & Wilkins, M. R. Methylation of Elongation Factor 1A: Where, Who, and Why? *Trends in Biochemical Sciences* **43**, 211–223 (2018).

104. Li, Z., Gonzalez, P. A., Sasvari, Z., Kinzy, T. G. & Nagy, P. D. Methylation of translation elongation factor 1A by the METTL10-like See1 methyltransferase facilitates tombusvirus replication in yeast and plants. *Virology* **448**, 43–54 (2014).

105. Swiercz, R., Person, M. D. & Bedford, M. T. Ribosomal protein S2 is a substrate for mammalian PRMT3 (protein arginine methyltransferase 3). *Biochem J* **386**, 85–91 (2005).

106. White, J. T. *et al.* Protein methylation and translation: Role of lysine modification on the function of yeast elongation factor 1A. *Biochemistry* **58**, 4997–5010 (2019).

107. Davydova, E. *et al.* Identification and characterization of a novel evolutionarily conserved lysine-specific methyltransferase targeting eukaryotic translation elongation factor 2 (eEF2). *J Biol Chem* **289**, 30499–30510 (2014).

108. Lu, S. C. & Mato, J. M. S-adenosylmethionine in liver health, injury, and cancer. *Physiol Rev* **92**, 1515–1542 (2012).

109. Hoffman, R. M. Methionine dependence in cancer cells - a review. *In Vitro* **18**, 421–428 (1982).

110. Mecham, J. O., Rowitch, D., Wallace, C. D., Stern, P. H. & Hoffman, R. M. The metabolic defect of methionine dependence occurs frequently in human tumor cell lines. *Biochem Biophys Res Commun* **117**, 429–434 (1983).

111. Módis, K. *et al.* Effect of S-adenosyl-L-methionine (SAM), an allosteric activator of cystathionine-β-synthase (CBS) on colorectal cancer cell proliferation and bioenergetics in vitro. *Nitric Oxide* **41**, 146–156 (2014).

112. Obata, F. *et al.* Nutritional Control of Stem Cell Division through S-Adenosylmethionine in Drosophila Intestine. *Developmental Cell* **44**, 741-751.e3 (2018).

113. Saito, Y. *et al.* Effect of essential amino acids on enteroids: Methionine deprivation suppresses proliferation and affects differentiation in enteroid stem cells. *Biochem Biophys Res Commun* **488**, 171–176 (2017).

114. Shiraki, N. *et al.* Methionine metabolism regulates maintenance and differentiation of human pluripotent stem cells. *Cell Metab* **19**, 780–794 (2014).

115. Lu, S. & Epner, D. E. Molecular mechanisms of cell cycle block by methionine restriction in human prostate cancer cells. *Nutr Cancer* **38**, 123–130 (2000).

116. Li, T. W. H. *et al.* Effects of S-adenosylmethionine and methylthioadenosine on inflammation-induced colon cancer in mice. *Carcinogenesis* **33**, 427–435 (2012).

117. Zsigrai, S. *et al.* S-Adenosylmethionine Treatment of Colorectal Cancer Cell Lines Alters DNA Methylation, DNA Repair and Tumor Progression-Related Gene Expression. *Cells* **9**, E1864 (2020).

118. Cave, D. D. *et al.* S-Adenosylmethionine-mediated apoptosis is potentiated by autophagy inhibition induced by chloroquine in human breast cancer cells. *J Cell Physiol* **233**, 1370–1383 (2018).

119. Yan, L. *et al.* S-Adenosylmethionine Affects Cell Cycle Pathways and Suppresses Proliferation in Liver Cells. *J Cancer* **10**, 4368–4379 (2019).

120. Muranen, T. *et al.* Inhibition of PI3K/mTOR Leads to Adaptive Resistance in Matrix-Attached Cancer Cells. *Cancer Cell* **21**, 227–239 (2012).

121. Zhao, C. *et al.* MAT2A promotes porcine adipogenesis by mediating H3K27me3 at Wnt10b locus and repressing Wnt/β-catenin signaling. *Biochim Biophys Acta Mol Cell Biol Lipids* **1863**, 132–142 (2018).

122. Sancak, Y. *et al.* The Rag GTPases bind raptor and mediate amino acid signaling to mTORC1. *Science* **320**, 1496–1501 (2008).

123. Bhatt, A. P. *et al.* Dual inhibition of PI3K and mTOR inhibits autocrine and paracrine proliferative loops in PI3K/Akt/mTOR-addicted lymphomas. *Blood* **115**, 4455–4463 (2010).

124. Shi, Y., Yan, H., Frost, P., Gera, J. & Lichtenstein, A. Mammalian target of rapamycin inhibitors activate the AKT kinase in multiple myeloma cells by up-regulating the insulin-like growth factor receptor/insulin receptor substrate-1/phosphatidylinositol 3-kinase cascade. *Mol Cancer Ther* **4**, 1533–1540 (2005).

125. Dai, C.-L. *et al.* Inhibition of Protein Synthesis Alters Protein Degradation through Activation of Protein Kinase B (AKT). *J Biol Chem* **288**, 23875–23883 (2013).

126. Zinck, R. *et al.* Protein synthesis inhibitors reveal differential regulation of mitogen-activated protein kinase and stress-activated protein kinase pathways that converge on Elk-1. *Mol Cell Biol* **15**, 4930–4938 (1995).

127. Mauer, J. *et al.* Reversible methylation of m6Am in the 5' cap controls mRNA stability. *Nature* **541**, 371–375 (2017).

128. Shearstone, J. R. *et al.* Global DNA demethylation during mouse erythropoiesis in vivo. *Science* **334**, 799–802 (2011).

129. Wong, P. *et al.* Gene induction and repression during terminal erythropoiesis are mediated by distinct epigenetic changes. *Blood* **118**, e128–e138 (2011).

130. Caboche, M. & Bachellerie, J. P. RNA methylation and control of eukaryotic RNA biosynthesis. Effects of cycloleucine, a specific inhibitor of methylation, on ribosomal RNA maturation. *Eur J Biochem* **74**, 19–29 (1977).

131. Yi, Y. *et al.* A PRC2-independent function for EZH2 in regulating rRNA 2′-O methylation and IRES-dependent translation. *Nat Cell Biol* **23**, 341–354 (2021).

132. Xiao, S. *et al.* Dimethylation of eEF1A at Lysine 55 Plays a Key Role in the Regulation of eEF1A2 on Malignant Cell Functions of Acute Myeloid Leukemia. *Technol Cancer Res Treat* **19**, 1533033820914295 (2020).

133. Jakobsson, M. E. *et al.* The dual methyltransferase METTL13 targets N terminus and Lys55 of eEF1A and modulates codon-specific translation rates. *Nat Commun* **9**, 3411 (2018).

134. Hua, X. *et al.* Effects of RNA Binding Proteins on the Prognosis and Malignant Progression in Prostate Cancer. *Front Genet* **11**, 591667 (2020).

135. Wu, Y.-Q., Ju, C.-L., Wang, B.-J. & Wang, R.-G. PABPC1L depletion inhibits proliferation and migration via blockage of AKT pathway in human colorectal cancer cells. *Oncol Lett* **17**, 3439–3445 (2019).

136. Rikova, K. *et al.* Abstract B197: Proteomic based analysis of ovarian cancer pathways. *Mol Cancer Ther* **12**, B197–B197 (2013).

137. Wu, Z. *et al.* A Chemical Proteomics Approach for Global Analysis of Lysine Monomethylome Profiling. *Mol Cell Proteomics* **14**, 329–339 (2015).

138. Craig, A. W. B., Haghighat, A., Yu, A. T. K. & Sonenberg, N. Interaction of polyadenylate-binding protein with the eIF4G homologue PAIP enhances translation. *Nature* **392**, 520–523 (1998).

139. Gray, N. K., Coller, J. M., Dickson, K. S. & Wickens, M. Multiple portions of poly(A)-binding protein stimulate translation in vivo. *EMBO J* **19**, 4723–4733 (2000).

140. Imataka, H., Gradi, A. & Sonenberg, N. A newly identified N-terminal amino acid sequence of human eIF4G binds poly(A)-binding protein and functions in poly(A)-dependent translation. *EMBO J* **17**, 7480–7489 (1998).

141. Derry, M. C., Yanagiya, A., Martineau, Y. & Sonenberg, N. Regulation of poly(A)-binding protein through PABP-interacting proteins. *Cold Spring Harb Symp Quant Biol* **71**, 537–543 (2006).

142. Jackson, R. J., Hellen, C. U. T. & Pestova, T. V. The mechanism of eukaryotic translation initiation and principles of its regulation. *Nat Rev Mol Cell Biol* **11**, 113–127 (2010).

143. Endres, L. *et al.* 2'-O-ribose methylation of transfer RNA promotes recovery from oxidative stress in Saccharomyces cerevisiae. *PLoS One* **15**, e0229103 (2020).

144. Liu, F. *et al.* ALKBH1-Mediated tRNA Demethylation Regulates Translation. *Cell* **167**, 816-828.e16 (2016).

145. Tuorto, F. *et al.* RNA cytosine methylation by Dnmt2 and NSun2 promotes tRNA stability and protein synthesis. *Nat Struct Mol Biol* **19**, 900–905 (2012).

146. Dumont, F. J. *et al.* Dominant mutations confer resistance to the immunosuppressant, rapamycin, in variants of a T cell lymphoma. *Cell Immunol* **163**, 70–79 (1995).

147. Lorenz, M. C. & Heitman, J. TOR mutations confer rapamycin resistance by preventing interaction with FKBP12-rapamycin. *J Biol Chem* **270**, 27531–27537 (1995).

148. Sarbassov, D. D., Guertin, D. A., Ali, S. M. & Sabatini, D. M. Phosphorylation and regulation of Akt/PKB by the rictor-mTOR complex. *Science* **307**, 1098–1101 (2005).

149. Tamburini, J. *et al.* Mammalian target of rapamycin (mTOR) inhibition activates phosphatidylinositol 3-kinase/Akt by up-regulating insulin-like growth factor-1 receptor signaling in acute myeloid leukemia: rationale for therapeutic inhibition of both pathways. *Blood* **111**, 379–382 (2008).

150. Dilling, M. B. *et al.* 4E-binding proteins, the suppressors of eukaryotic initiation factor 4E, are down-regulated in cells with acquired or intrinsic resistance to rapamycin. *J Biol Chem* **277**, 13907–13917 (2002).

151. Kaplan, B., Qazi, Y. & Wellen, J. R. Strategies for the management of adverse events associated with mTOR inhibitors. *Transplant Rev (Orlando)* **28**, 126–133 (2014).

A

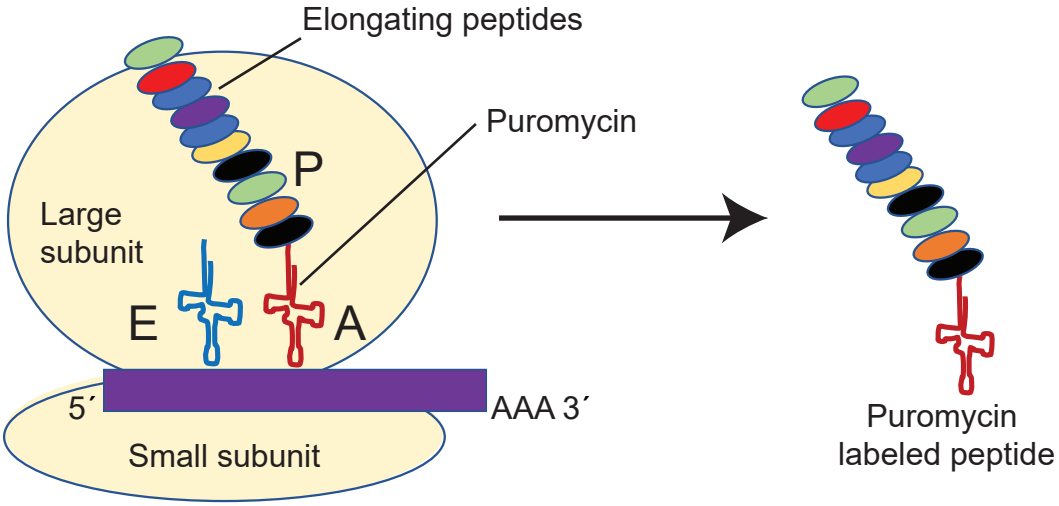
Elongating peptides
Puromycin
P
Large subunit
E
A
5´
AAA 3´
Small subunit
Puromycin labeled peptide

B

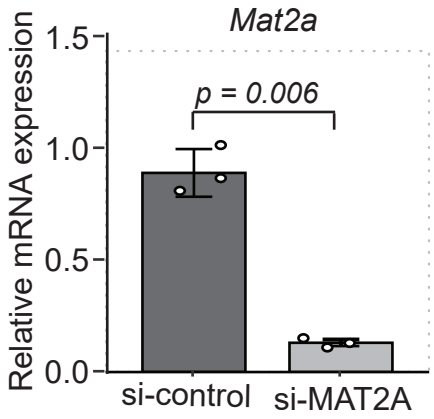
Mat2a
p = 0.006
Relative mRNA expression
1.5
1.0
0.5
0.0
si-control
si-MAT2A

C

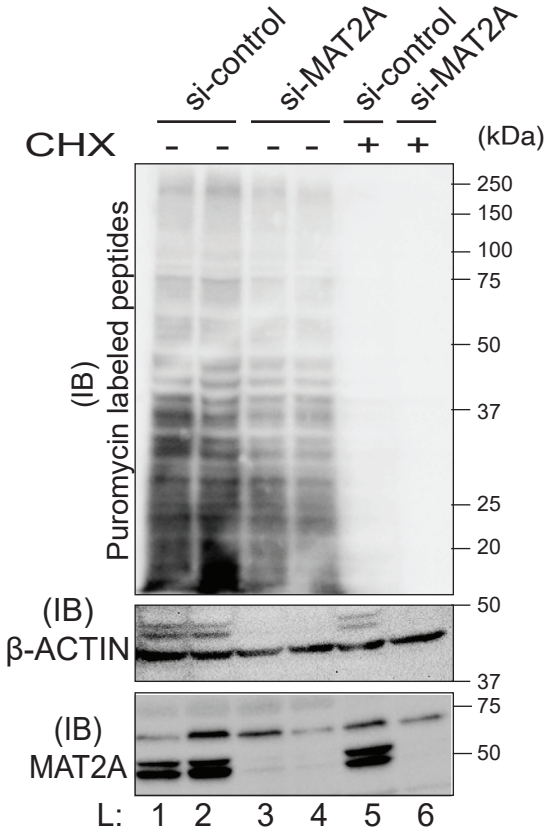
si-control
si-MAT2A
si-control
si-MAT2A
CHX
- - - - + +
(kDa)
(IB)
Puromycin labeled peptides
250
150
100
75
50
37
25
20
(IB)
β-ACTIN
50
37
(IB)
MAT2A
75
50
L: 1 2 3 4 5 6

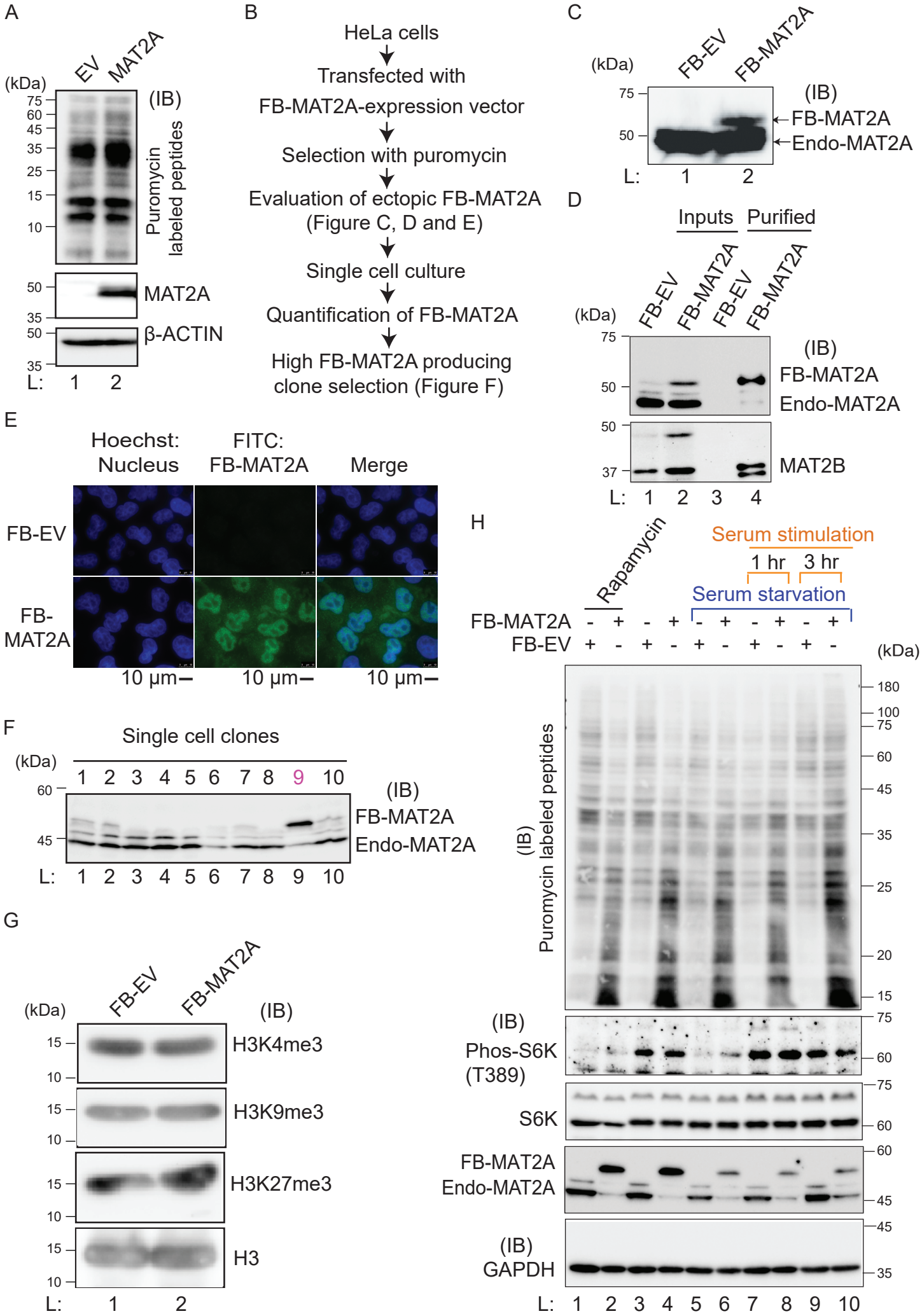
A
EV
MAT2A
(kDa)
75
60
45
35
25
15
10
(IB)
Puromycin labeled peptides
50
35
MAT2A
50
35
β-ACTIN
L: 1 2
B
HeLa cells
Transfected with
FB-MAT2A-expression vector
Selection with puromycin
Evaluation of ectopic FB-MAT2A (Figure C, D and E)
Single cell culture
Quantification of FB-MAT2A
High FB-MAT2A producing clone selection (Figure F)
C
FB-EV
FB-MAT2A
(kDa)
75
50
(IB)
FB-MAT2A
Endo-MAT2A
L: 1 2
D
Inputs
Purified
FB-EV
FB-MAT2A
FB-EV
FB-MAT2A
(kDa)
75
50
(IB)
FB-MAT2A
Endo-MAT2A
50
37
MAT2B
L: 1 2 3 4
E
Hoechst: Nucleus
FITC: FB-MAT2A
Merge
FB-EV
FB-MAT2A
10 μm
10 μm
10 μm
F
Single cell clones
(kDa)
1 2 3 4 5 6 7 8 9 10
60
45
(IB)
FB-MAT2A
Endo-MAT2A
L: 1 2 3 4 5 6 7 8 9 10
G
FB-EV
FB-MAT2A
(kDa)
(IB)
15
10
H3K4me3
H3K9me3
H3K27me3
H3
L: 1 2
H
Rapamycin
Serum stimulation
1 hr
3 hr
Serum starvation
FB-MAT2A - + - + - + - + - +
FB-EV + - + - + - + - + -
(kDa)
(IB)
Puromycin labeled peptides
180
100
75
60
45
35
25
20
15
(IB)
Phos-S6K (T389)
75
60
S6K
75
60
FB-MAT2A
Endo-MAT2A
60
45
(IB)
GAPDH
45
35
L: 1 2 3 4 5 6 7 8 9 10

A

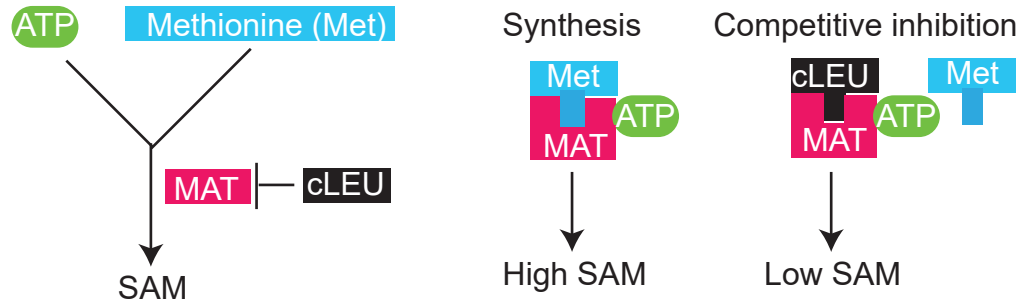
ATP
Methionine (Met)
MAT
cLEU
SAM
Synthesis
Met
ATP
MAT
High SAM
Competitive inhibition
cLEU
Met
ATP
MAT
Low SAM

B

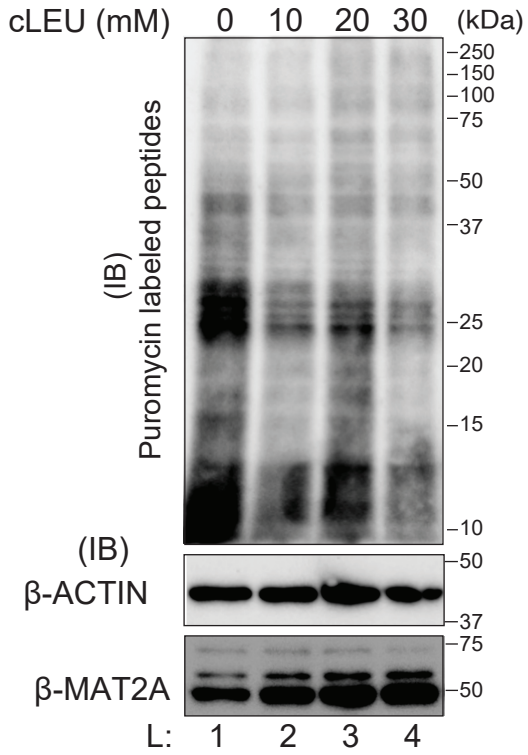
cLEU (mM) 0 10 20 30 (kDa)
(IB)
Puromycin labeled peptides
250
150
100
75
50
37
25
20
15
10
(IB)
β-ACTIN
50
37
β-MAT2A
75
50
L: 1 2 3 4

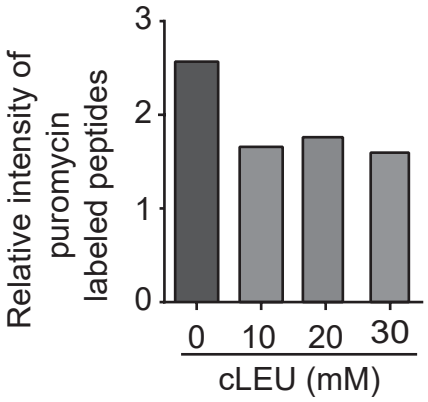
Relative intensity of puromycin labeled peptides
3
2
1
0
0 10 20 30
cLEU (mM)

Figure 4

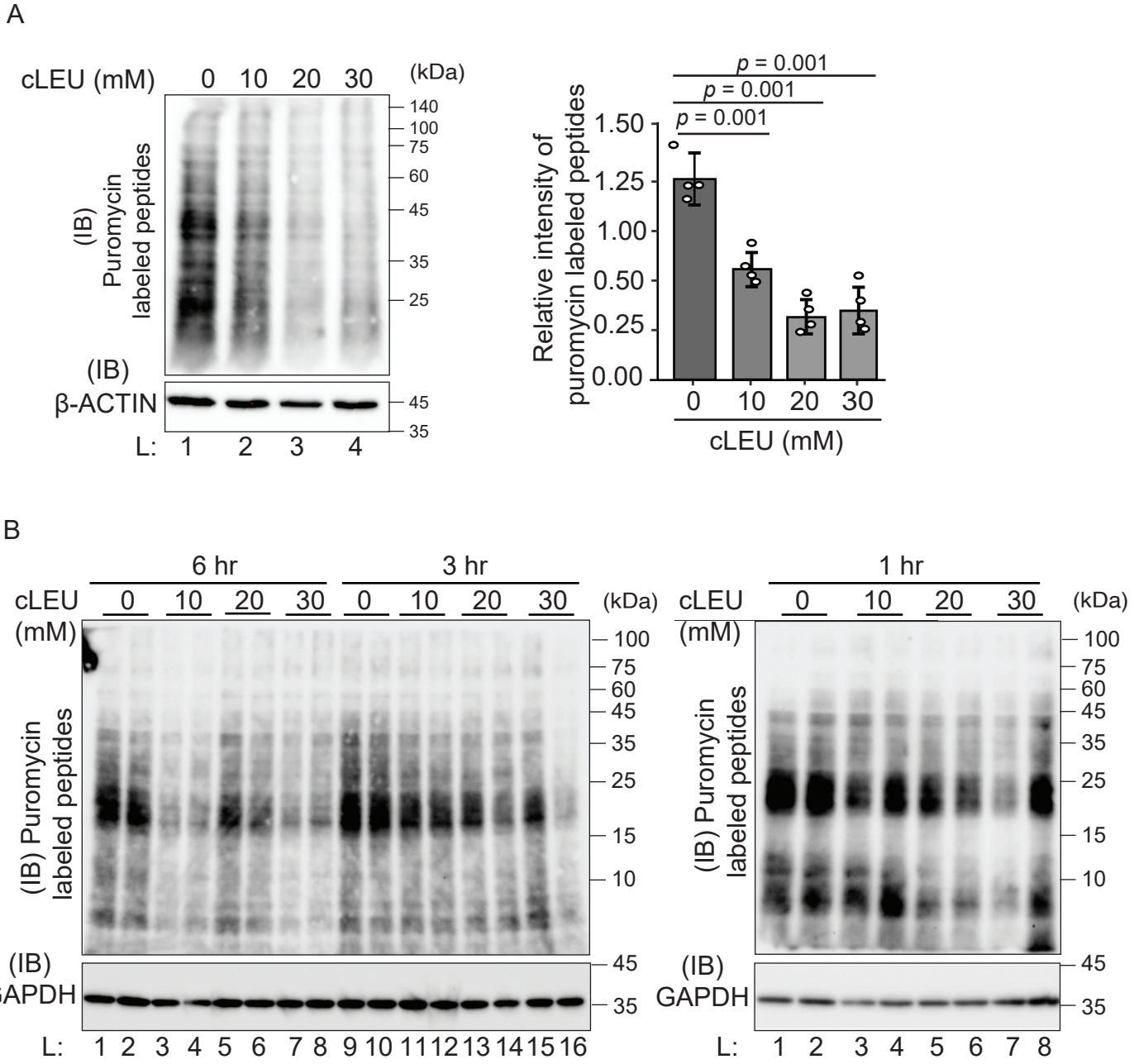
A
cLEU (mM) 0 10 20 30 (kDa)
(IB) Puromycin labeled peptides
140
100
75
60
45
35
25
(IB) β-ACTIN
45
35
L: 1 2 3 4
p = 0.001
p = 0.001
p = 0.001
Relative intensity of puromycin labeled peptides
1.50
1.25
1.00
0.50
0.25
0.00
0 10 20 30
cLEU (mM)
B
6 hr
3 hr
1 hr
cLEU (mM) 0 10 20 30 0 10 20 30 (kDa)
(IB) Puromycin labeled peptides
100
75
60
45
35
25
15
10
(IB) GAPDH
45
35
L: 1 2 3 4 5 6 7 8 9 10 11 12 13 14 15 16
cLEU (mM) 0 10 20 30 (kDa)
(IB) Puromycin labeled peptides
(IB) GAPDH
L: 1 2 3 4 5 6 7 8

Figure 5

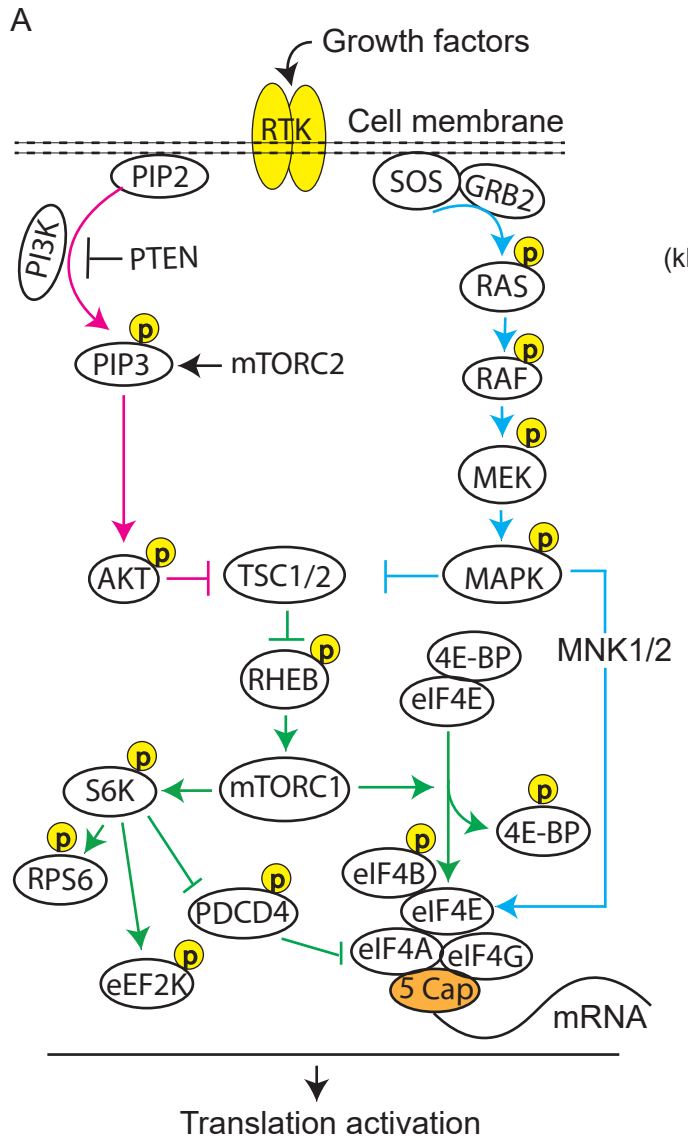
A
Growth factors
RTK
Cell membrane
PIP2
PI3K
PTEN
SOS
GRB2
RAS
RAF
MEK
PIP3
mTORC2
AKT
TSC1/2
MAPK
MNK1/2
RHEB
4E-BP
eIF4E
S6K
mTORC1
4E-BP
RPS6
eIF4B
PDCD4
eIF4E
eIF4A
eIF4G
eEF2K
5 Cap
mRNA
Translation activation

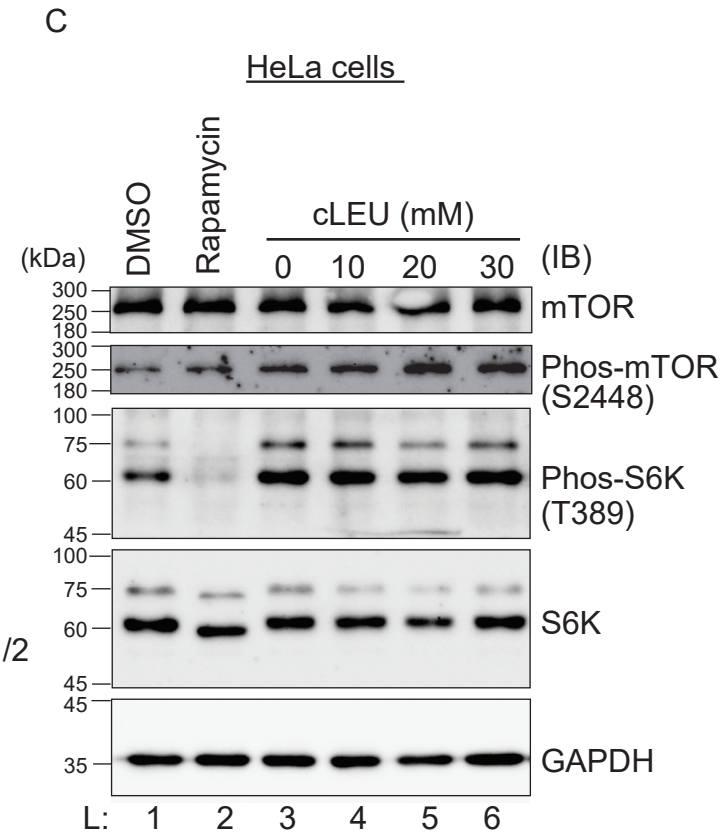
C
HeLa cells
DMSO
Rapamycin
cLEU (mM)
0 10 20 30
(kDa)
(IB)
mTOR
Phos-mTOR (S2448)
Phos-S6K (T389)
S6K
GAPDH
L: 1 2 3 4 5 6

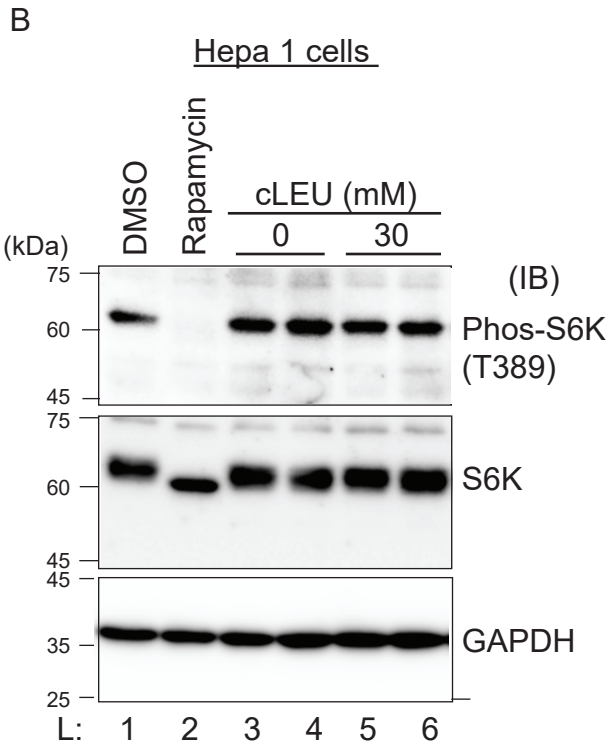
B
Hepa 1 cells
DMSO
Rapamycin
cLEU (mM)
0 30
(kDa)
(IB)
Phos-S6K (T389)
S6K
GAPDH
L: 1 2 3 4 5 6

Figure 6

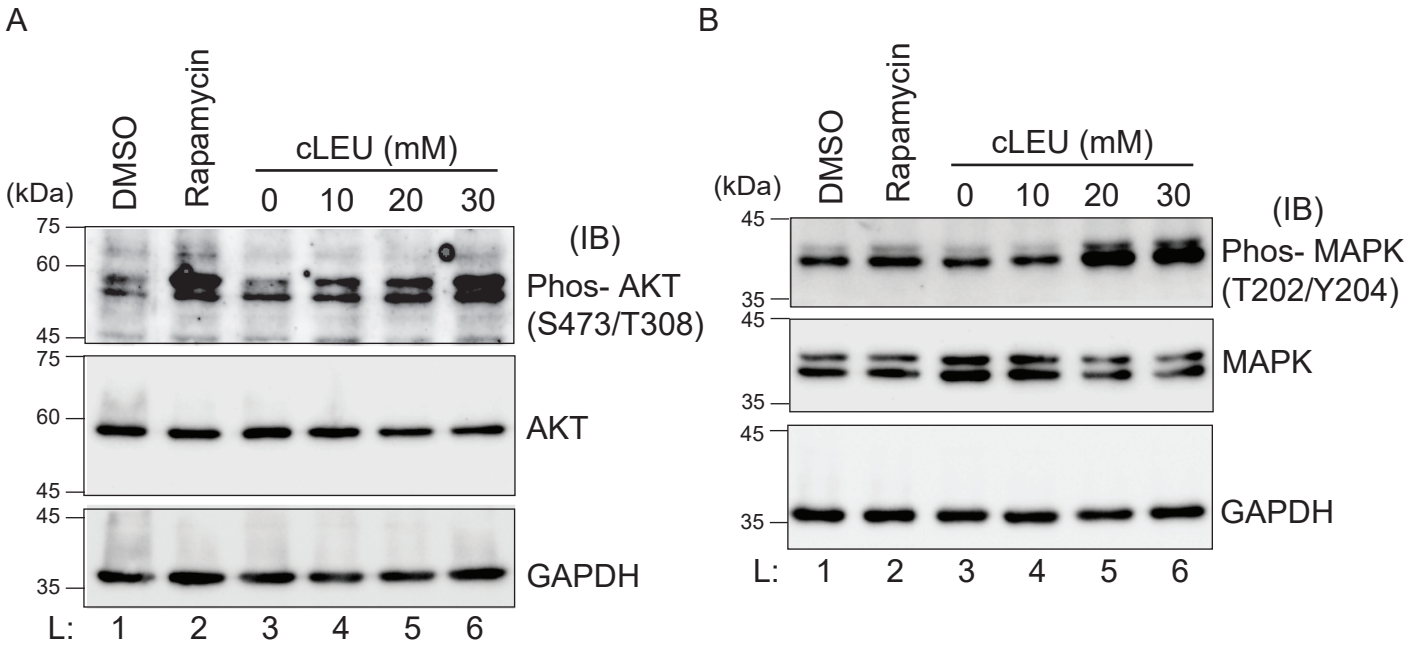
A
DMSO
Rapamycin
cLEU (mM)
0
10
20
30
(kDa)
75
60
45
(IB)
Phos- AKT
(S473/T308)
AKT
GAPDH
35
L:
1
2
3
4
5
6
B
MAPK
Phos- MAPK
(T202/Y204)

A

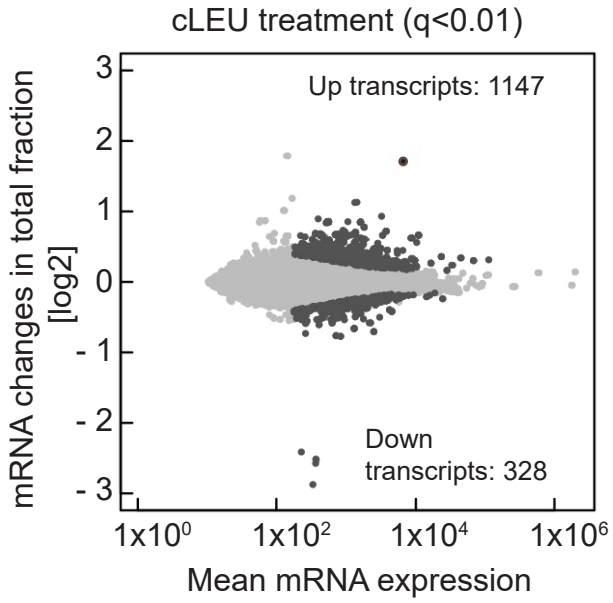

B

GO Term: Biological Process

Description	Count	*p* value	p.adjust.
Ribosome biogenesis	16	1.6e−13	3.9e−10
ncRNA processing	15	1.7e−10	8.6e−08

C

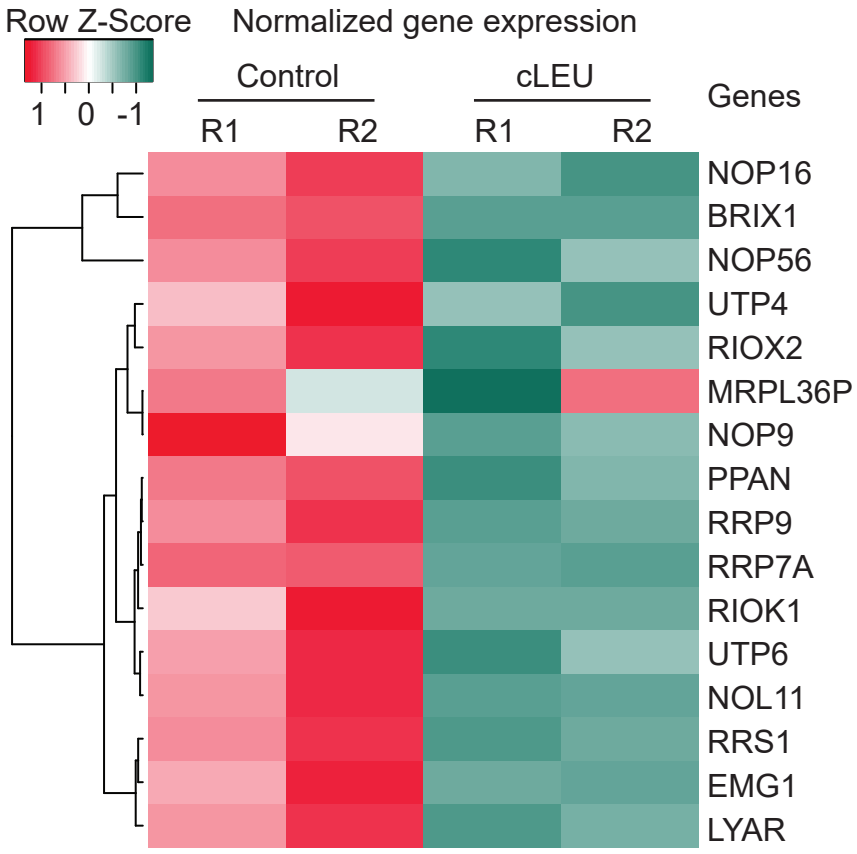

Figure 8

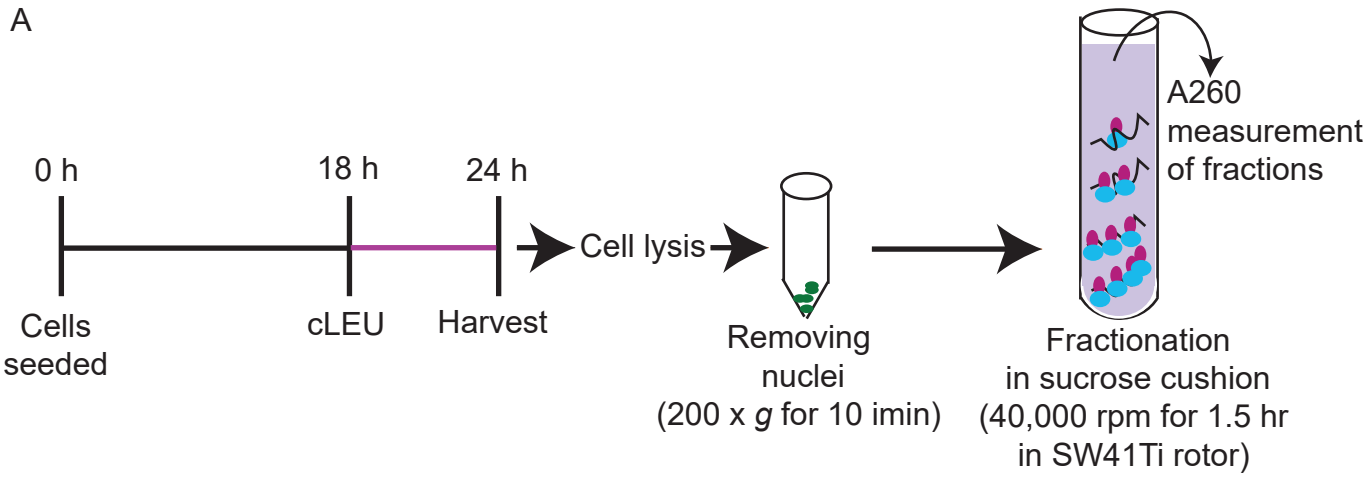
A
0 h
18 h
24 h
Cells seeded
cLEU
Harvest
Cell lysis
Removing nuclei (200 x g for 10 imin)
A260 measurement of fractions
Fractionation in sucrose cushion (40,000 rpm for 1.5 hr in SW41Ti rotor)

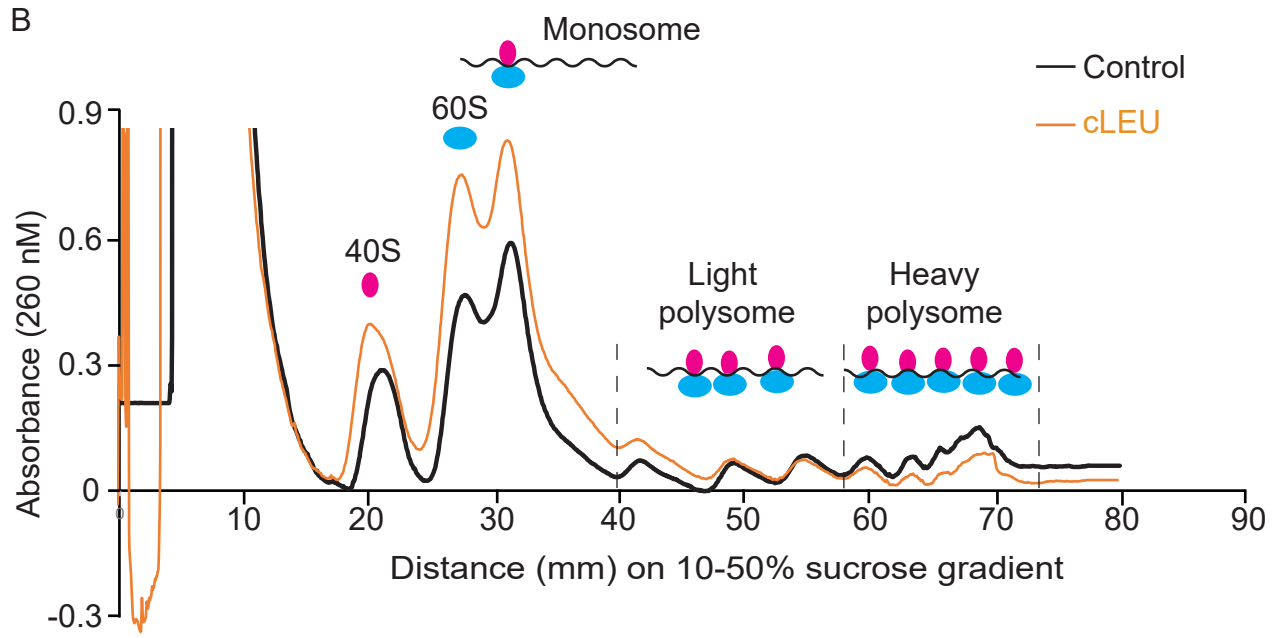
B
Monosome
60S
40S
Light polysome
Heavy polysome
Control
cLEU
Absorbance (260 nM)
0.9
0.6
0.3
0
-0.3
10
20
30
40
50
60
70
80
90
Distance (mm) on 10-50% sucrose gradient

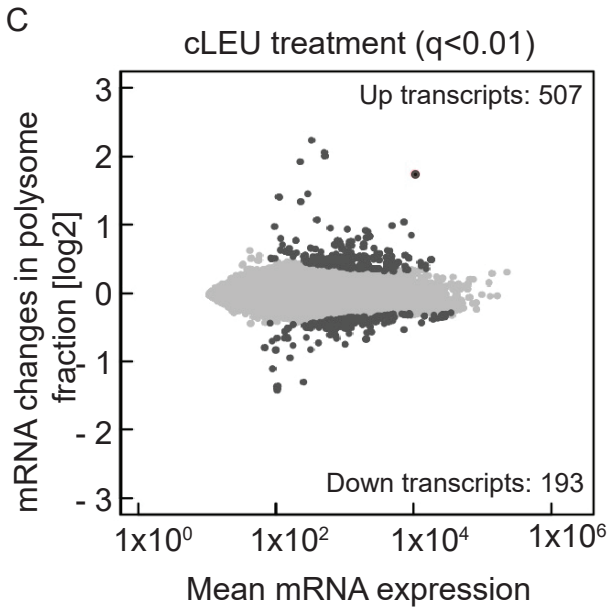
C
cLEU treatment (q<0.01)
Up transcripts: 507
Down transcripts: 193
mRNA changes in polysome fraction [log2]
3
2
1
0
- 1
- 2
- 3
1x10⁰
1x10²
1x10⁴
1x10⁶
Mean mRNA expression

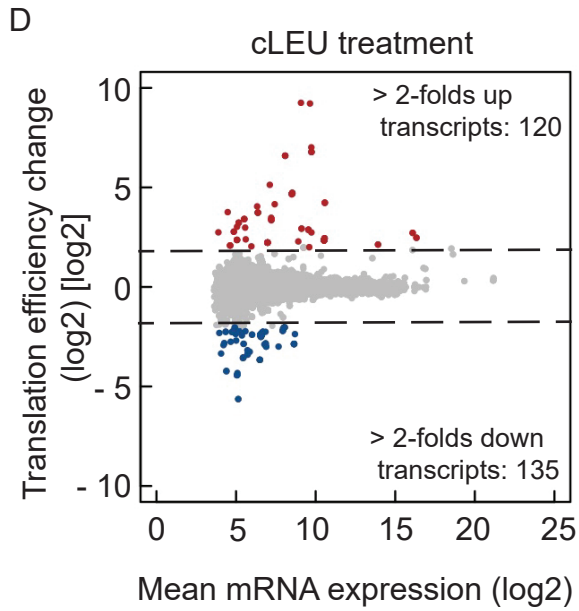
D
cLEU treatment
> 2-folds up transcripts: 120
> 2-folds down transcripts: 135
Translation efficiency change (log2) [log2]
10
5
0
- 5
- 10
0
5
10
15
20
25
Mean mRNA expression (log2)

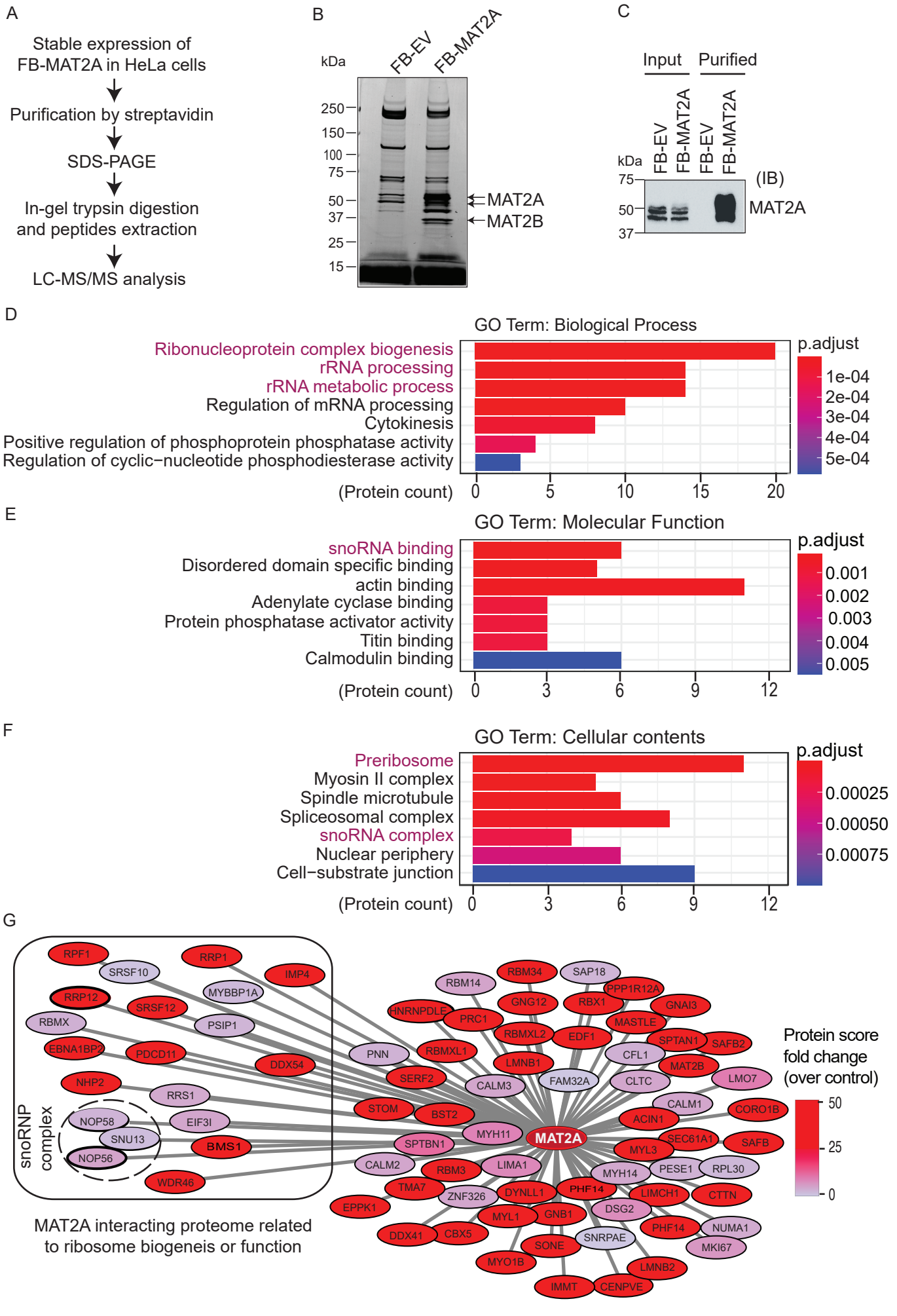
A
Stable expression of FB-MAT2A in HeLa cells
Purification by streptavidin
SDS-PAGE
In-gel trypsin digestion and peptides extraction
LC-MS/MS analysis
B
kDa
FB-EV
FB-MAT2A
250
150
100
75
50
37
25
15
MAT2A
MAT2B
C
Input
Purified
FB-EV
FB-MAT2A
FB-EV
FB-MAT2A
kDa
75
50
37
(IB)
MAT2A
D
GO Term: Biological Process
Ribonucleoprotein complex biogenesis
rRNA processing
rRNA metabolic process
Regulation of mRNA processing
Cytokinesis
Positive regulation of phosphoprotein phosphatase activity
Regulation of cyclic−nucleotide phosphodiesterase activity
(Protein count)
0
5
10
15
20
p.adjust
1e-04
2e-04
3e-04
4e-04
5e-04
E
GO Term: Molecular Function
snoRNA binding
Disordered domain specific binding
actin binding
Adenylate cyclase binding
Protein phosphatase activator activity
Titin binding
Calmodulin binding
(Protein count)
0
3
6
9
12
p.adjust
0.001
0.002
0.003
0.004
0.005
F
GO Term: Cellular contents
Preribosome
Myosin II complex
Spindle microtubule
Spliceosomal complex
snoRNA complex
Nuclear periphery
Cell−substrate junction
(Protein count)
0
3
6
9
12
p.adjust
0.00025
0.00050
0.00075
G
snoRNP complex
RPF1
SRSF10
RRP1
IMP4
MYBBP1A
RRP12
SRSF12
RBMX
PSIP1
EBNA1BP2
PDCD11
DDX54
NHP2
RRS1
NOP58
EIF3I
SNU13
BMS1
NOP56
WDR46
RBM14
RBM34
SAP18
PPP1R12A
GNG12
RBX1
GNAI3
HNRNPDLL
PRC1
MASTLE
RBMXL2
EDF1
SPTAN1
SAFB2
PNN
RBMXL1
CFL1
LMNB1
MAT2B
SERF2
CALM3
FAM32A
CLTC
LMO7
STOM
BST2
CALM1
CORO1B
ACIN1
MYH11
MAT2A
SEC61A1
SAFB
SPTBN1
MYL3
CALM2
RBM3
LIMA1
MYH14
PESE1
RPL30
TMA7
ZNF326
DYNLL1
PHF14
LIMCH1
CTTN
EPPK1
MYL1
GNB1
DSG2
PHF14
NUMA1
DDX41
CBX5
SNRPAE
MKI67
SONE
MYO1B
LMNB2
IMMT
CENPVE
Protein score fold change (over control)
50
25
0
MAT2A interacting proteome related to ribosome biogeneis or function

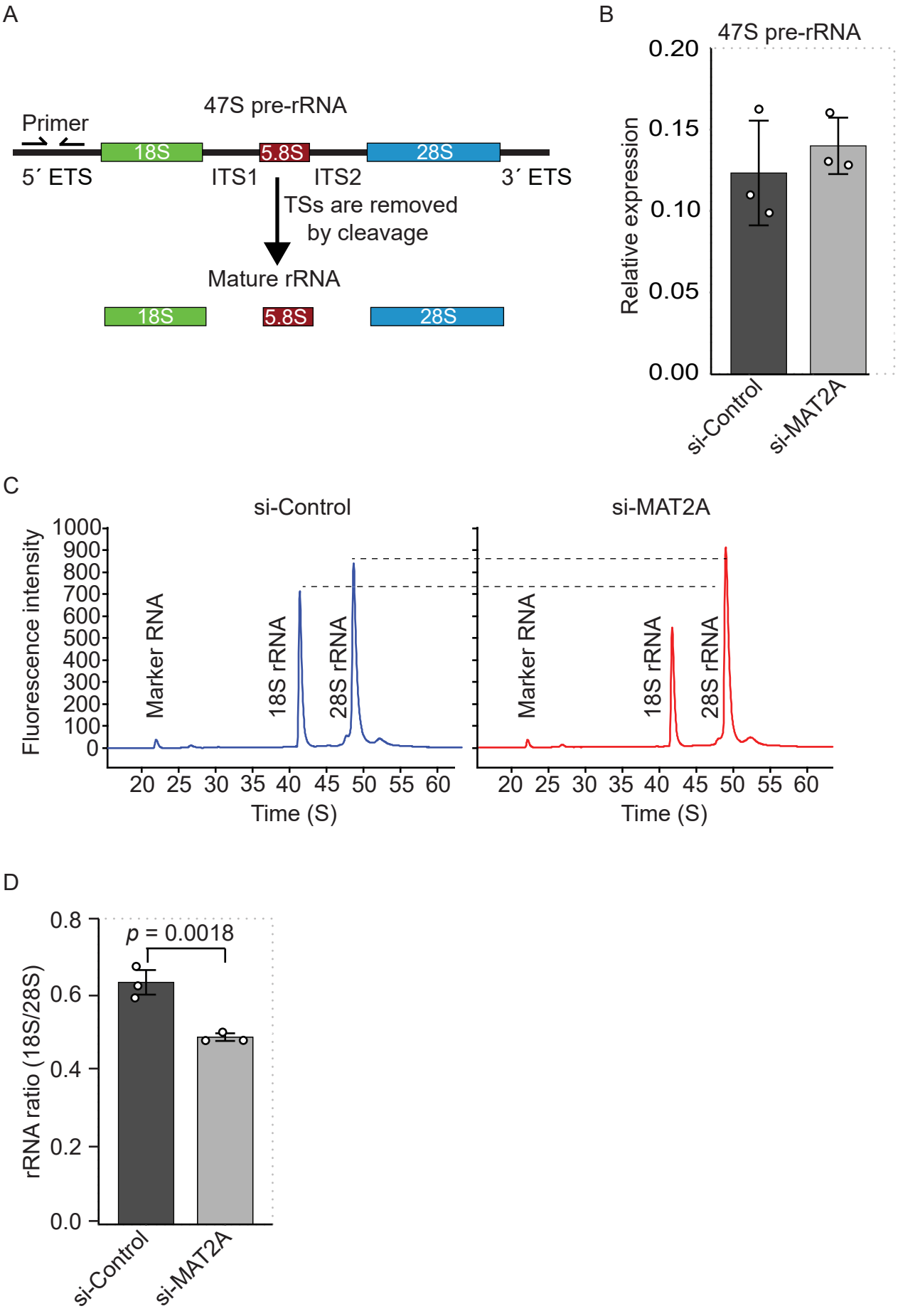
A
47S pre-rRNA
Primer
18S
5.8S
28S
5′ ETS
ITS1
ITS2
3′ ETS
TSs are removed
by cleavage
Mature rRNA
18S
5.8S
28S
B
47S pre-rRNA
Relative expression
0.20
0.15
0.10
0.05
0.00
si-Control
si-MAT2A
C
si-Control
si-MAT2A
Fluorescence intensity
1000
900
800
700
600
500
400
300
200
100
0
Marker RNA
18S rRNA
28S rRNA
20 25 30 35 40 45 50 55 60
Time (S)
D
p = 0.0018
rRNA ratio (18S/28S)
0.8
0.6
0.4
0.2
0.0
si-Control
si-MAT2A

A

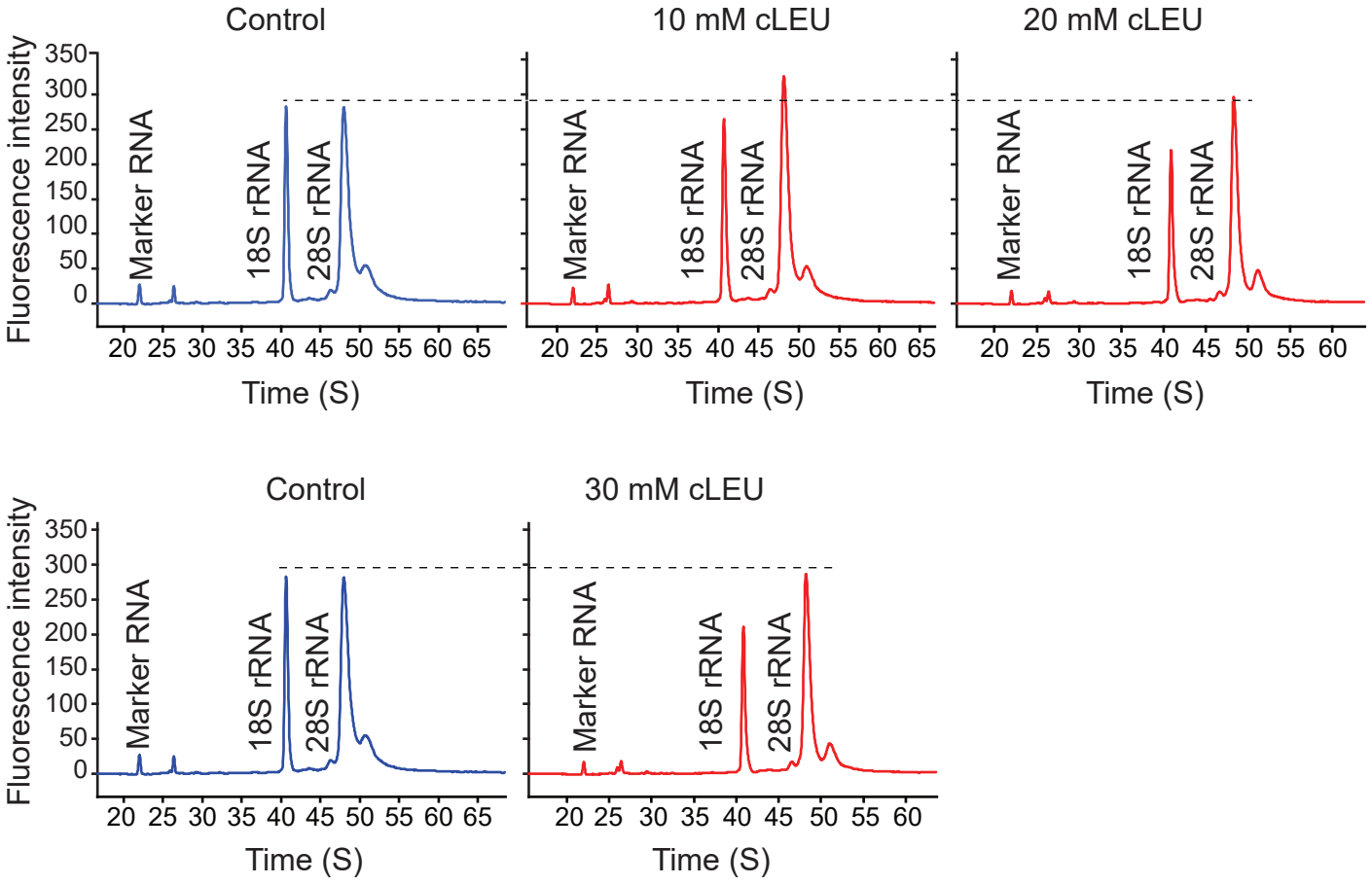
Control
10 mM cLEU
20 mM cLEU
Fluorescence intensity
Marker RNA
18S rRNA
28S rRNA
Time (S)
Control
30 mM cLEU

B

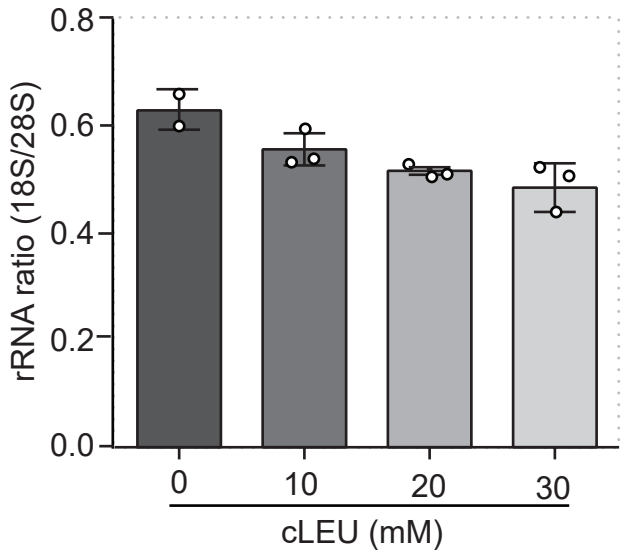
rRNA ratio (18S/28S)
cLEU (mM)

Figure 12

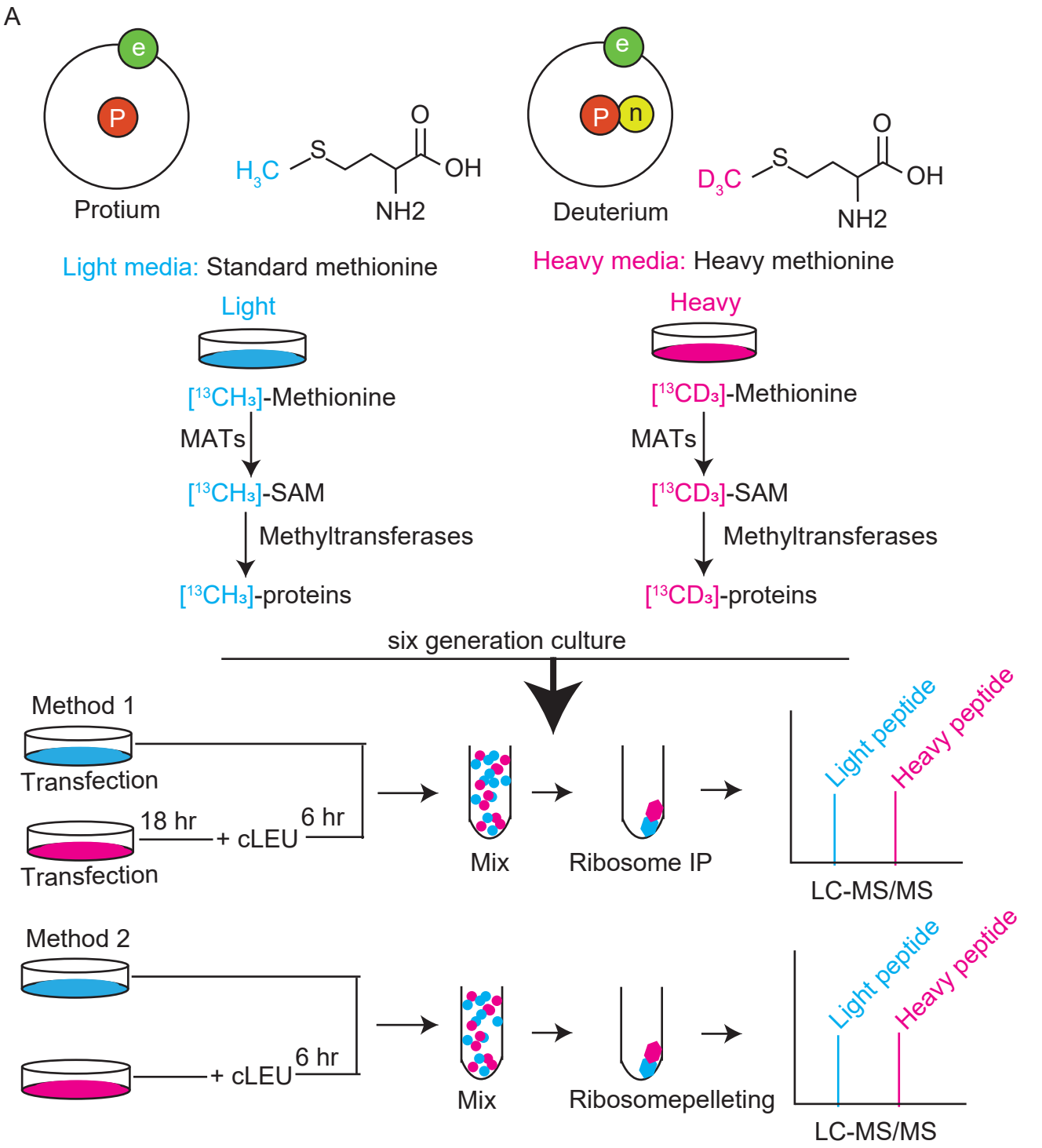
A
e
P
Protium
H3C
S
O
OH
NH2
e
P
n
Deuterium
D3C
S
O
OH
NH2
Light media: Standard methionine
Heavy media: Heavy methionine
Light
[13CH3]-Methionine
MATs
[13CH3]-SAM
Methyltransferases
[13CH3]-proteins
Heavy
[13CD3]-Methionine
MATs
[13CD3]-SAM
Methyltransferases
[13CD3]-proteins
six generation culture
Method 1
Transfection
18 hr
+ cLEU
6 hr
Transfection
Mix
Ribosome IP
Light peptide
Heavy peptide
LC-MS/MS
Method 2
+ cLEU
6 hr
Mix
Ribosomepelleting
Light peptide
Heavy peptide
LC-MS/MS

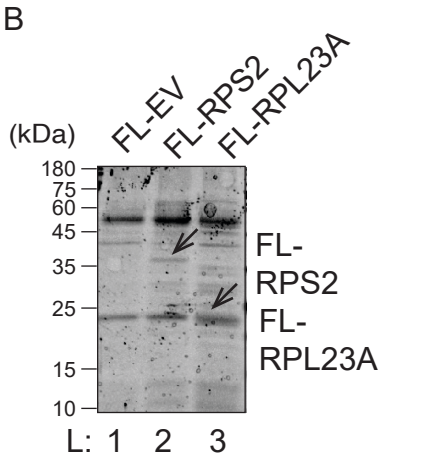
B
(kDa)
FL-EV
FL-RPS2
FL-RPL23A
180
75
60
45
35
25
15
10
FL-RPS2
FL-RPL23A
L: 1 2 3

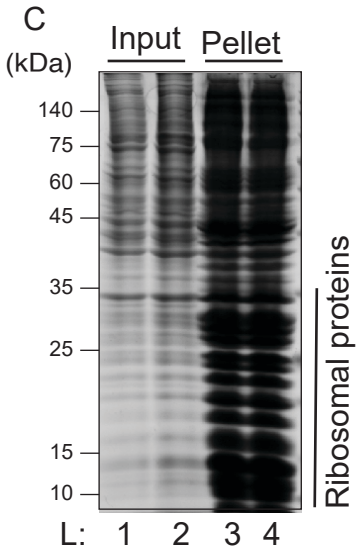
C
(kDa)
Input
Pellet
140
75
60
45
35
25
15
10
Ribosomal proteins
L: 1 2 3 4

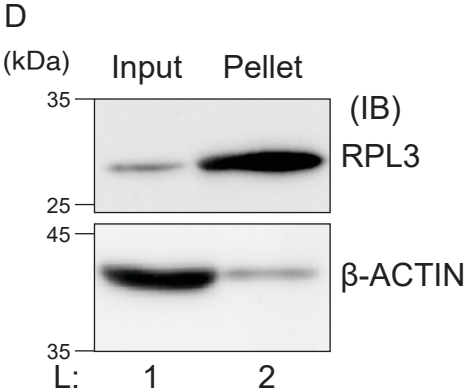
D
(kDa)
Input
Pellet
35
25
(IB)
RPL3
45
35
β-ACTIN
L: 1 2

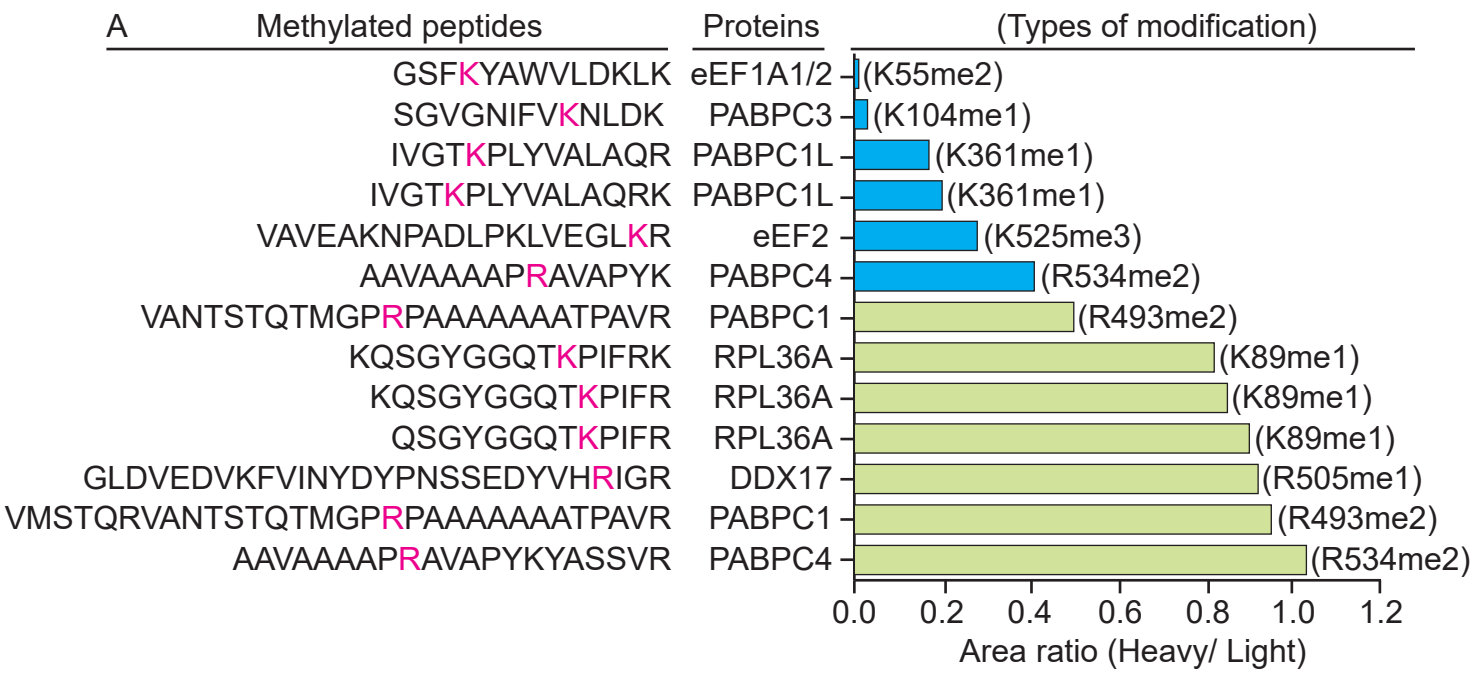
A
Methylated peptides
Proteins
(Types of modification)
GSFKYAWVLDKLK
eEF1A1/2
(K55me2)
SGVGNIFVKNLDK
PABPC3
(K104me1)
IVGTKPLYVALAQR
PABPC1L
(K361me1)
IVGTKPLYVALAQRK
PABPC1L
(K361me1)
VAVEAKNPADLPKLVEGLKR
eEF2
(K525me3)
AAVAAAAPRAVAPYK
PABPC4
(R534me2)
VANTSTQTMGPRPAAAAAAATPAVR
PABPC1
(R493me2)
KQSGYGGQTKPIFRK
RPL36A
(K89me1)
KQSGYGGQTKPIFR
RPL36A
(K89me1)
QSGYGGQTKPIFR
RPL36A
(K89me1)
GLDVEDVKFVINYDYPNSSEDYVHRIGR
DDX17
(R505me1)
VMSTQRVANTSTQTMGPRPAAAAAAATPAVR
PABPC1
(R493me2)
AAVAAAAPRAVAPYKYASSVR
PABPC4
(R534me2)
0.0
0.2
0.4
0.6
0.8
1.0
1.2
Area ratio (Heavy/ Light)

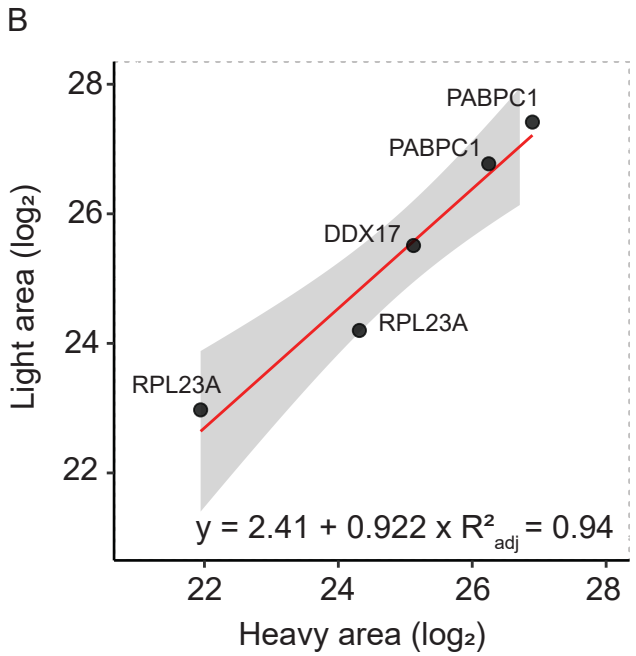
B
28
26
24
22
Light area (log₂)
PABPC1
PABPC1
DDX17
RPL23A
RPL23A
y = 2.41 + 0.922 x R²adj = 0.94
22
24
26
28
Heavy area (log₂)

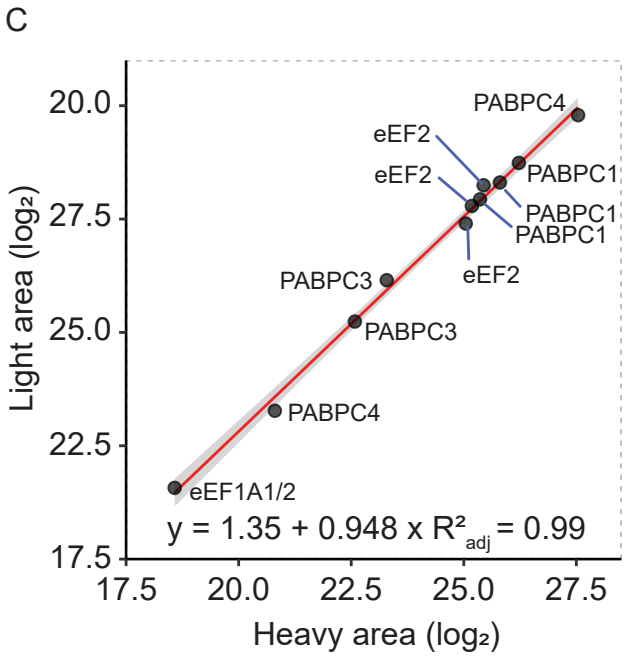
C
20.0
27.5
25.0
22.5
17.5
Light area (log₂)
PABPC4
eEF2
eEF2
PABPC1
PABPC1
PABPC1
eEF2
PABPC3
PABPC3
PABPC4
eEF1A1/2
y = 1.35 + 0.948 x R²adj = 0.99
17.5
20.0
22.5
25.0
27.5
Heavy area (log₂)

A

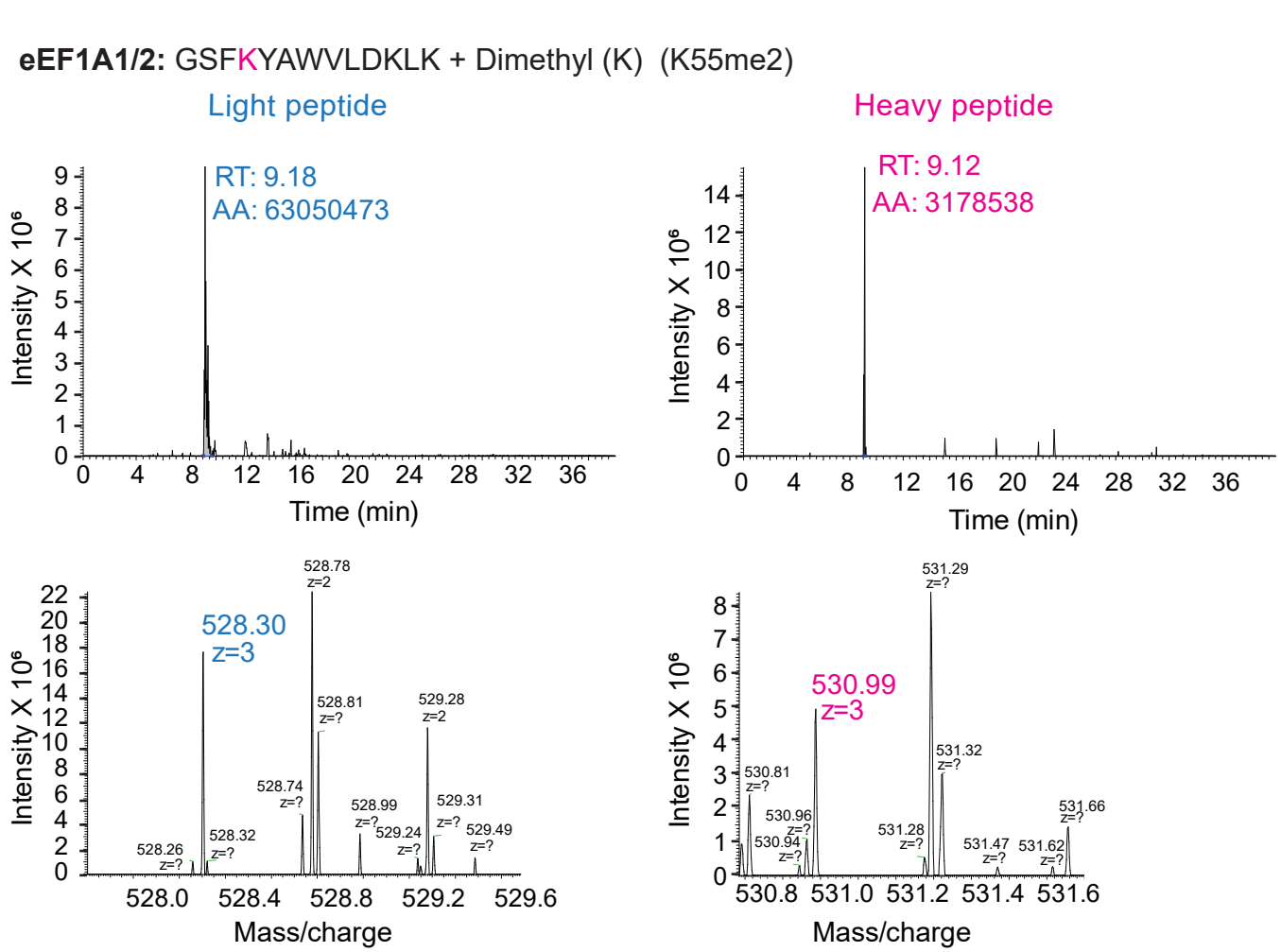
eEF1A1/2: GSFKYAWVLDKLK + Dimethyl (K) (K55me2)
Light peptide
Heavy peptide
RT: 9.18
AA: 63050473
RT: 9.12
AA: 3178538
Intensity X 10⁶
Time (min)
528.30
z=3
530.99
z=3
Mass/charge

B

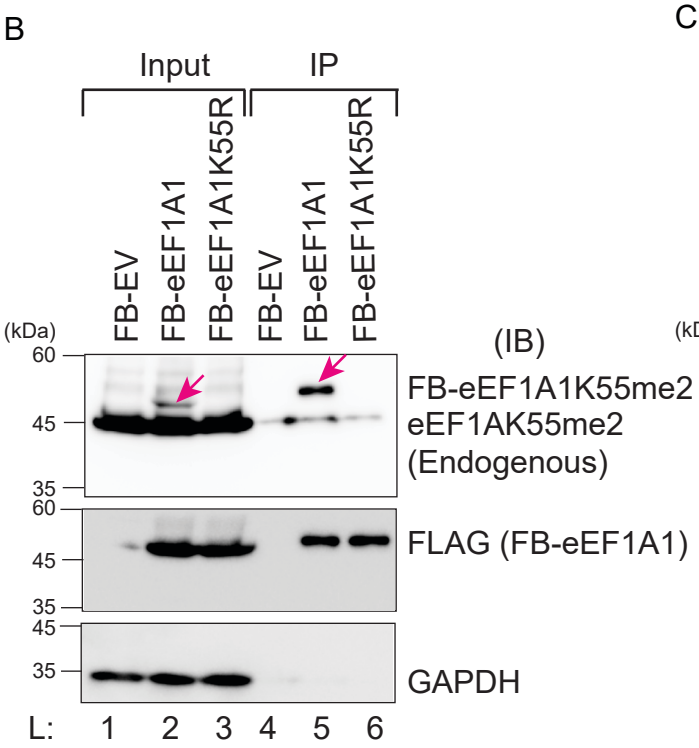
Input
IP
FB-EV
FB-eEF1A1
FB-eEF1A1K55R
(kDa)
(IB)
FB-eEF1A1K55me2
eEF1AK55me2
(Endogenous)
FLAG (FB-eEF1A1)
GAPDH
L: 1 2 3 4 5 6

C

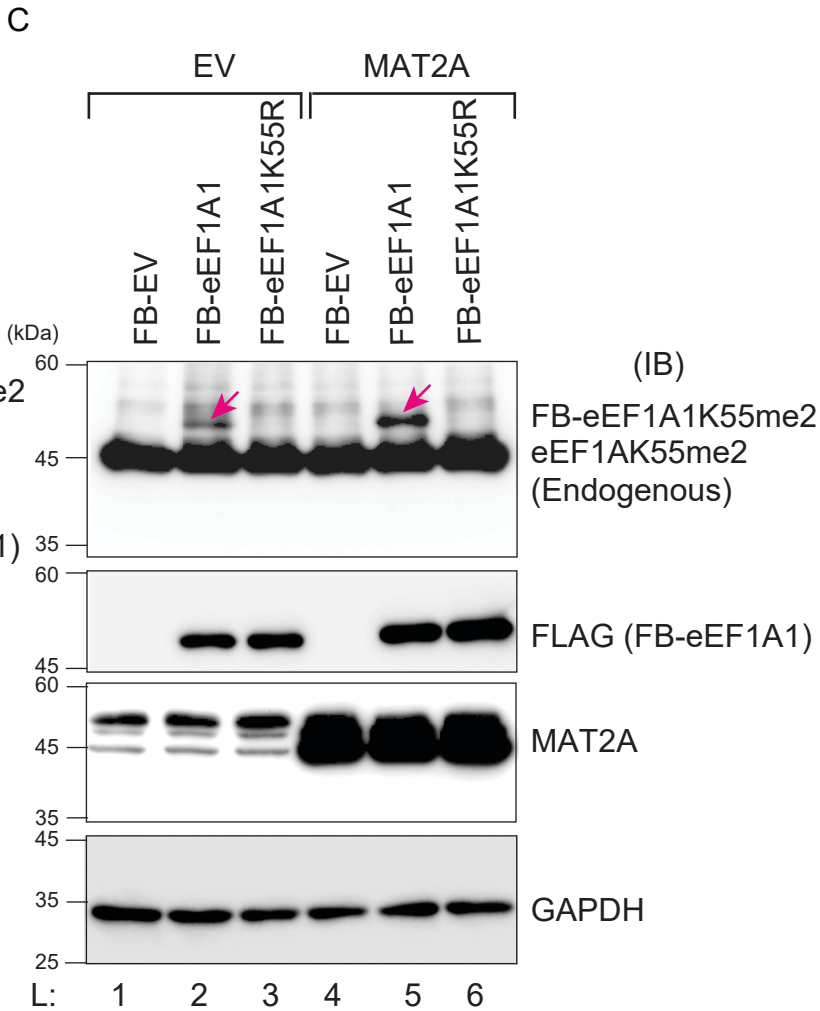
EV
MAT2A
FB-EV
FB-eEF1A1
FB-eEF1A1K55R
(kDa)
(IB)
FB-eEF1A1K55me2
eEF1AK55me2
(Endogenous)
FLAG (FB-eEF1A1)
MAT2A
GAPDH
L: 1 2 3 4 5 6

Figure 15

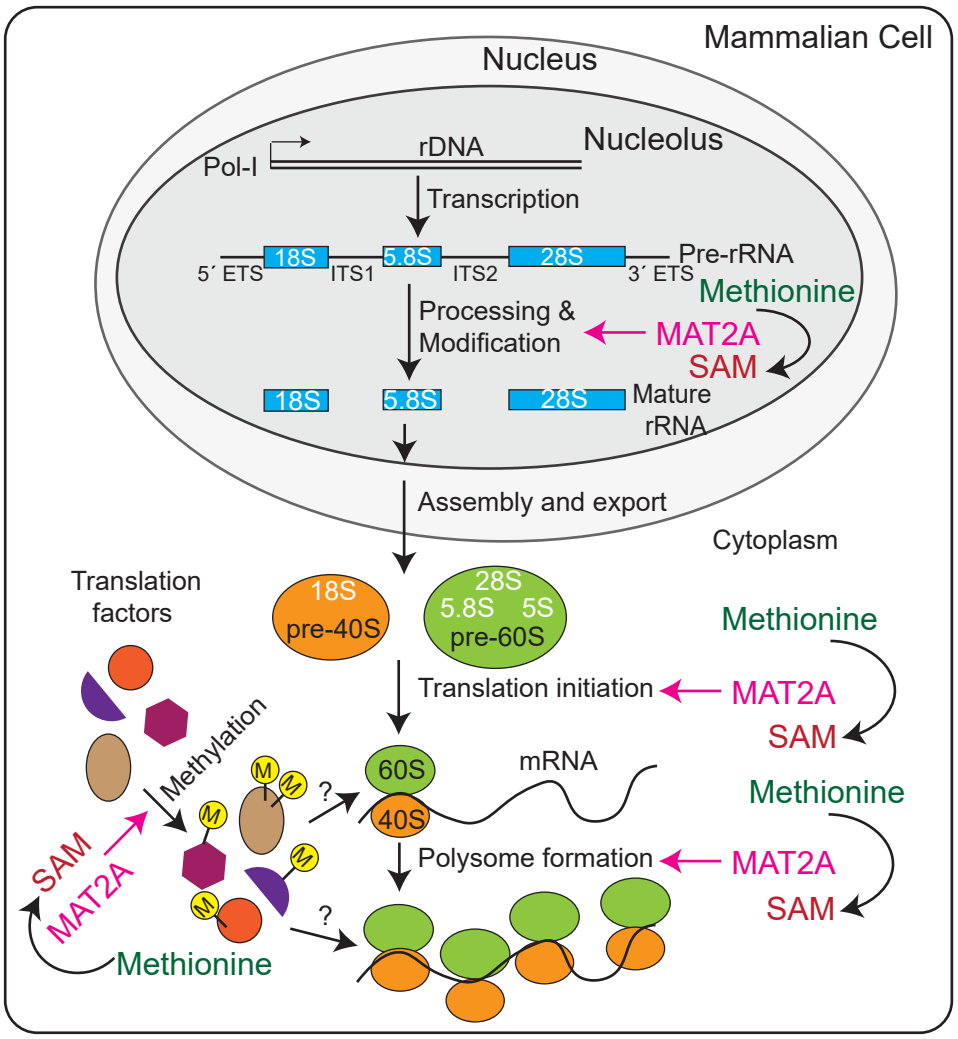
Mammalian Cell
Nucleus
Nucleolus
Pol-I
rDNA
Transcription
5´ ETS
18S
ITS1
5.8S
ITS2
28S
3´ ETS
Pre-rRNA
Methionine
Processing &
Modification
MAT2A
SAM
18S
5.8S
28S
Mature
rRNA
Assembly and export
Cytoplasm
Translation
factors
18S
pre-40S
28S
5.8S
5S
pre-60S
Methionine
Translation initiation
MAT2A
SAM
Methylation
60S
mRNA
40S
Methionine
SAM
MAT2A
Polysome formation
MAT2A
SAM
Methionine
?
?

Table 1

Number	Gene ID	Genes	TE. Change (log2)	Devience	padj.TE
1	rna-NM_020675.4	SPC25	3.759	0.872	1.000
2	rna-XM_011513398.2	ZNF595	2.083	5.952	1.000
3	rna-NM_001286054.1	ZNF595	2.083	5.952	1.000
4	rna-NM_182524.4	ZNF595	2.083	5.952	1.000
5	rna-NM_005514.8	HLA-B	2.039	2.741	1.000
6	rna-XR_926304.2	VARS	4.046	1.700	1.000
7	rna-XM_005249362.2	VARS	3.735	1.682	1.000
8	rna-NM_006295.3	VARS	3.735	1.682	1.000
9	rna-XM_024446537.1	VARS	3.735	1.682	1.000
10	rna-XM_017011246.1	VARS	3.735	1.682	1.000
11	rna-NM_001300906.2	IBTK	2.363	2.748	1.000
12	rna-NM_015525.4	IBTK	2.363	2.748	1.000
13	rna-XM_006715454.3	IBTK	2.363	2.748	1.000
14	rna-XM_006715453.3	IBTK	2.363	2.748	1.000
15	rna-XM_024447333.1	NAPRT	4.726	4.069	1.000
16	rna-XM_017013977.2	NAPRT	4.726	4.069	1.000
17	rna-XM_017013978.2	NAPRT	4.650	4.108	1.000
18	rna-XM_017013975.2	NAPRT	4.689	4.071	1.000
19	rna-XM_024447332.1	NAPRT	4.686	4.105	1.000
20	rna-XM_017013979.2	NAPRT	4.693	4.087	1.000
21	rna-XM_017013976.2	NAPRT	4.689	4.071	1.000
22	rna-NM_001363146.1	NAPRT	4.689	4.071	1.000
23	rna-NM_001363145.1	NAPRT	4.726	4.069	1.000
24	rna-NM_001286829.2	NAPRT	4.689	4.071	1.000
25	rna-NM_145201.6	NAPRT	4.689	4.071	1.000
26	rna-NM_138565.2	CTTN	6.781	1.666	0.000
27	rna-NM_005231.4	CTTN	6.781	1.666	0.000
28	rna-NM_001184740.2	CTTN	7.012	1.597	0.000
29	rna-XM_006718447.3	CTTN	6.775	1.647	0.000
30	rna-XM_006718448.4	CTTN	9.214	1.558	0.000
31	rna-XM_017017312.2	CTTN	9.251	1.567	0.000
32	rna-XR_001747729.1	HYOU1	2.229	3.402	1.000
33	rna-XR_002957117.1	HYOU1	2.229	3.402	1.000
34	rna-XM_005271392.4	HYOU1	2.229	3.402	1.000
35	rna-XM_005271393.3	HYOU1	2.229	3.402	1.000
36	rna-XM_017017095.1	HYOU1	2.229	3.402	1.000
37	rna-XM_017017097.1	HYOU1	2.229	3.402	1.000
38	rna-XM_017017096.1	HYOU1	2.229	3.402	1.000
39	rna-XM_005271394.3	HYOU1	2.229	3.402	1.000
40	rna-NM_001130991.3	HYOU1	2.229	3.402	1.000
41	rna-NM_006389.5	HYOU1	2.229	3.402	1.000
42	rna-NR_137631.1	NEDD8-MDP1	3.412	1.482	1.000
43	rna-NR_137630.1	NEDD8-MDP1	2.980	1.613	1.000
44	rna-NR_137632.1	NEDD8-MDP1	3.412	1.482	1.000
45	rna-NM_001199823.2	NEDD8-MDP1	3.408	1.483	1.000
46	rna-NM_006156.3	NEDD8	2.392	1.863	1.000
47	rna-NR_024058.1	YWHAE	2.439	0.791	1.000
48	rna-NM_006761.5	YWHAE	2.439	0.791	1.000
49	rna-XM_017025005.2	YWHAE	2.439	0.791	1.000
50	rna-XM_005256784.4	YWHAE	2.439	0.791	1.000
51	rna-XR_002958293.1	PRPF31	6.592	2.515	1.000
52	rna-XR_935789.3	PRPF31	6.592	2.515	1.000
53	rna-XM_006723137.4	PRPF31	6.592	2.515	1.000
54	rna-NM_015629.4	PRPF31	6.592	2.515	1.000
55	gene-RNA45SN1	RNA45SN1	2.470	3.020	1.000
56	rna-NR_145819.1	RNA45SN1	2.470	3.020	1.000
57	gene-RNA18SN1	RNA18SN1	2.130	5.373	1.000
58	rna-NR_145820.1	RNA18SN1	2.130	5.373	1.000
59	gene-RNA28SN1	RNA28SN1	2.717	2.564	1.000
60	rna-NR_145822.1	RNA28SN1	2.717	2.564	1.000
61	rna-NM_006140.5-2	CSF2RA	3.225	2.358	1.000
62	rna-NM_172246.3-2	CSF2RA	3.225	2.358	1.000

Table 1 (Continue)

Number	Gene ID	Genes	TE. Change (log2)	Devience	padj.TE
63	rna-NM_172249.3-2	CSF2RA	3.024	2.388	1.000
64	rna-NM_172245.3-2	CSF2RA	3.225	2.358	1.000
65	rna-NM_001364241.2-2	HNRNPH1	2.346	0.959	1.000
66	rna-NM_001364227.2-2	HNRNPH1	2.346	0.959	1.000
67	rna-NM_001364236.2-2	HNRNPH1	2.346	0.959	1.000
68	rna-NM_001364237.2-2	HNRNPH1	2.346	0.959	1.000
69	rna-NM_001364251.2-2	HNRNPH1	2.346	0.959	1.000
70	rna-NM_001364254.2-2	HNRNPH1	2.346	0.959	1.000
71	rna-NM_001364242.2-2	HNRNPH1	2.346	0.959	1.000
72	rna-NM_001364240.2-2	HNRNPH1	2.346	0.959	1.000
73	rna-NM_001364247.2-2	HNRNPH1	2.346	0.959	1.000
74	rna-NM_001364228.2-2	HNRNPH1	2.346	0.959	1.000
75	rna-NM_005520.3-2	HNRNPH1	2.346	0.959	1.000
76	rna-NM_001364231.2-2	HNRNPH1	2.346	0.959	1.000
77	rna-NM_001364230.2-2	HNRNPH1	2.346	0.959	1.000
78	rna-NM_001363572.2-2	HNRNPH1	2.346	0.959	1.000
79	rna-NM_001364250.2-2	HNRNPH1	2.348	0.957	1.000
80	rna-NM_001364252.2-2	HNRNPH1	2.346	0.959	1.000
81	rna-NM_001364255.2-2	HNRNPH1	2.346	0.959	1.000
82	rna-NM_001364248.2-2	HNRNPH1	2.346	0.959	1.000
83	rna-NM_001364246.2-2	HNRNPH1	2.346	0.959	1.000
84	rna-NM_001364244.2-2	HNRNPH1	2.346	0.959	1.000
85	rna-NM_001364229.2-2	HNRNPH1	2.346	0.959	1.000
86	rna-NM_001257293.2-2	HNRNPH1	2.346	0.959	1.000
87	rna-NM_001364232.2-2	HNRNPH1	2.346	0.959	1.000
88	rna-NM_001364245.2-2	HNRNPH1	2.346	0.959	1.000
89	rna-NM_001364238.2-2	HNRNPH1	2.346	0.959	1.000
90	rna-NM_001364243.2-2	HNRNPH1	2.346	0.959	1.000
91	rna-NM_001364239.2-2	HNRNPH1	2.346	0.959	1.000
92	rna-NM_001364233.1-2	HNRNPH1	2.341	0.960	1.000
93	rna-NM_001364225.1-2	HNRNPH1	2.341	0.960	1.000
94	rna-NM_001364253.1-2	HNRNPH1	2.341	0.960	1.000
95	rna-NM_001364235.1-2	HNRNPH1	2.341	0.960	1.000
96	rna-NM_001364234.1-2	HNRNPH1	2.341	0.960	1.000
97	rna-NM_001364226.1-2	HNRNPH1	2.341	0.960	1.000
98	rna-NM_004551.3-2	NDUFS3	2.286	4.870	1.000
99	rna-NM_001028.3-2	RPS25	2.737	0.830	1.000
100	rna-NM_003366.4-2	UQCRC2	2.743	3.511	1.000
101	rna-NM_013234.4-2	EIF3K	2.873	1.033	1.000
102	rna-NM_001300992.2-2	EIF3K	2.873	1.033	1.000
103	rna-NM_001308393.2-2	EIF3K	2.873	1.033	1.000
104	rna-NM_001005335.2-2	HNRNPL	2.000	4.722	1.000
105	rna-NR_147845.1-2	NMRAL1	3.348	2.166	1.000
106	rna-NM_001351994.1-2	NMRAL1	3.384	2.148	1.000
107	rna-NM_020677.6-2	NMRAL1	3.384	2.148	1.000
108	rna-NM_001305142.3-2	NMRAL1	3.393	2.110	1.000
109	rna-NM_001351996.2-2	NMRAL1	3.476	2.054	1.000
110	rna-NM_001305141.3-2	NMRAL1	3.393	2.110	1.000
111	rna-NM_001351995.2-2	NMRAL1	3.398	2.105	1.000
112	rna-NM_139215.3-2	TAF15	2.930	3.800	1.000
113	rna-NM_003487.4-2	TAF15	2.930	3.800	1.000
114	rna-NM_012138.4-2	AATF	4.155	3.411	1.000
115	rna-NR_104195.1-2	PSMB3	4.226	1.225	1.000
116	rna-NR_104194.1-2	PSMB3	4.239	1.224	1.000
117	rna-NM_002795.4-2	PSMB3	4.226	1.225	1.000
118	rna-NM_001114093.2-2	LSM14A	2.777	1.063	1.000
119	rna-NM_015578.3-2	LSM14A	2.777	1.063	1.000
120	rna-NM_006295.3-3	VARS	5.129	2.082	1.000

Table 2

Number	Gene ID	Genes	TE change (log2)	Devience	padj. TE
1	rna-NM_001014840.2	CUTA	-3.56686351	2.86135269	0.999989744
2	rna-NM_001014837.2	CUTA	-3.547651155	2.86624632	0.999989744
3	rna-NM_001014838.2	CUTA	-3.547651155	2.86624632	0.999989744
4	rna-NM_015921.3	CUTA	-3.547651155	2.86624632	0.999989744
5	rna-NM_001014433.2	CUTA	-3.56686351	2.86135269	0.999989744
6	rna-XM_011516409.3	BCAP29	-2.82751943	0.88568938	0.999989744
7	rna-XM_017012438.2	BCAP29	-2.920913118	0.9497051	0.999989744
8	rna-XM_017012437.2	BCAP29	-2.82751943	0.88568938	0.999989744
9	rna-XM_011519959.2	MTCH2	-2.860213396	5.141995	0.999989744
10	rna-XM_011519960.3	MTCH2	-2.860213396	5.141995	0.999989744
11	rna-XM_011519961.2	MTCH2	-2.860213396	5.141995	0.999989744
12	rna-NM_001317232.1	MTCH2	-2.864432665	5.14793275	0.999989744
13	rna-NM_001317233.1	MTCH2	-2.864432665	5.14793275	0.999989744
14	rna-NM_001317231.1	MTCH2	-2.864432665	5.14793275	0.999989744
15	rna-XM_006718172.2	MTCH2	-2.864432665	5.14793275	0.999989744
16	rna-XM_017017462.2	MTCH2	-2.864432665	5.14793275	0.999989744
17	rna-NM_014342.4	MTCH2	-2.864432665	5.14793275	0.999989744
18	rna-NR_106990.1	MIR7703	-2.857761259	2.05288012	0.999989744
19	rna-MIR7703	MIR7703	-2.857761259	2.05288012	0.999989744
20	rna-NR_051979.1	IPO4	-5.63368935	1.46325516	0.999989744
21	rna-NM_024658.4	IPO4	-5.63368935	1.46325516	0.999989744
22	rna-NM_003366.4	UQCRC2	-2.220197556	0.99670826	0.999989744
23	rna-XM_017022815.2	NPIPB9	-2.3113244	1.11681976	0.999989744
24	rna-NR_037609.1	SLX1B-SULT1A4	-3.346056793	2.78485268	0.999989744
25	rna-NM_001256264.2	FLII	-2.414506947	4.068364	0.999989744
26	rna-NM_001256265.2	FLII	-2.423619721	4.07472799	0.999989744
27	rna-NM_002018.4	FLII	-2.414506947	4.068364	0.999989744
28	rna-XM_005256558.3	FLII	-2.414506947	4.068364	0.999989744
29	rna-XM_005256556.4	FLII	-2.414506947	4.068364	0.999989744
30	rna-XM_005256555.4	FLII	-2.414506947	4.068364	0.999989744
31	rna-NM_018154.3	ASF1B	-2.268748557	1.13061456	0.999989744
32	rna-XR_002958336.1	PSMC4	-2.990131048	22.9646289	0.999989744
33	rna-NM_153001.2	PSMC4	-2.99646747	22.8318884	0.999989744
34	rna-NM_006503.4	PSMC4	-2.99646747	22.8318884	0.999989744
35	rna-XR_001754916.2	CBS	-2.039565585	3.52782029	0.999989744
36	rna-XR_002958634.1	CBS	-2.041773108	3.55392433	0.999989744
37	rna-XR_001754915.1	CBS	-2.206398065	3.40952608	0.999989744
38	rna-XR_001754917.2	CBS	-2.081144757	3.64099957	0.999989744
39	rna-XM_017028491.2	CBS	-2.039565585	3.52782029	0.999989744
40	rna-XM_024452140.1	CBS	-2.032077645	3.49775323	0.999989744
41	rna-XM_024452137.1	CBS	-2.034377752	3.49905455	0.999989744
42	rna-XM_011529774.2	CBS	-2.198025855	3.39937909	0.999989744
43	rna-NM_001320298.1	CBS	-2.038347317	3.5454755	0.999989744
44	rna-XM_024452139.1	CBS	-2.030911816	3.51494089	0.999989744
45	rna-NM_001178008.2	CBS	-2.038347317	3.5454755	0.999989744
46	rna-XM_024452138.1	CBS	-2.030911816	3.51494089	0.999989744
47	rna-NM_001178009.3	CBS	-2.039565585	3.52782029	0.999989744
48	rna-NM_000071.2	CBS	-2.038347317	3.5454755	0.999989744
49	rna-XM_011529777.2	CBS	-2.032750799	3.56136616	0.999989744
50	rna-XM_024452136.1	CBS	-2.027621884	3.53166481	0.999989744
51	rna-NM_001321072.1	CBS	-2.200429094	3.40092178	0.999989744
52	rna-XM_011529783.2	CBS	-2.194286257	3.41562073	0.999989744
53	rna-NM_001082579.2	RBFOX2	-2.298407607	2.24256284	0.999989744
54	rna-XM_017028688.1	RBFOX2	-2.266905052	2.23743377	0.999989744
55	rna-XM_005261432.2	RBFOX2	-2.266905052	2.23743377	0.999989744
56	rna-XM_005261429.2	RBFOX2	-2.266905052	2.23743377	0.999989744
57	rna-XM_006724186.2	RBFOX2	-2.266905052	2.23743377	0.999989744
58	rna-XM_005261433.2	RBFOX2	-2.266905052	2.23743377	0.999989744
59	rna-XM_005261430.2	RBFOX2	-2.266905052	2.23743377	0.999989744
60	rna-XM_005261428.2	RBFOX2	-2.266905052	2.23743377	0.999989744
61	rna-XM_006724188.2	RBFOX2	-2.266905052	2.23743377	0.999989744
62	rna-XM_006724187.2	RBFOX2	-2.266905052	2.23743377	0.999989744

Table 2 (Continue)

Number	Gene ID	Genes	TE change (log2)	Devience	padj. TE
63	rna-XM_006724185.2	RBFOX2	-2.266905052	2.23743377	0.999989744
64	rna-NM_001082578.3	RBFOX2	-2.266905052	2.23743377	0.999989744
65	rna-NM_001349999.1	RBFOX2	-2.298407607	2.24256284	0.999989744
66	rna-XM_017028686.1	RBFOX2	-2.369189397	2.2100612	0.999989744
67	rna-XM_024452189.1	RBFOX2	-2.351155042	2.21541517	0.999989744
68	rna-XM_017028697.1	RBFOX2	-2.351155042	2.21541517	0.999989744
69	rna-XM_006724189.3	RBFOX2	-2.37710312	2.20786807	0.999989744
70	rna-NM_001349995.2	RBFOX2	-2.37710312	2.20786807	0.999989744
71	rna-NM_001349994.2	RBFOX2	-2.37710312	2.20786807	0.999989744
72	rna-NM_001349990.2	RBFOX2	-2.37710312	2.20786807	0.999989744
73	rna-NM_001349982.2	RBFOX2	-2.37710312	2.20786807	0.999989744
74	rna-NM_001349992.2	RBFOX2	-2.37710312	2.20786807	0.999989744
75	rna-NM_001349989.2	RBFOX2	-2.37710312	2.20786807	0.999989744
76	rna-NM_001349991.2	RBFOX2	-2.37710312	2.20786807	0.999989744
77	rna-NM_001349996.2	RBFOX2	-2.37710312	2.20786807	0.999989744
78	rna-XM_017028687.2	RBFOX2	-2.37710312	2.20786807	0.999989744
79	rna-XM_024452188.1	RBFOX2	-2.37710312	2.20786807	0.999989744
80	rna-XM_024452191.1	RBFOX2	-2.41498206	2.20186088	0.999989744
81	rna-XM_006724192.2	RBFOX2	-2.41498206	2.20186088	0.999989744
82	rna-XM_017028691.1	RBFOX2	-2.41498206	2.20186088	0.999989744
83	rna-XM_017028690.1	RBFOX2	-2.41498206	2.20186088	0.999989744
84	rna-XM_017028698.1	RBFOX2	-2.497289609	2.30650386	0.999989744
85	rna-XM_017028696.1	RBFOX2	-2.497289609	2.30650386	0.999989744
86	rna-XM_017028693.1	RBFOX2	-2.497289609	2.30650386	0.999989744
87	rna-XM_006724191.1	RBFOX2	-2.497289609	2.30650386	0.999989744
88	rna-XM_024452190.1	RBFOX2	-2.253600004	2.47870685	0.999989744
89	rna-NM_001082576.3	RBFOX2	-2.497289609	2.30650386	0.999989744
90	rna-NM_001349983.2	RBFOX2	-2.497289609	2.30650386	0.999989744
91	rna-NM_001082577.3	RBFOX2	-2.497289609	2.30650386	0.999989744
92	rna-NM_001031695.4	RBFOX2	-2.497289609	2.30650386	0.999989744
93	rna-NM_001349998.2	RBFOX2	-2.497289609	2.30650386	0.999989744
94	rna-NM_014309.4	RBFOX2	-2.497289609	2.30650386	0.999989744
95	rna-NM_001349997.2	RBFOX2	-2.497289609	2.30650386	0.999989744
96	rna-XM_024452192.1	RBFOX2	-2.41498206	2.20186088	0.999989744
97	rna-XM_006724194.2	RBFOX2	-2.41498206	2.20186088	0.999989744
98	rna-XM_006724193.3	RBFOX2	-3.402000211	2.13710035	0.999989744
99	rna-NR_028057.2-2	PLCXD1	-2.436761145	2.80518028	0.999989744
100	rna-NR_163416.1-2	PLCXD1	-2.225390943	2.57855033	0.999989744
101	rna-NR_135623.1-2	CD99	-2.229665722	4.05456978	0.999989744
102	rna-NM_002414.5-2	CD99	-2.229665722	4.05456978	0.999989744
103	rna-NM_001321368.2-2	CD99	-2.229665722	4.05456978	0.999989744
104	rna-NM_001321370.2-2	CD99	-2.229665722	4.05456978	0.999989744
105	rna-NM_001122898.3-2	CD99	-2.229665722	4.05456978	0.999989744
106	rna-NM_001321369.2-2	CD99	-2.229665722	4.05456978	0.999989744
107	rna-NM_001142298.2-2	SQSTM1	-2.835549644	0.88701589	0.999989744
108	rna-NM_001142299.2-2	SQSTM1	-2.839825952	0.88850262	0.999989744
109	rna-NM_003900.5-2	SQSTM1	-2.88390826	0.86839552	0.999989744
110	rna-NM_005526.4-2	HSF1	-3.177246502	10.2427556	0.087588672
111	rna-NM_001077180.2-2	METTL9	-2.033801717	1.6386866	0.999989744
112	rna-NM_016025.5-2	METTL9	-2.033801717	1.6386866	0.999989744
113	rna-NM_001398.3-2	ECH1	-3.369731566	3.88550589	0.999989744
114	rna-NM_014060.3-2	MCTS1	-4.215217177	0.11355506	0
115	rna-NM_001137554.2-2	MCTS1	-4.238777214	0.1667025	0
116	rna-NM_024830.5-2	LPCAT1	-2.755456433	0.89735799	0.999989744
117	rna-NM_003313.4-2	TSTA3	-2.252503311	1.15462316	0.999989744
118	rna-NM_001317783.2-2	TSTA3	-2.252503311	1.15462316	0.999989744
119	rna-NM_003311.4-2	PHLDA2	-2.692716607	1.16271568	0.999989744
120	rna-NM_001201479.2-2	CORO7-PAM16	-3.255547542	0.85148089	0.999989744
121	rna-NM_016069.11-2	PAM16	-4.32309204	0.83225905	0.999989744
122	rna-NM_006445.4-2	PRPF8	-2.994815656	1.9810357	0.999989744
123	rna-NR_125756.1-2	CHCHD10	-3.661022501	6.15403322	0.999989744
124	rna-NR_125755.1-2	CHCHD10	-3.661022501	6.15403322	0.999989744

Table 2 (Continue)

Number	Gene ID	Genes	TE change (log2)	Devience	padj. TE
125	rna-NM_213720.3-2	CHCHD10	-3.661022501	6.15403322	0.999989744
126	rna-NM_001301339.2-2	CHCHD10	-3.661022501	6.15403322	0.999989744
127	rna-NM_002415.2-2	MIF	-2.3683965	1.44886328	0.999989744
128	rna-NM_001084392.1-2	DDT	-2.395103639	1.26808824	0.999989744
129	rna-NM_001355.4-2	DDT	-2.395103639	1.26808824	0.999989744
130	rna-NM_004638.4-6	PRRC2A	-2.355166159	2.63175527	0.999989744
131	rna-NM_080686.3-6	PRRC2A	-2.355166159	2.63175527	0.999989744
132	rna-NM_014260.3-5	PFDN6	-4.431289966	1.06311755	0.999989744
133	rna-NM_001265596.1-5	PFDN6	-4.431289966	1.06311755	0.999989744
134	rna-NM_001185181.3-5	PFDN6	-4.413902723	1.06777478	0.999989744
135	rna-NM_001265595.2-5	PFDN6	-4.431289966	1.06311755	0.999989744

Table 3

								Control		Ratio vs control	
No.	Gene symbol	Protein name	Protein score	Protein matches significance	Protein sequence significance	Proteuncover	Unique peptides	Protein score	Protein matches	Scores	peptide matches
1	MAT2A	Methionine adenosyltransferase 2A	12807	577	66	76.5	577	111	4	115	144
2	MAT2B	Methionine adenosyltransferase 2B	4785	193	43	86.8	193	.	.	.	.
3	LMO7	Lim domain 7	794	47	40	24.2	47	79	6	10	8
4	MKI67	Marker of proliferation ki-67	598	35	33	12.2	35	84	7	7	5
5	LIMA1	Lim domain and actin binding 1	596	24	17	27.7	24	69	4	9	6
6	RBMX	Rna binding motif protein, x-linked	542	28	18	38.9	28	128	5	4	6
7	RBM14	Rna binding motif protein 14	350	15	12	21.8	15	61	4	6	4
8	SPTBN1	Spectrin beta, non-erythrocytic 1	349	12	12	7.4	12	29	1	12	12
9	GNAI3	G protein subunit alpha i3	329	12	10	35.3	9	.	.	.	.
10	RBMXL1	Rna binding motif protein, x-linked like 1	255	13	9	23.1	13	.	.	.	.
11	EDF1	Endothelial differentiation related factor 1	247	9	7	39.9	9	.	.	.	.
12	NOP56	Nop56 ribonucleoprotein	217	10	8	14.8	10	38	3	6	3
13	SAFB2	Scaffold attachment factor B2	199	11	10	15.1	9	.	.	.	.
14	CBX5	Chromobox 5	171	6	5	25.7	5	.	.	.	.
15	STOM	Stomatin	168	5	5	20.5	5	.	.	.	.
16	MYH11	Myosin heavy chain 11	167	7	6	3	7	18	1	9	7
17	NUMA1	Nuclear mitotic apparatus protein 1	165	5	4	3.6	5	35	1	5	5
18	CLTC	Clathrin heavy chain	164	5	5	3.6	5	31	2	5	3
19	DSG2	Desmoglein 2	161	6	6	7.2	6	20	1	8	6
20	BST2	Bone marrow stromal cell antigen 2	159	4	4	18.3	4	.	.	.	.
21	CTTN	Cortactin	152	5	4	16.4	5	.	.	.	.
22	IMMT	Inner membrane mitochondrial protein	152	4	3	5.1	4	.	.	.	.
23	CALM1	Calmodulin 1	148	7	5	46.3	7	28	1	5	7
24	CALM2	Calmodulin 2	148	7	5	46.3	7	28	1	5	7
25	CALM3	Calmodulin 3	148	7	5	46.3	7	28	1	5	7
26	ZNF326	Zinc finger protein 326	147	4	4	10.5	4	28	1	5	4
27	SAFB	Scaffold attachment factor B	143	10	8	13.4	8	.	.	.	.
28	NOP58	Nop58 ribonucleoprotein	140	7	6	12.9	7	39	1	4	7
29	PES1	Pescadillo ribosomal biogenesis factor 1	140	6	5	8.2	6	37	1	4	6
30	RRS1	Ribosome biogenesis regulator homolog	138	9	6	24.7	9	28	1	5	9
31	GNG12	G protein subunit gamma 12	136	3	3	26.4	3	.	.	.	.
32	SPTAN1	Spectrin alpha, non-erythrocytic 1	136	7	7	4.6	7	.	.	.	.
33	SNU13	Snu13 homolog, sno-RNP	133	5	5	39.8	5	53	1	3	5
34	CFL1	Cofilin 1	131	6	5	17.5	6	31	1	4	6
35	DYNLL1	Dynein light chain lc8-type 1	128	3	3	39.3	3	.	.	.	.
36	PPP1R12A	Protein phosphatase 1 regulatory 12A	127	8	7	10.8	8	.	.	.	.
37	ACIN1	Apoptotic chromatin condensation inducer 1	126	5	4	4.5	5	.	.	.	.
38	EBNA1BP2	Ebna1 binding protein 2	122	4	4	12.7	4	.	.	.	.
39	SERF2	Small edrk-rich factor 2	117	4	3	18.6	4	.	.	.	.
40	EIF3I	Eukaryotic translation initiation factor 3I	116	4	4	21.5	4	22	1	5	4
41	LMNB2	Lamin B2	115	3	3	4.7	3	.	.	.	.
42	PNN	Pinin, desmosome associated protein	112	6	5	7.4	6	28	1	4	6
43	LMNB1	Lamin B1	108	3	3	7.5	3	.	.	.	.
44	MYBBP1A	Myb binding protein 1A	107	8	8	7.5	8	37	1	3	8
45	RRP12	Ribosomal rna processing 12 homolog	107	6	6	6.8	6	.	.	.	.
46	LIMCH1	Lim and calponin homology domains 1	105	3	3	4.2	3	.	.	.	.
47	CENPV	Centromere protein V	103	5	4	21.5	5	.	.	.	.
48	PSIP1	Pc4 and sfrs1 interacting protein 1	102	6	5	13.2	6	29	1	4	6
49	NHP2	Nhp2 ribonucleoprotein	100	5	3	26.1	5	.	.	.	.
50	MYL1	Myosin light chain 1	96	3	2	8.2	3	.	.	.	.
51	MYL3	Myosin light chain 3	96	3	2	8.2	3	.	.	.	.
52	MYH14	Myosin heavy chain 14	92	5	4	2.3	5	18	1	5	5
53	PRC1	Protein regulator of cytokinesis 1	91	5	5	8.2	5	.	.	.	.
54	RBM34	Rna binding motif protein 34	86	3	3	9.5	3	.	.	.	.
55	GNB1	G protein subunit beta 1	84	6	6	17.9	4	.	.	.	.

Table 3 (Continue)

								Control		Ratio vs control	
No.	Gene symbol	Protein name	Protein score	Protein matches significance	Protein sequence significance	Proteuncover	Unique peptides	Protein score	Protein matches	Scores	peptide matches
56	SAP18	Sin3a associated protein 18	76	5	3	24.2	5	22	1	3	5
57	FAM32A	Family with sequence similarity 32 member A	73	5	5	36.6	5	50	1	1	5
58	SRSF10	Serine and arginine rich splicing factor 10	73	5	5	24	5	42	1	2	5
59	MYO1B	Myosin IB	71	5	5	7.2	5	.	.	.	.
60	SON	Son dna binding protein	71	3	3	1.4	3	.	.	.	.
61	DDX54	Dead-box helicase 54	69	3	3	4.4	3	.	.	.	.
62	RPL30	Ribosomal protein l30	67	5	4	51.3	5	22	1	3	5
63	DDX41	Dead-box helicase 41	65	3	2	3.1	3	.	.	.	.
64	PDCD11	Programmed cell death 11	64	3	3	2	3	.	.	.	.
65	SEC61A1	Sec61 translocon alpha 1 subunit	63	3	3	4.8	3	.	.	.	.
66	RRP1	Ribosomal rna processing 1	61	3	3	7.6	3	.	.	.	.
67	RBMXL2	Rna binding motif protein, x-linked like 2	58	5	4	9.7	5	.	.	.	.
68	EPPK1	Epiplakin 1	56	4	4	1.2	3	.	.	.	.
69	RBX1	Ring-box 1	56	3	2	17.6	3	.	.	.	.
70	RPF1	Ribosome production factor 1 homolog	55	3	2	8	3	.	.	.	.
71	IMP4	Imp4 homolog, u3 sno-RNP	54	3	3	13.4	3	.	.	.	.
72	CORO1B	Coronin 1b	52	3	3	12.3	3	.	.	.	.
73	SNRPA	Small nuclear ribonucleoprotein polypeptide A	50	5	5	23.8	5	35	1	1	5
74	TMA7	Translation machinery associated 7 homolog	46	3	2	18.8	3	.	.	.	.
75	WDR46	Wd repeat domain 46	46	3	2	3.9	3	.	.	.	.
76	RBM3	Rna binding motif	44	3	3	22.3	3	.	.	.	.
77	PHF14	Phd finger protein 14	43	5	2	4.1	5	.	.	.	.
78	BMS1	Bms1, ribosome biogenesis factor	42	3	3	3.6	3	.	.	.	.
79	SRSF12	Serine and arginine rich splicing factor 12	35	2	2	8.4	2	.	.	.	.
80	HNRNPDL	Heterogeneous nuclear rNP d like	30	3	3	10	3	.	.	.	.
81	MASTL	Microtubule associated ser/thr kinase like	20	4	2	4.1	4	.	.	.	.

Table 4

Number	Uniport entry no.	Protein description	Gene symbol	Peptide sequence	Modifications	Normalized area (averaging duplicate peptides)		Normalized area ratio (Heavy peptide/ Light peptide)
						Light peptide	Heavy peptide	
Peptides from FLAG-RPL23A complex proteins								
1	Q86V81	THO complex subunit 4	ALYREF	NRGAGGFGGGGGTR	Dimethyl (R)	10.77	9.24	0.86
2	Q86V81	THO complex subunit 4	ALYREF	NRGAGGFGGGGGTR	Dimethyl (R)	5.59	4.14	0.74
3	Q99700	Ataxin-2	ATXN2	VSAGRGSISSGLEFVS HNPPSEAATPPVAR	Methyl (R)	0.16	0.34	2.15
4	Q92841	Probable ATP-dependent RNA helicase	DDX17	GLDVEDVKFVINYDY PNSSEDYVHRIGR	Methyl (R)	0.12	0.11	0.92
5	P17066	Heat shock 70 kDa protein 6	HSPA6	TTPSYVAFTDTERLV GDAAK	Methyl (R)	2.24	0.26	0.12
6	P11940	Polyadenylate-binding protein 1	PABPC1	VANTSTQTMGPRPAA AAAAATPAVR	Dimethyl (R)	0.56	0.59	1.06
7	P11940	Polyadenylate-binding protein 1	PABPC1	VANTSTQTMGPRPA AAAAAATPAVR	Dimethyl (R)	1.13	1.09	0.97
8	P11940	Polyadenylate-binding protein 1	PABPC1	VMSTQRVANTSTQT MGPRPAAAAAAATP AVR	Dimethyl (R)	0.14	0.12	0.87
9	Q9H361	Polyadenylate-binding protein 3	PABPC3	SGVGNIFVKNLDK	Methyl (K)	6.61	0.02	0.00
10	Q9H361	Polyadenylate-binding protein 3	PABPC3	SGVGNIFVKNLDK	Methyl (K)	92.62	0.37	0.00
11	P38159	RNA-binding motif protein, X chromosome	RBMX	VEADRPGKLFIGGLN TETNEKALEAVFGKY GR	Trimethyl (K)	1.17	0.39	0.34
12	P83881	60S ribosomal protein L36a	RPL36A	QSGYGGQTKPIFR	Methyl (K)	5.10	3.74	0.73
13	P83881	60S ribosomal protein L36a	RPL36A	KQSGYGGQTKPIFR	Methyl (K)	3.91	3.19	0.82
Peptides from ultracentrifuged purified ribosome								
14	P68104	Elongation factor 1-alpha 1/2	EEF1A1/2	GSFKYAWVLDKLK	Dimethyl (K)	1144.78	8.12	0.01
15	P13639	Elongation factor 2	EEF2	VAVEAKNPADLPKL VEGLKR	Trimethyl (K)	1.81	0.50	0.28
16	P11940	Polyadenylate-binding protein 1	PABPC1	VANTSTQTMGPRPAA AAAAATPAVR	Dimethyl (R)	1.91	0.63	0.33
17	P11940	Polyadenylate-binding protein 1	PABPC1	VANTSTQTMGPRPAA AAAAATPAVR	Dimethyl (R)	3.62	1.33	0.37
18	P11940	Polyadenylate-binding protein 1	PABPC1	VMSTQRVANTSTQT MGPRPAAAAAAATP AVR	Dimethyl (R)	0.10	0.06	0.62
19	P11940	Polyadenylate-binding protein 1	PABPC1	VMSTQRVANTSTQT MGPRPAAAAAAATP AVR	Dimethyl (R)	0.56	0.58	1.03
20	Q4VXU2	Polyadenylate-binding protein 1 like	PABPC1L	IVGTKPLYVALAQR	Methyl (K)	0.69	0.14	0.21
21	Q4VXU2	Polyadenylate-binding protein 1 like	PABPC1L	IVGTKPLYVALAQR	Methyl (K)	0.21	0.02	0.08
22	Q4VXU2	Polyadenylate-binding protein 1 like	PABPC1L	IVGTKPLYVALAQRK	Methyl (K)	0.17	0.04	0.20
23	Q9H361	Polyadenylate-binding protein 3	PABPC3	SGVGNIFVKNLDK	Methyl (K)	10.46	2.60	0.25

Table 4 (Continue)

Number	Uniport entry no.	Protein description	Gene symbol	Peptide sequence	Modifications	Normalized area (averaging duplicate peptides)		Normalized area ratio (Heavy peptide/ Light peptide)
						Light peptide	Heavy peptide	
Peptides from ultracentrifuged purified ribosome								
24	Q13310	Polyadenylate-binding protein 4	PABPC4	AAVAAAAP**R**AVAPY K	Dimethyl (R)	0.20	0.08	0.41
25	Q13310	Polyadenylate-binding protein 4	PABPC4	AAVAAAAP**R**AVAPY KYASSVR	Dimethyl (R)	0.22	0.23	1.03
26	Q969Q0	60S ribosomal protein L36a	RPL36A	QSGYGGQT**K**PIFR	Methyl (K)	12.96	13.8 7	1.07
27	Q969Q0	60S ribosomal protein L36a	RPL36A	QSGYGGQT**K**PIFR	Methyl (K)	4.78	4.76	1.00
28	Q969Q0	60S ribosomal protein L36a	RPL36A	KQSGYGGQT**K**PIFR	Methyl (K)	1.01	1.00	0.99
29	Q969Q0	60S ribosomal protein L36a	RPL36A	KQSGYGGQT**K**PIFRK	Methyl (K)	0.27	0.22	0.82

Table 5

Number	Uniport entry no.	Protein description	Gene symbol	Peptide sequence	Modifications	Normalized area (averaging duplicate peptides)		Normalized area ratio (Heavy peptide/ Light peptide)
						Light peptide	Heavy peptide	
1	Q86V81	THO complex subunit 4	ALYREF	NRGAGGFGGGGGTR	Dimethyl (R)	8.18	6.69	0.82
2	Q99700	Ataxin-2	ATXN2	VSAGRGSISSGLEFVSHNPPSEAATPPVAR	Methyl (R)	0.16	0.34	2.15
3	Q92841	Probable ATP-dependent RNA helicase	DDX17	GLDVEDVKFVINYDYPNSSEDYVHRIGR	Methyl (R)	0.12	0.11	0.92
4	P68104	Elongation factor 1-alpha 1/2	EEF1A1/2	GSFKYAWVLDKLK	Dimethyl (K)	1144.78	8.12	0.01
5	P13639	Elongation factor 2	EEF2	VAVEAKNPADLPKLVEGLKR	Trimethyl (K)	1.81	0.50	0.28
6	P17066	Heat shock 70 kDa protein 6	HSPA6	TTPSYVAFTDTERLVGDAAK	Methyl (R)	2.24	0.26	0.12
7	P11940	Polyadenylate-binding protein 1	PABPC1	VANTSTQTMGPRPAAAAAAATPAVR	Dimethyl (R)	1.80	0.91	0.50
8	P11940	Polyadenylate-binding protein 1	PABPC1	VMSTQRVANTSTQTMGPRPAAAAAAATPAVR	Dimethyl (R)	0.27	0.26	0.95
9	Q4VXU2	Polyadenylate-binding protein 1 like	PABPC1L	IVGTKPLYVALAQR	Methyl (K)	0.45	0.08	0.18
10	Q4VXU2	Polyadenylate-binding protein 1 like	PABPC1L	IVGTKPLYVALAQRK	Methyl (K)	0.18	0.04	0.20
11	Q9H361	Polyadenylate-binding protein 3	PABPC3	SGVGNIFVKNLDK	Methyl (K)	36.56	0.99	0.03
12	Q13310	Polyadenylate-binding protein 4	PABPC4	AAVAAAAPRAVAPYK	Dimethyl (R)	0.20	0.08	0.41
13	Q13310	Polyadenylate-binding protein 4	PABPC4	AAVAAAAPRAVAPYKYASSVR	Dimethyl (R)	0.22	0.23	1.03
14	P38159	RNA-binding motif protein, X chromosome	RBMX	VEADRPGKLFIGGLNTETNEKALEAVFGKYGR	Trimethyl (K)	1.17	0.39	0.34
15	P83881	60S ribosomal protein L36a	RPL36A	QSGYGGQTKPIFR	Methyl (K)	5.51	4.98	0.90
16	P83881	60S ribosomal protein L36a	RPL36A	KQSGYGGQTKPIFR	Methyl (K)	2.46	2.10	0.85
17	Q969Q0	60S ribosomal protein L36a	RPL36A	KQSGYGGQTKPIFRK	Methyl (K)	0.27	0.22	0.82